APPROVAL SHEET

Title of Thesis: Multiscale Tensile Characterization and Repeatability of Additively Manufactured 17-4 PH Stainless Steel

Name of Candidate: Madeline Grace Selby
Master of Science, 2022

Thesis and Abstract Approved:

_____

Dr. Marc Zupan
Associate Professor
Department of Mechanical Engineering

Date Approved: 29 April 2022

ABSTRACT

Title of Document:	MULTISCALE TENSILE CHARACTERIZATION AND REPEATABILITY OF ADDITIVELY MANUFACTURED 17-4 PH STAINLESS STEEL
	Madeline Grace Selby, Master of Science, 2022
Directed By:	Dr. Marc Zupan, Associate Professor, Department of Mechanical Engineering

Additive manufacturing (AM) presents a new opportunity to revolutionize manufacturing by producing intricate, customized components that traditional manufacturing cannot readily produce. Metal AM has been targeted as a viable manufacturing operation to create precipitation hardened stainless steel alloys for next-generation marine vehicle systems due to the material's high strength and corrosion resistance. This study examines heat treated AM 17% Chromium – 4% Nickel precipitation hardened (17-4 PH) stainless steel material manufactured using powder bed fusion on an EOS M290 machine. Six geometrically identical builds were produced to assess AM repeatability with material characterization across varying length scales. Multiscale tensile testing at the micro-, meso-, and macroscale presents a methodology to study the material both locally and globally and draw comparisons across the different length scales. Results indicate that

tensile testing must occur at different length scales to fully characterize AM 17-4 PH stainless steel material.

MULTISCALE TENSILE CHARACTERIZATION AND REPEATABILITY OF ADDITIVELY MANUFACTURED 17-4 PH STAINLESS STEEL

By

Madeline Grace Selby

Thesis submitted to the Faculty of the Graduate School of the
University of Maryland, Baltimore County, in partial fulfillment
of the requirements for the degree of
Master of Science
2022

Dedication

To my grandfather, James Svoboda, the first researcher in my family.

Acknowledgements

I want to start by thanking my advisor, Dr. Marc Zupan, for his guidance and support starting from when I joined the lab as an undergraduate student. Joining his lab encouraged me to pursue research for my career and I am forever grateful for his help seeking out Ph.D. programs. His encouragement and enthusiasm provided me with the motivation and determination to be the best researcher I can be. Next, I want to thank my unofficial co-advisor, Dr. Michael Duffy for his endless assistance and advice throughout my time in the MMCL. His knowledge of this project and every single piece of lab equipment made the entire process easier and more successful. Thank you for giving me the tour of the lab and showing your excitement for research when I was in your machine design class and struggling to build an RC car.

I want to thank all my lab mates in the MMCL. Your friendship and support mean the world to me, and I could not have made it this far without you. João Santos has taught me so many things while I have been in the lab: how to polish, how to grade lab reports, how to write a research paper, how to survive graduate classes, and so much more. I very much appreciate his willingness to help with any problem I had in the lab or with classes. Matt Dusek made this research team the best group I have ever been on for a project. He kept me motivated to write my literature review and helped me power through all the painful parts of this work. I have always been able to rely on Matt in every aspect of the lab and as a friend. Being able to walk through thesis ideas together and jointly run experiments made this entire process so much more enjoyable. Julianna Posey created a welcoming environment in the lab and quickly became a close friend. She helped improve the difficult times in the lab and always acted as a resource I could talk to.

Jocelyn Wilkins helped me stay sane by video chatting while I polished and helped me move through the mesosamples much faster than I would have on my own.

I want to thank Olivia Bailey and Liz Emberger for their unwavering friendship since freshman year. Their encouragement and support throughout my entire time at UMBC has helped me be successful and stay sane while doing it.

Finally, I want to thank my family for their encouragement and dedication to helping me throughout my first year of graduate school. My brother, Max, sent me updates of his book which served as excellent distractions/breaks in my writing. From the bottom of my heart, I want to thank my parents, Sandy and Chip, for always supporting me and pushing me to do my best. Their love and support helped me make it through my degrees at UMBC.

Table of Contents

List of Tables

List of Figures

List of Abbreviations

17-4 PH	17% Chromium - 4% Nickel Precipitation Hardened
AM	Additive Manufacturing
CAD	Computer-Aided Design
DED	Direct Energy Deposition
DIC	Digital Image Correlation
DMLM	Direct Metal Laser Melting
DMLS	Direct Metal Laser Sintering
EBM	Electron Beam Melting
L-PBF	Laser Powder Bed Fusion
NSWC	Naval Surface Warfare Center
NSWCCD	Naval Surface Warfare Center Carderock Division
PBF	Powder Bed Fusion
SLA	Stereolithography
SLM	Selective Laser Melting
SLS	Selective Laser Sintering
UMBC	University of Maryland, Baltimore County
UTS	Ultimate Tensile Strength
YS	Yield Strength

1. Introduction

1.1 Background

This work was developed in partial fulfillment of the UMBC degree requirements for a Master of Science in Mechanical Engineering. This thesis is the product of an Educational Partnership Agreement between the University of Maryland, Baltimore County (UMBC) and Naval Surface Warfare Center Carderock Division (NSWCCD). This project was developed to characterize the properties and repeatability of additively manufactured (AM) 17% Chromium – 4% Nickel precipitation hardened (17-4 PH) stainless steel structures. The 17-4 PH material was selected due to its high strength and corrosion resistance which are suitable for intense marine environments. NSWCCD provided UMBC with structures from Naval Surface Warfare Center Panama City (NSWC Panama City) for this study. This partnership between NSWCCD and UMBC applies UMBC's unique microtensile characterization efforts with the ongoing evaluation of AM at NSWCCD, facilitating future collaboration between the research institutions.

1.2 Motivation

Additive manufacturing (AM) presents a new possibility to revolutionize manufacturing by producing intricate, customized components that traditional manufacturing cannot readily produce. Metal AM has been targeted as a viable manufacturing process for next-generation vehicle systems due to its unique capabilities. The Navy has identified AM as a novel technique to create weight-optimized and unique components to enhance vehicle performance, with the potential for manufacturing use while underway. However, AM is considered a disruptive technology where typical qualification and characterization methods cannot always be applied. Therefore, new

characterization methodologies must occur to understand the behavior of this material compared to its traditionally manufactured counterparts. Characterization across varying length scales presents a methodology to study the material locally and globally.

1.3 Aims and Scope

The aim of this work is to add to the limited literature on AM 17-4 PH stainless steel by conducting multiscale tensile testing. The proposed methodology will determine mechanical properties from micro-, meso-, and macroscale tensile samples and draw comparisons across these different length scales. The micro- and mesoscale samples will introduce a localized look into the material's mechanical properties while the macroscale samples present a globalized analysis method.

This work falls under an overarching study to assess the repeatability of AM 17-4 PH stainless steel by analyzing various geometric structures and build orientations. The scope of this work is limited to the repeatability across multiscale tensile testing to determine mechanical properties.

1.4 Thesis Overview

Chapter 2 presents an overview of the relevant studies necessary to understand the scope of this work. It includes a detailed introduction to additive manufacturing (AM), including the methodology, various processes, and applications, followed by a more thorough overview of metal AM with details on powder bed fusion (PBF), processing operations, and post-processing treatments. This section concludes with a thorough investigation into 17-4 PH stainless steel, with a particular emphasis on the effect of AM on the material and the published mechanical properties. Chapter 3 explains the specific AM 17-4 PH stainless steel material used in this study, including the build geometry. It

includes the microsample and mesosample tensile testing techniques, such as sample preparation, the systems used, and data analysis methods. Chapter 4 evaluates the results obtained from the mechanical testing across length scales. Mechanical properties including yield strength, ultimate tensile strength, and strain to failure, are presented with a statistical comparison across length scales. Chapter 5 presents the conclusions from the entire work and recommends future work to expand upon this study.

2. State of the Art

2.1 Introduction

The additive manufacturing (AM) process introduces a novel technique to create intricately manufactured parts that cannot be created through traditional means. To optimize the AM process, material selection must be optimized to undergo the complex thermal cycles from AM. This study evaluates the behavior of additively manufactured 17% Chromium – 4% Nickel precipitation hardened (17-4 PH) stainless steel which enables the creation of components for next-generation marine vehicle systems due to AM's intricacy and the material's high strength and corrosion resistance.

This state of the art will introduce additive manufacturing, the many AM processes, and their industrial applications. It will then delve into the specifics of metal AM including the different modes of material delivery, processing parameters, and the necessary post-processing treatments. The state of the art will then examine the specifics of additively manufactured 17-4 PH stainless steel, focusing on the microstructural implications from the manufacturing process and the mechanical properties from different thermal post-processing treatments.

2.2 Additive Manufacturing (AM)

2.2.1. AM Overview

Additive manufacturing (AM) is defined as a process of creating a 3D part by joining materials together layer by layer [1]. AM was developed as a technology to enable custom, intricate part design while reducing material waste and manufacturing time [2]. When AM was first commercialized in the 1980s, it was primarily used for conceptual models and prototyping [3]. Through recent innovations, the technology has

transformed from rapid prototyping to rapid manufacturing using more advanced materials and processes [4]. AM drives innovation because it provides the ability to manufacture complex geometries on-demand, and it is creating a paradigm shift from design for manufacturing to manufacturing for design [4].

The generalized process and individual steps for AM processes are seen in Figure 1. The first step of the AM process is to create a 3D model, generally designed using computer-aided design (CAD) software or a 3D scan of an existing object [5]. To convert the 3D model into a format that the AM machine will understand, the CAD software must first save the 3D model as an STL file [6]. The acronym STL is widely believed to derive from the word stereolithography or even standard triangle language or standard tessellation language [7]. The STL file format describes the surface of the 3D model using connected triangles [8]. This file is then imported into a slicing software, often called the "slicer," which converts the 3D model into specific printing instructions for the AM machine. The slicer cuts the STL file into horizontal layers, using predetermined settings such as infill percentage or layer height, and determines the appropriate tool path for the machine [7]. The information created from the slicer is saved as a GCode file and sent to the machine. The system then manufactures the 3D model by forming each layer through the selective placement of material, guided by the 2D slices [5].

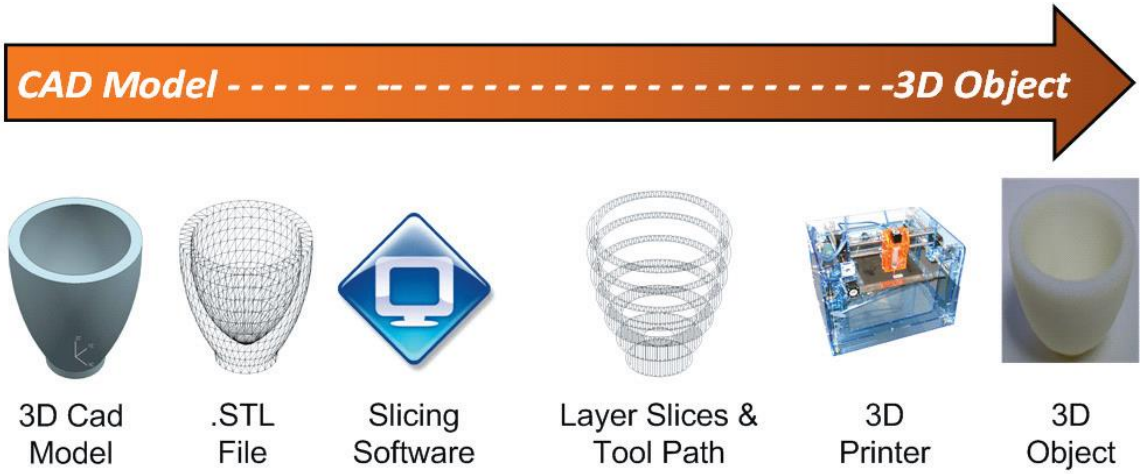

Figure 1 Generalized AM process [5].

2.2.2. AM Processes

The ASTM F42 committee categorizes AM processes into seven different areas [1], as seen in Table 1. These seven categories are defined based on the layer deposition and layer-to-layer bonding methods. They also vary based on process's starting materials, including liquid, filament/paste, powder, or solid sheet [4].

Table 1 AM processes and equipment manufacturers [4].

Process Category	Process/Technology	Material	Manufacturer(s)
Vat photopolymerization	SLA (Stereolithography)	UV curable resins	Asiga 3D Systems EnvisionTEC Rapidshape
		Waxes	DWS
		Ceramics	Lithoz
Material jetting	MJM (Multi-Jet Modeling)	UV curable resins	3D Systems Stratasys
		Waxes	Solidscape
Binder jetting	3DP (3D Printing)	Composites Polymers, ceramics Metals	3D Systems Voxeljet ExOne
Material extrusion	FDM (Fused Deposition Modeling)	Thermoplastics	Stratasys MakerBot RepRap Bits from Bytes Fabbster Delta Micro Factory Corporation Beijing Tiertime
		Waxes	ChocEdge Essential Dynamics Fab@Home
Powder bed fusion	SLS (Selective Laser Sintering)	Thermoplastics	EOS Blueprinter 3D Systems
		Metals	3Geometry Matsuura 3D Systems
	SLM (Selective Laser Melting)	Metals	EOS SLM Solutions Concept Laser 3D Systems Realizer Renishaw
	EBM (Electron Beam Melting)	Metals	Arcam Sciaky
Sheet lamination	LOM (Laminated Object Manufacturing)	Paper Metals Thermoplastics	Mcor Technologies Fabrisonic Solido
Directed energy deposition	LMD/LENS (Laser Metal Deposition)	Metals	Optomec DM3D Irepa Laser
	EBAM (Electron Beam AM)	Metals	Sciaky

Vat photopolymerization was the first AM process to be successfully commercialized in the 1980s [3]. This process uses UV light to selectively cure the top layer of a vat of liquid photopolymer resin. This curing causes the exposed areas to solidify into a solid part, and the part is lowered to allow additional uncured resin to flow over the top for selective curing next. The benefits to vat photopolymerization include the ability to create high levels of accuracy and smooth surface finishes in a component [9]. However, the process is slow, and the available materials are limited and tend to have a relatively high material cost [2].

Material jetting is an AM process where droplets of material are selectively deposited layer by layer and cured with UV light after each deposited layer. Thermally molten materials may also be used in this process; they are selectively deposited and then solidify at room temperature. Material jetting enables high levels of part accuracy and can easily use multiple materials and colors in a single part. Both the size and the limited useable materials affect the widespread adoption of this process [9].

The process of binder jetting involves the selective deposition of liquid bonding agents to powdered material. Depending on the material, the part can be used as-built, cured, or fired in a furnace. Benefits to this process include high productivity for a wide range of materials and full color printing [9]. However, the produced parts display relatively weak material properties, which must be considered when using binder jetting [2].

Material extrusion is an AM process that selectively deposits melted material through a heated extrusion nozzle in a designated path. This process repeats layer by layer to create the full 3D part [2]. This method of AM has become well-known and

prevalent and has even been implemented in office and academic environments. Material extrusion is inexpensive and creates parts that can have good structural properties [9]. The process does have low accuracy and can have some difficulty fabricating overly complex parts [2].

Powder bed fusion (PBF) uses a laser or electron beam to selectively melt a bed of powder, layer by layer, to create the 3D part. The unmelted powder acts as support material for any overhang features on the part. PBF allows for high levels of complexity, a wide variety of materials, and little to no post-processing to remove support material [9]. However, this process is relatively expensive, limited in size, and the part's surface finish is constrained by the powder particle size [2].

Sheet lamination is a technique that stacks and laminates sheets of material together. The sheets are cut to the correct shape before lamination to form the proper 3D shape. This process has the benefits of high speed and low cost (for non-metal materials) [9]. The drawbacks of sheet lamination are the limited materials and geometric constraints [2].

Directed energy deposition (DED) uses either powder or wire fed through a nozzle into a melt pool on the part's surface where a laser or electron beam adheres it. DED can essentially be considered a type of automated welding process. Some key advantages of DED include no limitation in direction or axis, extremely high deposition rates, and the ability to repair damaged components and add features [9]. Limitations include lowered accuracies and required post-processing. Additionally, current research examines the capability of AM hybrid systems which combine DED systems with the

benefits of traditional subtractive manufacturing such as milling to improve part tolerances [2, 10].

2.2.3. Applications

Industrial applications of AM are particularly relevant in the aerospace, automotive, biomedical, and military sectors, with additional growth in other sectors. These industries benefit from designs with weight optimization, faster customization, part consolidation, topology optimization, and more [2]. In general, AM is suitable for low-volume production applications, components with complex geometries, expensive or difficult to manufacture materials, and quick design change requirements [11].

The aerospace sector relies on various technical and economic objectives for manufacturing, including functional performance, lead time reduction, light-weighting, complexity, and cost management [12]. AM provides a potential solution to meet these goals and surpass the capabilities of the traditional manufacturing processes previously used. Currently, the main advantage of using AM in aerospace applications is lead time reduction due to the complexity of the parts. Traditional tooling methods create long lead times for the complicated structures required for aerospace applications, whereas AM techniques require far less tooling [12]. Airbus took advantage of AM to develop titanium brackets for the Airbus A350 XWB, seen in Figure 2, and achieved a 75% reduced manufacturing time and 30% lighter structure [13].

Figure 2 AM PBF bracket for Airbus A350 XWB manufactured of Ti6Al4V [13, 14].

Aerospace components generally require advanced, specialty materials, such as titanium, special steels, or ultrahigh temperature ceramics, which are difficult, costly, and time-consuming to fabricate using traditional methods and typically manufactured in small batches [4]. Additionally, conventional forms of manufacturing create large quantities of scrap, which are challenging to recycle [15]. AM enables complex geometries while also reducing waste and thus lowering the manufacturing cost of parts for aerospace applications [4, 15]. AM techniques allow high-performance to weight ratio which, when applied to aerospace components, creates lightweight structures which reduce cost and emissions [13].

Similar to the aerospace sector, the automotive industry requires components to be lightweight, complex, and able to be consolidated into single components. Reduced weight combined with design complexity improves vehicle performance and reduces the time spent on assembly and the cost of the part [16]. The automotive industry has explored the use of AM in designing and developing specific components to improve the time spent in the development cycle and the cost for manufacturing. AM automotive

components have already been used in luxury, low-volume vehicles for structural and functional parts and in racing vehicles which typically use lightweight alloys with complex structures [4, 17].

The biomedical field is another industry area that significantly benefits from AM technologies. Medical applications of AM include medical models, implants, components of medical devices, splints, prostheses, and biomanufacturing [18]. These applications require high complexity, customization, patient-specific necessities, and small production amounts [13]. The design freedom provided by AM presents the opportunity to create these complex, customizable, and extremely precise structures. It also allows the control of the internal structures and microarchitecture, which can be essential for tissue regeneration and integration into the body [19].

2.3 Metal Additive Manufacturing

2.3.1. Metal AM Overview

While there are seven types of AM, as examined in Section 2.2.2, only five processes are typically used when producing metal AM structures in industry, seen in Figure 3 [2].

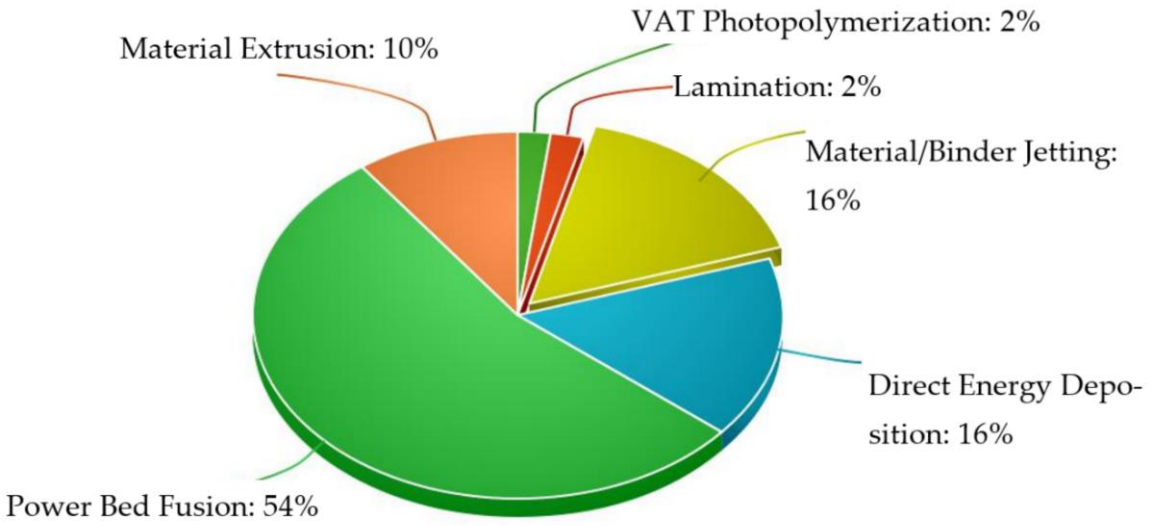

Figure 3 Industrial use of metal AM in 2020 [2].

Of these five categories, powder bed fusion (PBF) and directed energy deposition (DED) are the most available systems on the market [20]. Table 2 lists the common metal AM technologies and commercial machine suppliers within the PBF and DED categories.

Table 2 Metal AM processes and commercial machine suppliers. Adapted from [21].

AM Category	Technology	Commercial Machine Supplier
Powder Bed Fusion (PBF)	Direct Metal Laser Sintering (DMLS)	EOS
	Selective Laser Melting (SLM)	SLM Solutions
	LaserCUSING	Concept Laser
	Laser Melting (LM)	Renishaw
	Selective Laser Sintering (SLS)	3D Systems
	Electron Beam Melting (EBM)	Arcam
	Laser Metal Fusion (LMF)	Trumpf
Directed Energy Deposition (DED)	Direct Manufacturing (DM)	Sciaky
	Laser-Engineered Net Shaping (LENS)	Optomec
	Direct Metal Deposition (DMD)	DM3D Technology
	Wire Arc Additive Manufacturing (WAAM)	Not provided
	Laser Metal Deposition (LMD)	Trumpf
	Direct Metal Printing	3D Systems

2.3.2. Metal AM Systems

As defined by Frazier, metal AM systems can be classified into three broad categories: powder bed systems, powder feed systems, and wire feed systems [22]. Powder feed and wire feed systems both fall under the previously identified category directed energy deposition (DED) [22]. This review will examine all three metal AM categories, focusing on powder bed systems due to their relevance to this research.

2.3.2.1. Powder Bed Systems

ASTM defines powder bed fusion (PBF) as "an additive manufacturing process in which thermal energy selectively fuses regions of a powder bed" [23]. These systems account for the majority of available metal AM systems on the market due to their exceptional resolution [20, 24]. The powder bed process can alternatively be called selective laser sintering (SLS), selective laser melting (SLM), direct metal laser sintering (DMLS), direct metal laser melting (DMLM), and electron beam melting (EBM), also seen in Table 2. Laser PBF (L-PBF) systems may use either melting or sintering to selectively fuse each powder layer, but current systems tend to use melting to create full-density parts. Melting systems allow for the re-melting of previous layers as the current layer is melted, and the melting process better adheres the current layer to the previous layers [24, 25].

Figure 4 presents the basic process for L-PBF systems, where the dashed line represents an enclosed chamber usually filled with inert gas [20].

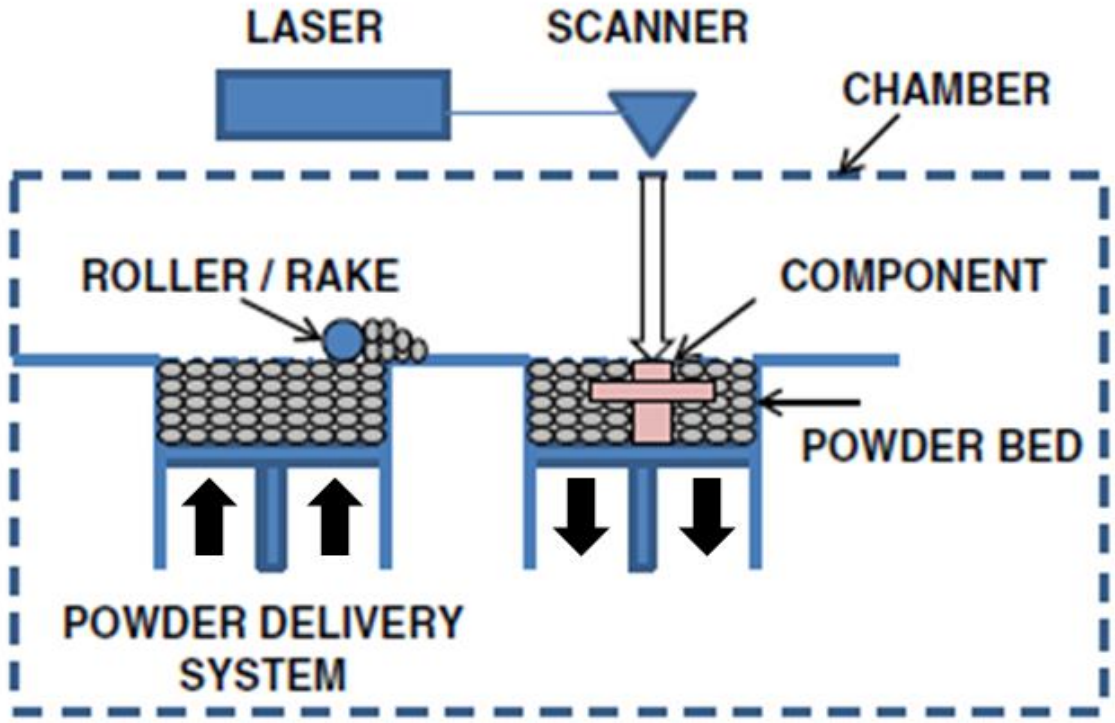

Figure 4 Generic metal AM laser powder bed system [22].

The system uses two beds: one to provide the reserve powder and one to support the build during manufacturing. A roller or a rake pushes a thin layer (20 – 60 μm) of fresh powder from the reserve bed to the build platform [20, 26]. The laser selectively fuses the powder to create each layer of the component. After each layer is selectively fused, the reserve powder bed moves up, and the build platform holding the component moves down to apply a new layer of powder and continue the process [11, 20, 22, 25]. The un-fused powder on the build platform acts as a support structure for the part [27].

The build chamber for PBF systems is an enclosed space with a controlled operating atmosphere based on the energy source and material. When exposed to air, metal powders tend to oxidize and collect moisture [24]. To prevent this interaction, laser systems typically operate in an inert atmosphere with either nitrogen or argon gas filling

the build chamber or flowing over the powder bed. The inert gas flow protects the component from oxygen and clears “spatter” and metal fumes created from the laser [25, 28]. Instead of an inert gas environment, EBM systems operate in a vacuum chamber [20]. Both laser and electron beam PBF systems occur in a heated chamber set to a pre-determined temperature based on the process: around 100°C for laser and 700°C for electron beam [29]. The build platform is an additional thermally necessary component as it serves as the primary path to dissipate heat [24].

The laser scanning strategy dictates the manufacturing of each build layer. This strategy describes the motion of the laser beam across the surface of each powder layer [30]. L-PBF systems incorporate two different components of scanning: the core hatching pass and the contour pass, seen in Figure 5.

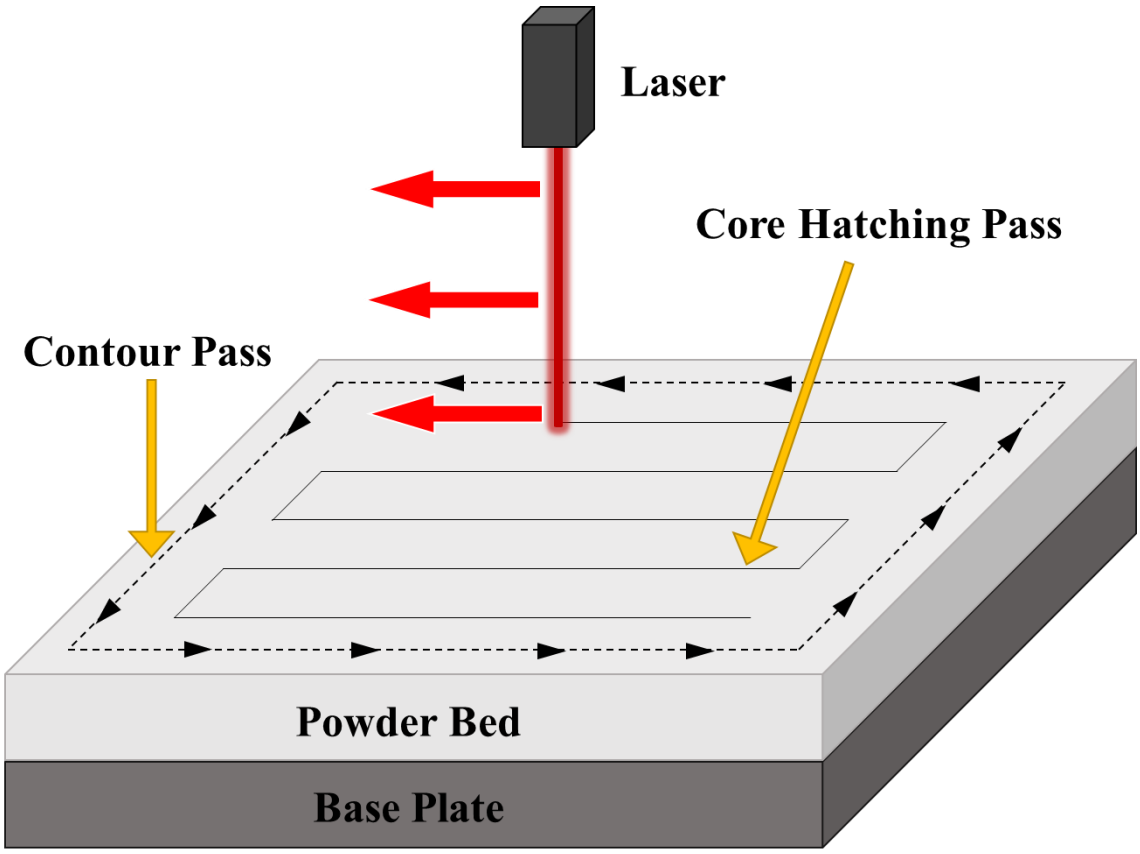

Figure 5 Selective laser fusing contour pass and core hatching pass [31].

Various scanning paths can be used to fill the core region of the part. Figure 6 shows example scanning strategies for the core hatch.

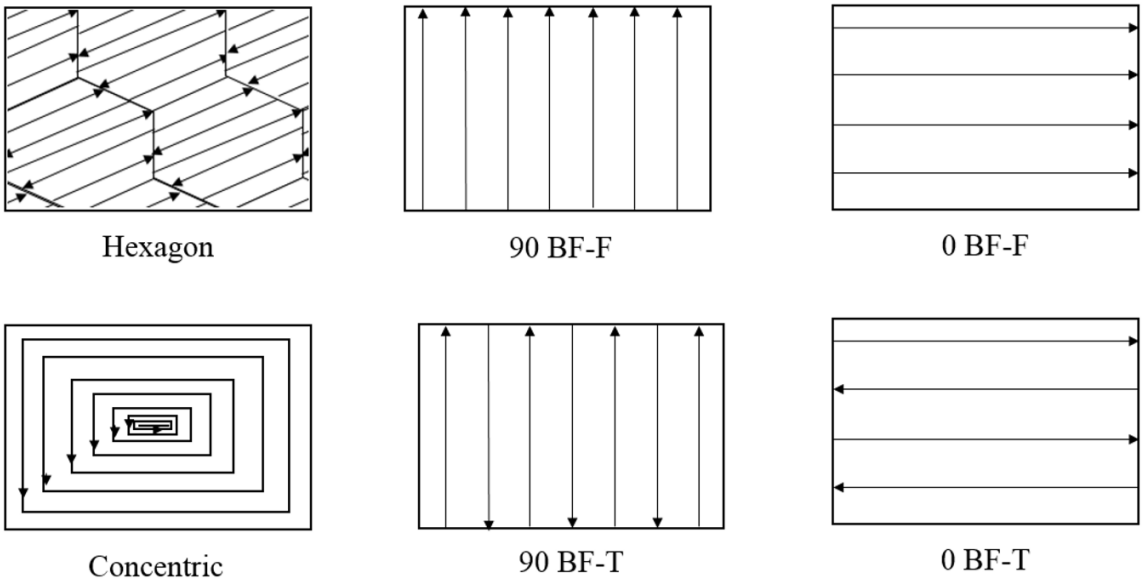

Figure 6 Schematic representation of possible hatch patterns [32].

After fusing the core region, the outer surface of the part tends to be rough due to the discontinuous scanning lines on the outer surface [33]. The laser re-passes over the part edges to melt the contours, or the boundaries between the part and the powder bed, thus counteracting the rough surface. This additional laser pass is called the contour pass or contour scan [24, 33]. Scanning strategies and processing parameters can affect the part's density, mechanical properties, part tolerances, and residual stress [25].

After the part is completed, the un-fused powder must be removed from the build platform and the part. To a certain extent, this unused powder can be recycled for use in future builds [27]. Once the excess powder is removed, the part must be separated from the build platform, typically through wire electrical discharge machining (EDM) or an abrasive saw [24]. Post-processing operations tend to be required to improve the as-built part for use. These operations can include thermal treatments to improve mechanical properties and reduce residual stresses or surface finishing to improve the rough surface [11, 24]. Additional discussion of post-processing will occur in Section 2.3.4.

Powder bed systems have the capability to produce high resolution and complex features while maintaining dimensional control due to the thin layers and the use of powder for support material [22]. Compared to other metal AM systems, powder bed systems have a much more significant size limitation, and it tends to be expensive due to the cost of metal powder [2].

2.3.2.2. Powder Feed Systems

Powder feed systems blow a stream of powder through a nozzle into a molten metal pool where a laser heat source fuses a thin layer onto the build surface in the desired shape [2, 24]. The powder is blown through the nozzle using an inert carrier gas or gravity feed. A stream of shielding gas flows over the build surface to prevent oxidation in the molten weld pool [29]. Two styles of powder feed systems exist on the market: a system where the build platform is stationary but the deposition head moves and a system where the deposition head is stationary but the build platform moves [22]. Figure 7 shows the generic process for a powder feed system.

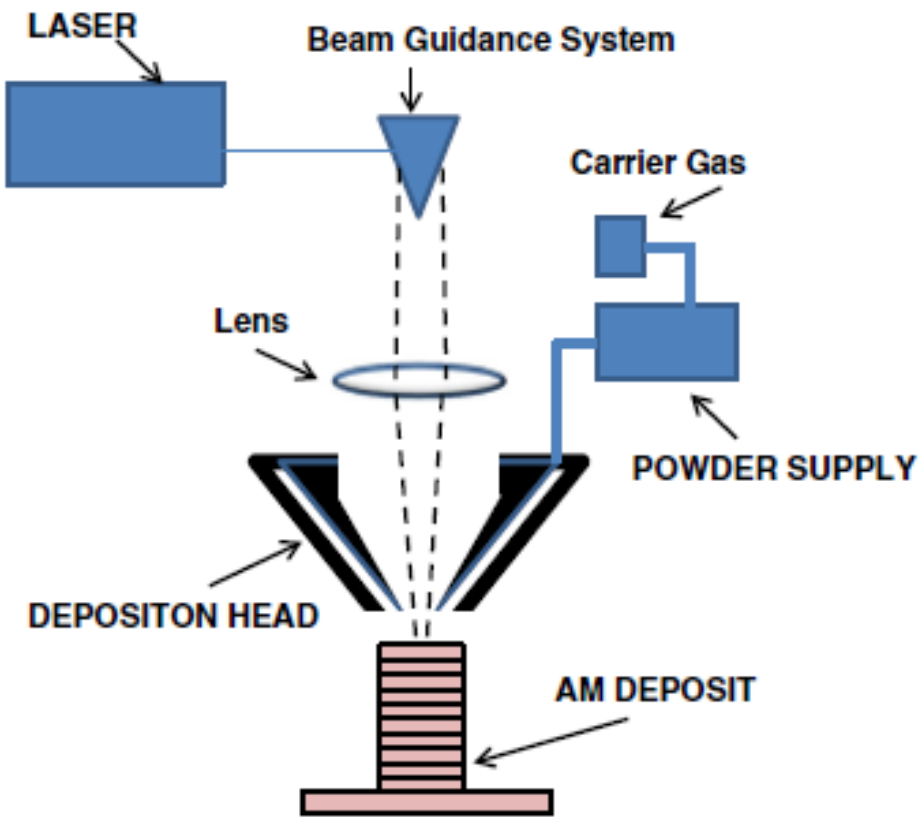

Figure 7 Generic metal AM powder feed system [22].

Powder feed systems have a larger build volume than powder bed systems, and they can repair damaged components or add features to a pre-existing part surface [2, 22]. These systems have lower resolution and part detail than powder bed systems and typically require additional machining after manufacturing [11].

2.3.2.3. Wire Feed Systems

Wire feed systems are similar to powder feed systems, except they use metal wire instead of powder as feedstock. The wire feedstock is directed into a molten metal pool, and a single layer is fused using an electron beam, laser, or plasma arc for the energy source [22, 29]. These systems operate in either a fully inert atmosphere or with an inert gas shroud to protect the molten metal from oxygen. Some wire feed systems are

extensions of welding technologies and can use robotic welding machines to create parts using multi-pass welding [2, 24]. Wire feed systems can have the build substrate in a stationary position or on a rotating axis to allow for more complex geometries [2]. Figure 8 shows a basic diagram for a wire feed system.

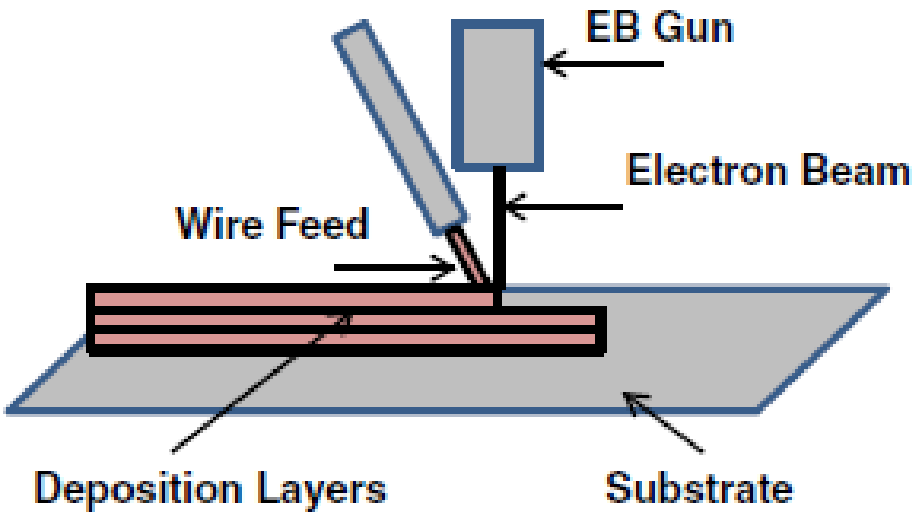

Figure 8 Generic metal AM wire feed system [22].

The main benefits of wire feed systems are the high deposition rates and large build volumes [22]. These systems can use commercially available welding wire which tends to be less expensive than metal powder [29]. Wire feed systems sacrifice part detail and surface finish and thus, require extensive post-build machining [11, 22].

2.3.3. Processing Parameters

Creating satisfactory AM parts using L-PBF heavily relies on using the ideal processing parameters during the manufacturing process. Both the structure and the properties of the manufactured component depend on the processing parameters [34]. Generally, processing parameters can be sorted into four categories: laser, scan, powder, and temperature, with the corresponding parameters listed in Table 3 [35].

Table 3 PBF processing parameter categories. Adapted from [35].

Processing Parameter Category	Processing Parameter
Laser	Laser power Spot size Pulse duration Pulse frequency
Scan	Scan speed Scan spacing Scan Pattern
Powder	Particle shape, size, and distribution Powder bed density Layer thickness Material properties
Temperature	Powder bed temperature Powder feeder temperature Temperature uniformity

A visual representation of typical processing parameters can be seen in Figure 9. Many processing parameters are interdependent and interact with each other [35]. When suboptimal processing parameters are used, defects can occur in the material such as porosity and residual stresses, creating distortion and a lack of geometric precision [30, 36].

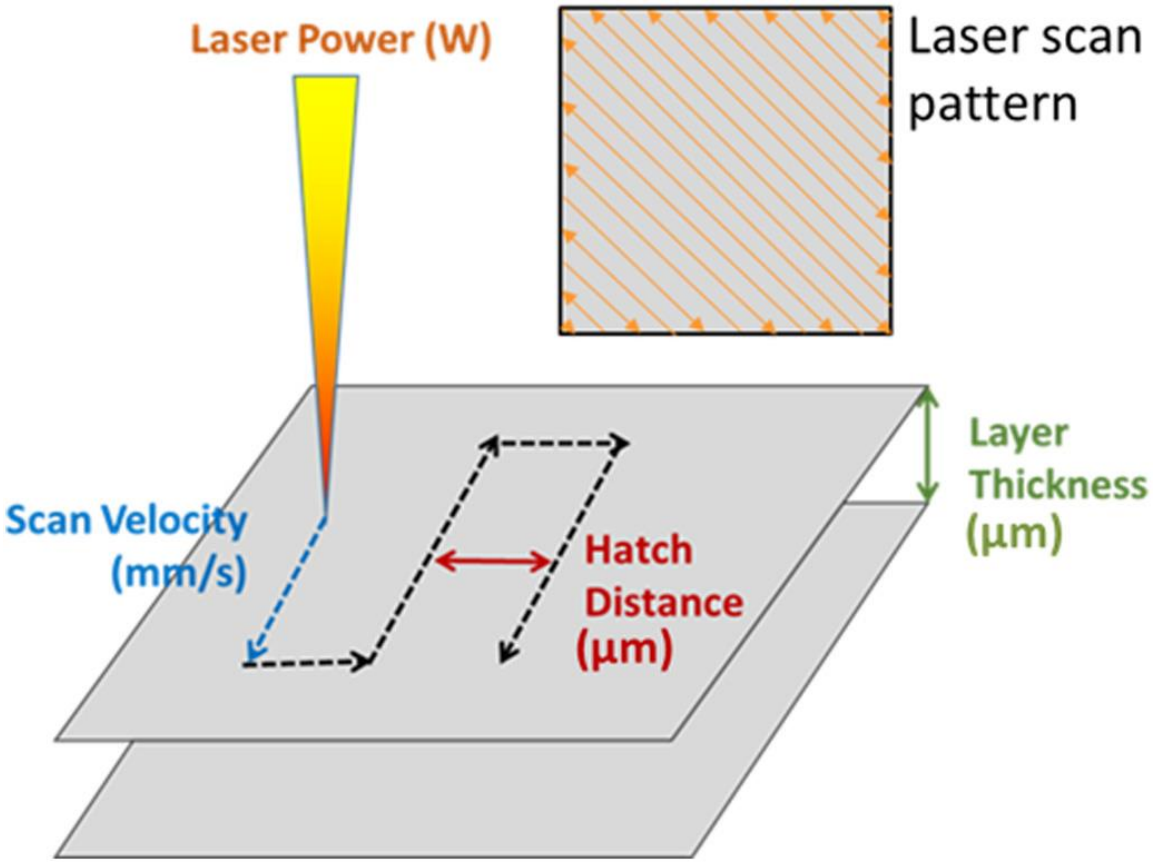

Figure 9 Typical processing parameters for PBF systems [36]

2.3.4. Post-Processing

AM parts are not ready for use directly out of the machine; they require additional post-processing steps to improve the quality of the parts. Excess powder must be removed, and the part must be separated from the build substrate before the part can go into use. Typically, AM parts undergo a thermal treatment process to improve performance. They frequently are machined to improve the surface finish since as-built AM parts exhibit high surface roughnesses [24].

2.3.4.1. Thermal Post-Processing

Thermal post-processing, or heat treatments, are used to relieve residual stress, reduce porosity, achieve ideal microstructure, and improve the mechanical performance

of an AM part [24]. These heat treatments homogenize the microstructure and increase ductility at the cost of lowering tensile strength [37]. Due to the differences between traditionally manufactured parts and AM parts, specific heat treatments need to be developed for AM material rather than simply using traditional heat treatments [20, 35].

Most metal AM parts require a stress relieving operation, primarily due to the residual stresses present in the material [2]. Residual stresses are caused by the inherent, thermally cyclic process of AM as previous layers are re-melted and cooled during the melting of new layers. A thermal stress relief occurs at an elevated temperature where atomic diffusion increases and atoms move from high stress regions to lower stress regions, resulting in a relief of internal stresses. These treatments must be performed at specific temperatures that are high enough to permit atomic mobility but occur over a short enough timeframe to suppress undesired grain recrystallization and growth [24].

After stress relief, precipitation hardened materials, such as 17-4 PH stainless steel, typically undergo a solution treatment (Condition A) followed by aging to obtain the desired precipitates. The chosen solution treatment temperature must be above the solvus temperature to ensure it dissolves all unwanted phases, essentially “resetting” the material’s matrix. The solution treatment must occur for long enough that the precipitates dissolve but short enough to restrict grain growth. Aging occurs next to create and grow precipitate phases. The previous solution treatment eliminated the original phase structures, so the aging process does not need to consider those previous phase structures [24].

2.3.4.2. Surface Finishing

The poor surface finish of as-built metal AM parts generally requires modification due to performance and aesthetic reasons [35], which impedes industry-wide adoption [38]. The poor surface finish occurs due to imperfections and defects such as stair-stepping from the inherently layered nature of AM, partially fused powder, part geometry, surface orientation, and balling effects [39]. An example of the stair-stepping effect due to the layer by layer deposition can be seen in Figure 10a, along with roughness from other aspects of the manufacturing process in Figure 10b.

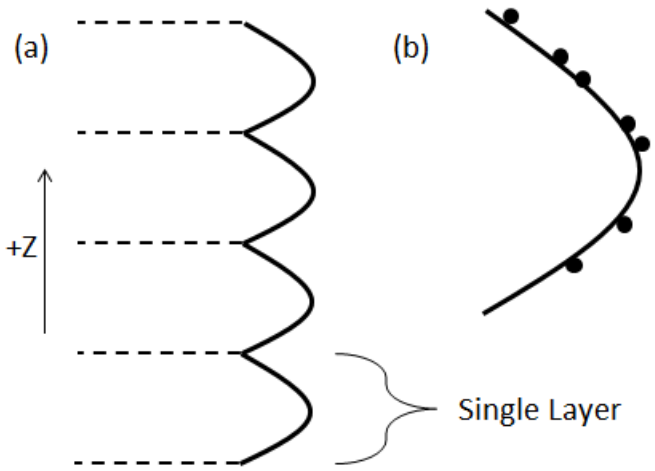

Figure 10 Poor surface finish due to a) layer roughness and b) actual surface roughness [24].

High surface roughness for AM parts restricts dimensional accuracy and provides locations for stress concentration sites which contribute to early crack initiation [39]. This premature crack initiation can create lower fatigue limits in as-built AM parts than AM parts polished or machined after manufacturing [20, 40]. Since the poor surface finish negatively impacts the material's performance, a variety of post-treatments have been

developed to mitigate the effects. Maleki sorts these surface treatments into four main categories: material removal, no material removal, coating, and hybrid treatments [39]. Figure 11 shows the specific treatments corresponding to each category.

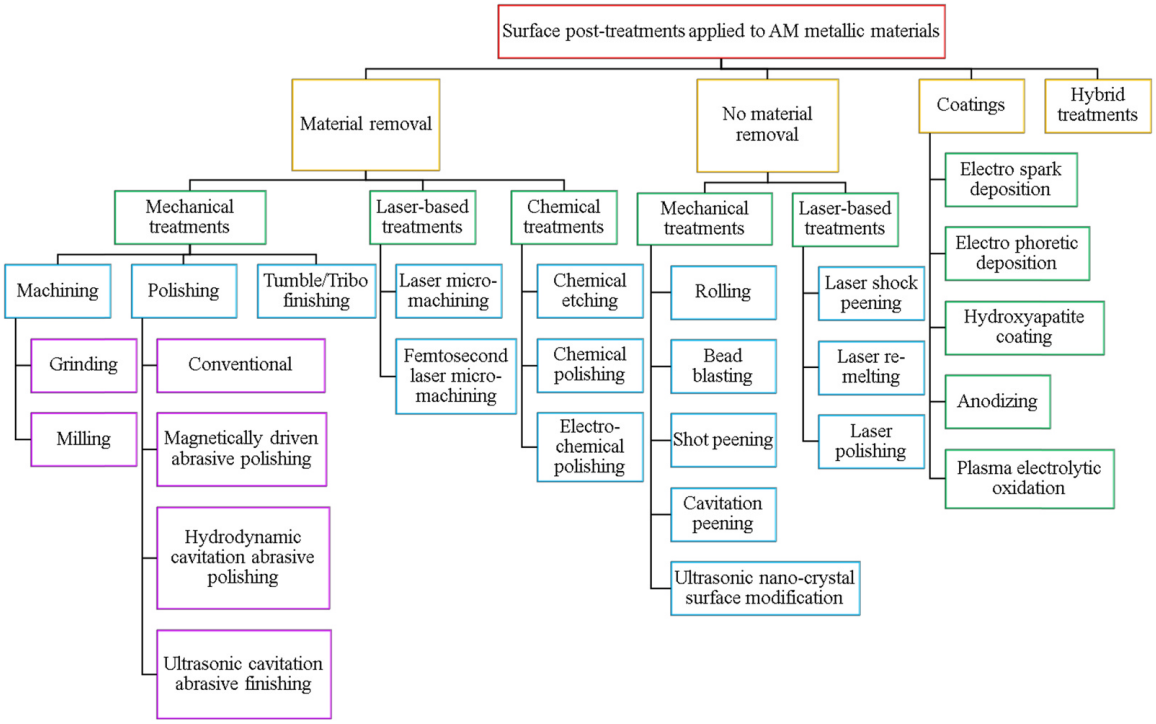

Figure 11 Surface post-treatments for AM metals [39]

2.4 AM Tension-Compression Asymmetry

Traditionally manufactured metallic materials typically exhibit similar tensile and compressive behaviors. However, it has been found that AM metals do not tend to exhibit this same behavior [41, 42]. A study by Cyr examined an AM maraging steel (MS1) manufactured using DMLS and found that the material exhibited high tension-compression asymmetry [41]. Additional work examined heat treated AM Ti-6Al-4V produced using DMLS and determined that the strain values from compression testing were higher than for tension testing, indicating that the material exhibited a more ductile

behavior under compression loading [42]. AM Ti-6Al-4V fabricated using Electron Beam Melting (EBM) similarly presented tension-compression asymmetry with higher compressive yield strengths than tensile yield strengths [43]. Alongside more traditional metal alloys, the high entropy alloy (HEA) $Al_{0.3}$CoCrFeNi manufactured using direct laser fabrication showed significant tension-compression asymmetry, specifically in its work hardening rate and ductility [44]. In general, the literature for AM material compression testing is lacking compared to the abundant studies on tensile testing. As such, only tensile testing will be presented as part of this study.

2.5 AM of 17-4 PH Stainless Steel

2.5.1. 17-4 PH Stainless Steel

The need for AM metals with good printability for varied applications requiring high strength and corrosion resistance has caused AM researchers to look to 17-4 PH stainless steel [45]. Table 4 presents the chemical composition of the EOS 17-4 PH stainless steel powder used in this study. The major alloying elements are chromium (Cr), nickel (Ni), and copper (Cu). The addition of chromium creates corrosion resistance in the alloy by creating a passive layer of Cr_2O_3 oxide. The nickel acts as an austenite stabilizer, improving the material's corrosion resistance. Copper precipitates form and grow during the aging heat treatment, strengthening the material [46].

Table 4 Chemical composition of EOS 17-4 PH stainless steel powder [47].

Element	Weight Percent (%)
Chromium (Cr)	15.00 - 17.00
Nickel (Ni)	3.00 - 5.00
Copper (Cu)	3.00 - 5.00
Silicon (Si)	≤ 1.00
Manganese (Mn)	≤ 1.00
Carbon (C)	≤ 0.07
Phosphorus (P)	≤ 0.040
Sulfur (S)	≤ 0.030
Niobium (Nb) + Tantalum (Ta)	0.15 - 0.45
Iron (Fe)	balance

2.5.2. Microstructure

In general, there are three different microstructural phases in PH stainless steel: δ-ferrite (bcc), austenite (fcc), and martensite (bcc). During the solid-state phase transformation, the microstructure typically changes from δ-ferrite to austenite to martensite. However, the cyclic heating/cooling throughout laser powder bed fusion creates non-equilibrium microstructures for 17-4 PH stainless steel, making the microstructure far more unique than ones created using conventional manufacturing methods [48]. Commercially wrought 17-4 PH stainless steel generally consists of a fully bcc martensitic structure [46, 49]. However, it is common to also have some quantity of retained austenite in the microstructure due to the austenite-stabilizing nickel content [46].

Zai's L-PBF PH martensitic stainless steel review identifies contradictory and inconsistent microstructural findings in the existing literature [48]. Looking specifically at as-built L-PBF 17-4 PH stainless steel, some studies identified that the microstructure contained martensite and some quantity of retained austenite [50-53]. Other literature

reported either a fully δ-ferrite microstructure [54] or a dominantly δ-ferritic one [55]. The highly similar crystal structures of δ-ferrite, ferrite, and martensite contribute to the difficulties in identifying the microstructural components of as-built 17-4 PH stainless steel samples [48]. Additionally, the gas environments used to atomize the powder and manufacture the components impact the microstructure of the as-built material. Table 5 shows that either a bcc-martensite microstructure or fcc-austenite microstructure will be produced depending on if argon or nitrogen gas is used during atomization and fabrication.

Table 5 17-4 PH primary phases based on atomization and fabrication conditions [56].

Powder Type	Argon Gas Fabrication	Nitrogen Gas Fabrication
Argon Atomized (α)	α (bcc-martensite) (Ar/Ar)	α (bcc-martensite) (Ar/N_2)
Nitrogen Atomized (γ)	α (bcc-martensite) (N_2/Ar)	γ (fcc-austenite) (N_2/ N_2)

The thermally cyclic nature of AM creates unique heating, melting, and solidification conditions not typically seen in traditional manufacturing methods. These conditions can create microstructural heterogeneities, anisotropy, and residual stresses (as previously mentioned in Section 2.3.4.1 Thermal Post-Processing), which must be improved using heat treatments [48]. Different heat treatment parameters can considerably impact the amount of retained austenite [51, 53], and a solution treatment can create a finer and more uniform microstructure than as-built material [55]. Figure 12 shows a brief example of the differences in 17-4 PH stainless steel microstructure in the as-built, homogenized, and wrought conditions.

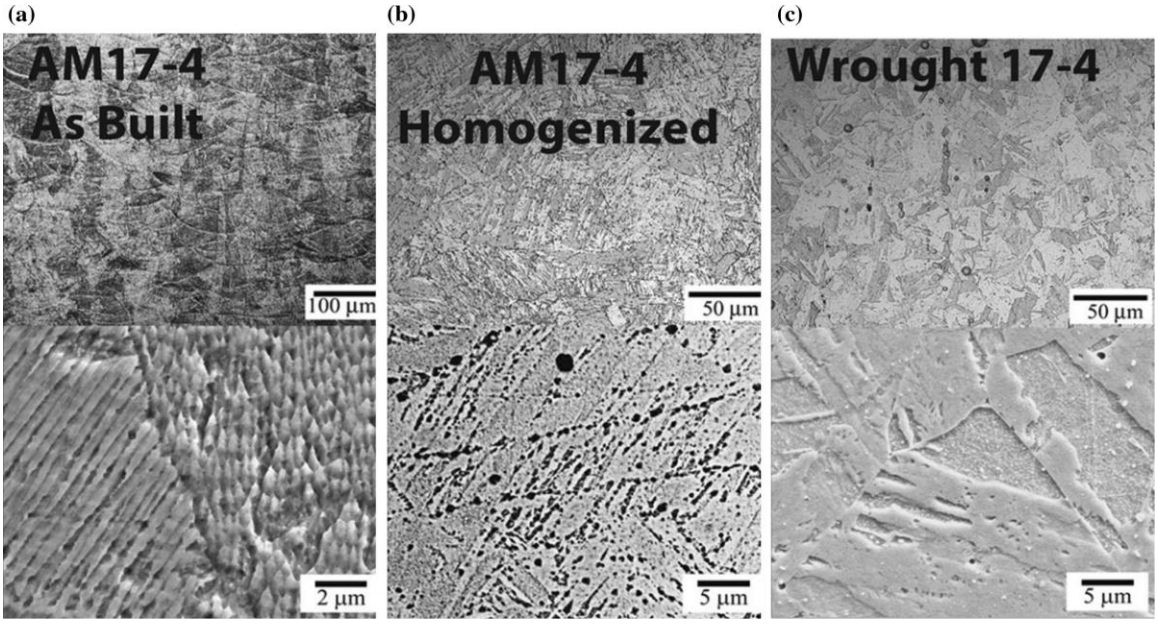

Figure 12 Optical micrographs of 17-4 PH stainless steel: a) as-built, b) after homogenization treatment, and c) wrought microstructures. Micrographs were taken parallel to build direction for the AM images and parallel to the rolling direction for the wrought image [45].

AM creates a new opportunity to control microstructure for specific applications and in turn, influence the mechanical properties as desired [20, 56].

2.5.3. Mechanical Properties

Due to the unique manufacturing process of AM, extensive mechanical characterization is required to implement it as a viable manufacturing option. As mentioned previously, a variety of factors can impact AM material's mechanical behavior, including the type of AM process, processing parameters, post-processing, and microstructure. This section presents an overview of the mechanical properties of AM 17-4 PH stainless steel in literature, with a focus on microstructural and thermal post-processing impacts. Table 6 summarizes these mechanical properties of L-PBF 17- PH stainless steel. The reported results are from ASTM standard size tensile samples, and all

samples were manufactured using either argon- or water-atomized powder as opposed to nitrogen-atomized.

Table 6 Summary of mechanical properties of AM 17-4 PH in literature with different heat treatments.

Machine Type	Condition	Orientation	0.2% Yield Strength (MPa)	UTS (MPa)	Strain to Failure (%)	Ref
EOS M280	As-Built	Vertical	661±24	1255±3	16.2±2.5	[53]
EOS M280	H900[1]	Vertical	945±12	1417±6	15.5±1.3	[53]
EOS M280	H1025	Vertical	870±25	1358±8	13.3±1.5	[53]
EOS M280	H1150	Vertical	1005±15	1319±2	11.1±0.4	[53]
EOS M280	Condition A[2]	Vertical	939±9	1188±6	9.0±1.5	[53]
EOS M280	CA-H900	Vertical	1352±18	1444±2	4.6±0.4	[53]
EOS M280	CA-H1025	Vertical	1121±9	1172±2	9.6±1.7	[53]
EOS M280	CA-H1150	Vertical	859±11	1017±15	16.6±1.2	[53]
ProX 100	As-Built	Vertical	580	940	5.8	[52]
ProX 101	As-Built	Horizontal	650	1060	14.5	[52]
ProX 102	CA-H900	Vertical	1020	1150	2.8	[52]
ProX 103	CA-H900	Horizontal	1250	1410	11	[52]
EOS M290	As-Built	Vertical	861.3±44.7	924.2±65.9	20.1±1.5	[47]
EOS M290	As-Built	Horizontal	860.6±75.7	886.0±70.4	19.9±1.2	[47]
EOS M290	Atmospheric HT[3]	Vertical	1242.6±10.1	1345.5±2.8	12.6±0.9	[47]
EOS M290	Atmospheric HT	Horizontal	1235.5±8.7	1340.0±5.9	13.5±0.9	[47]

[1]H900 (480°C for 1 hr), H1025 (550°C for 4 hr), H1150 (620°C for 4 hr); [2]Condition A (CA) (1040°C for 30 min); [3]Argon Atmospheric HT (CA followed by 460°C for 1 hr)

AM 17-4 PH stainless steel tends to have increased strength and hardness but reduced ductility compared to traditionally manufactured 17-4 PH stainless steel [45, 46]. Studies cite the refined microstructure of AM parts and microstructural precipitates as the cause for increased strength [57]. The percentage of austenite compared to martensite in the microstructure also impacts the mechanical properties since austenite is softer and the precipitation hardening only occurs in martensite [46]. The reduced ductility can be attributed to the porosity inherent in AM [52]. Heat treatments also tend to improve the

strength of AM 17-4 PH stainless steel compared to as-built material, seen in Table 6. Improved strength can also be attributed to the microstructural changes and precipitation hardening effects [48].

3. Materials and Methods

3.1 Materials

The additively manufactured (AM) 17% Chromium – 4% Nickel precipitation hardened (17-4 PH) stainless steel material examined in this work was manufactured by Naval Surface Warfare Center Panama City (NSWC Panama City) and provided to UMBC by Naval Surface Warfare Center Carderock Division (NSWCCD). The material was manufactured from argon atomized powder supplied by EOS using the EOS M290 direct metal laser sintering (DMLS) system under an argon environment. Figure 13 shows the EOS M290 system.

Figure 13 EOS M290 DMLS machine [58].

The system's technical specifications are presented in Figure 14. A goal of this study is to evaluate the repeatability of AM, specifically, the repeatability of a specific EOS M290

DMLS system. As such, all samples were manufactured using the standard processing parameters recommended by EOS. Additionally, all material underwent a thermal post-processing treatment which Section 3.3 will address further.

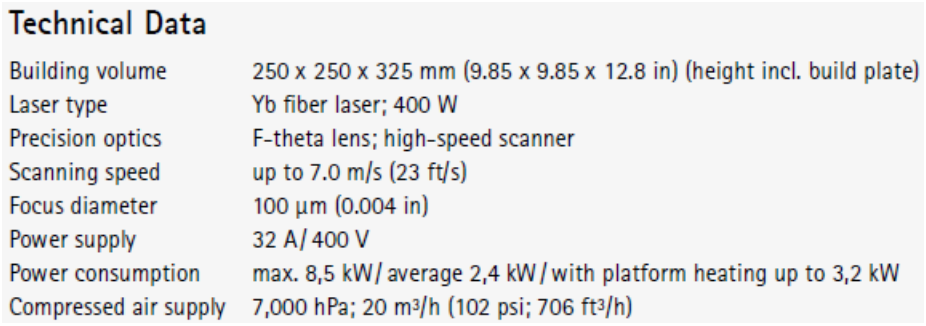

Technical Data

Building volume	250 x 250 x 325 mm (9.85 x 9.85 x 12.8 in) (height incl. build plate)
Laser type	Yb fiber laser; 400 W
Precision optics	F-theta lens; high-speed scanner
Scanning speed	up to 7.0 m/s (23 ft/s)
Focus diameter	100 µm (0.004 in)
Power supply	32 A / 400 V
Power consumption	max. 8,5 kW / average 2,4 kW / with platform heating up to 3,2 kW
Compressed air supply	7,000 hPa; 20 m³/h (102 psi; 706 ft³/h)

Figure 14 EOS M290 technical specifications [58].

The nominal chemical composition of the EOS 17-4 PH stainless steel powder used in this study is presented in Table 7.

Table 7 Nominal chemical composition of EOS 17-4 PH stainless steel powder [47].

Element	Weight Percent (%)
Chromium (Cr)	15.00 - 17.00
Nickel (Ni)	3.00 - 5.00
Copper (Cu)	3.00 - 5.00
Silicon (Si)	≤ 1.00
Manganese (Mn)	≤ 1.00
Carbon (C)	≤ 0.07
Phosphorus (P)	≤ 0.040
Sulfur (S)	≤ 0.030
Niobium (Nb) + Tantalum (Ta)	0.15 - 0.45
Iron (Fe)	balance

Table 8 presents the particle size distribution, the powder density, and the general powder process data of the EOS powder used in this study.

Table 8 EOS 17-4 PH stainless steel powder particle size distribution, powder density, and general powder process data [47].

Particle Size	
D50[4]	36-44 μm
Particles >53 μm[5]	Max 6.0 wt.-%
Particles >63 μm[5]	Max 1.0 w.-%
Powder Density	
Apparent density[6]	Mean 3.83 g/cm^3
Tap density[7]	Mean 4.7 g/cm^3
General process data	
Layer thickness	40 μm
Volume rate	3.32 mm^3/s (11.95 cm^3/h)

[4]According to ASTM B822; [5]According to ASTM B214; [6]According to ASTM B212, ASTM B329 & ASTM B417; [7]According to ASTM B527.

During build manufacturing at NSWC Panama City, all powder was obtained from the same feedstock lot. Initial manufacturing intended to use only "virgin powder," i.e., powder not previously used during an AM operation; however, this supply was limited throughout production. As such, recycled powder, i.e., loose powder from a previous AM operation, supplemented the virgin powder supply. The details of the first use of recycled feedstock were not tracked as is typical in large-scale manufacturing operations. This lack of record keeping will likely occur as AM production scales to a size similar to traditional manufacturing operations. The combined usage of virgin and recycled powders is indicative of an authentic manufacturing environment and demonstrates the resultant repeatability likely seen in a production environment.

3.2 Overview of Build Layout

NSWCCD and UMBC collaborated to develop a build layout with various structures intended to influence both the thermal history and build procedure based on the geometric features and the build height. The various structures were designed to ensure

that each build layer has the same area overall, thus requiring the same manufacturing time. Figure 15 shows the layout of the six builds provided by NSWC Panama City for this study.

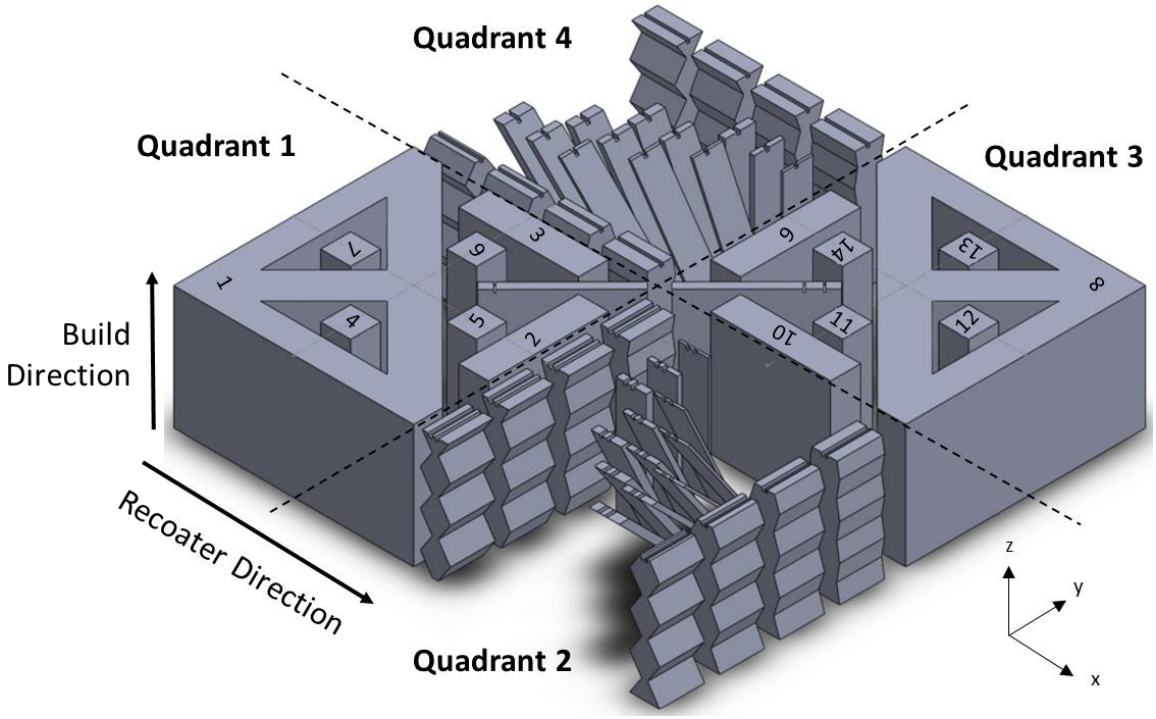

Figure 15 Build plate layout.

The builds were designed with two different quadrant layouts, each repeated twice in a different orientation with respect to the powder recoated direction. Quadrants 2 and 4 supplied zig zag and angled thin fin structures, both with different thicknesses and build angles. Figure 16 indicates the locations of these structures on the build.

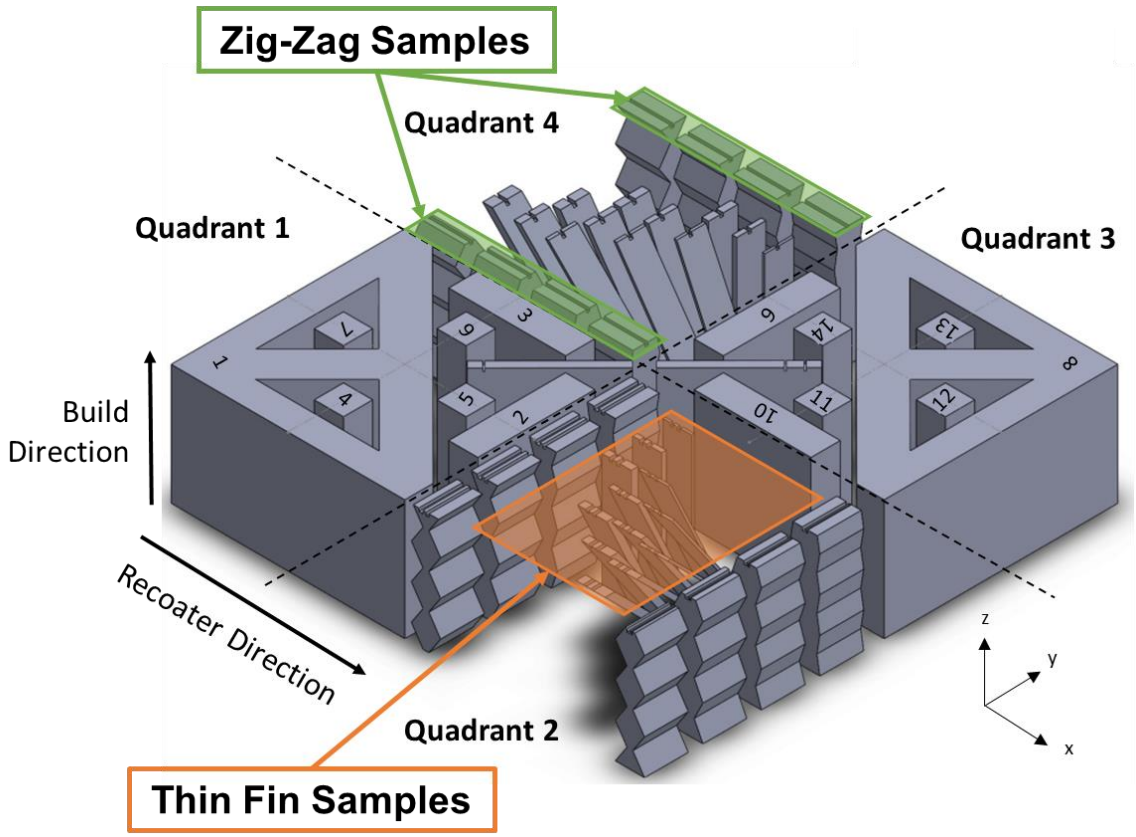

Figure 16 Highlighted sections of zig zag and thin fin structures.

The eight zig zag structures had one of two base types (narrow or wide) with one of four width reductions (20%, 40%, 60%, 80%), and the twelve thin fin structures had one of three thicknesses (1mm, 2mm, 3mm) and were built at one of four build angles (90°, 65°, 55°, 45°). Previous work studied these quadrant 2 structures, evaluating hardness, surface roughness, and microstructure in as-built material [31] and heat treated material [59, 60]. Quadrants 1 and 3 provided bulk specimens to cut out microscale, mesoscale, and macroscale (ASTM E8 round bar) tension samples, henceforth called round bar samples. Each build was broken down into different coupons, numerically labeled in Figure 15. Coupons 1-5 were used for the tension samples in this study, highlighted in Figure 17.

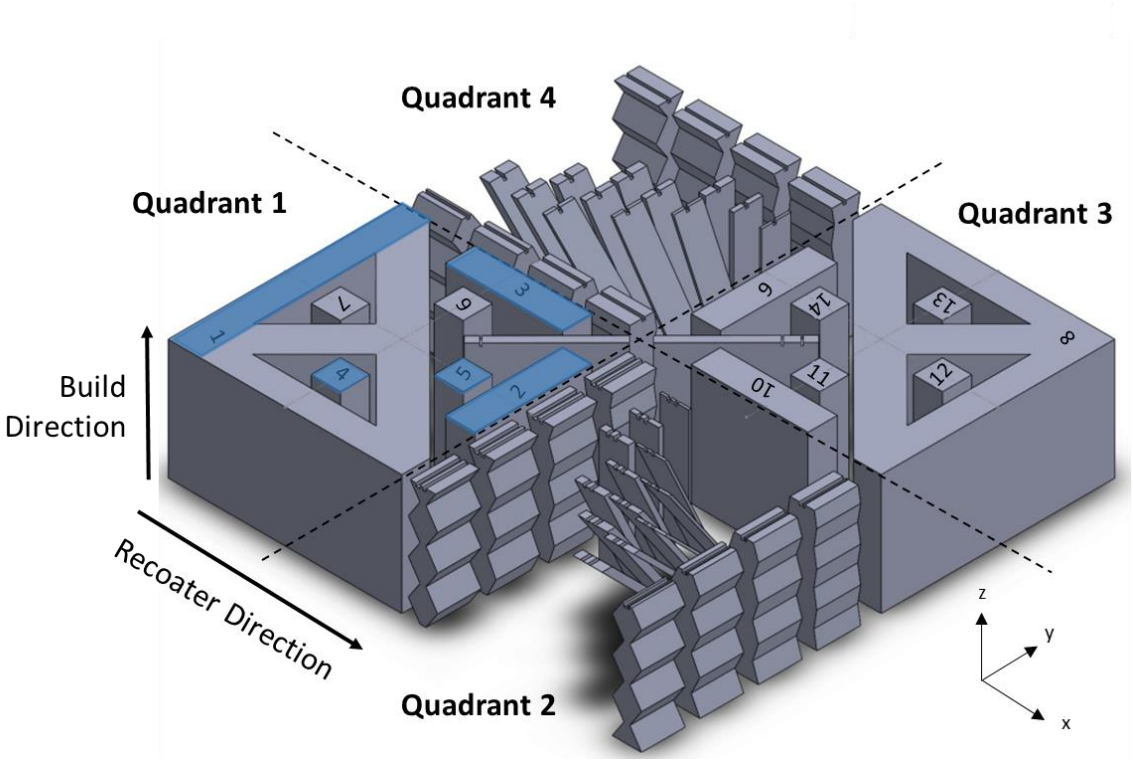

Figure 17 Highlighted sections of bulk material where tension samples were extracted.

From the highlighted blocks, coupons 2 and 3 were used to extract all three types of tension samples: microsamples, mesosamples, and round bar samples. Figure 18 shows the locations where the tension samples were extracted.

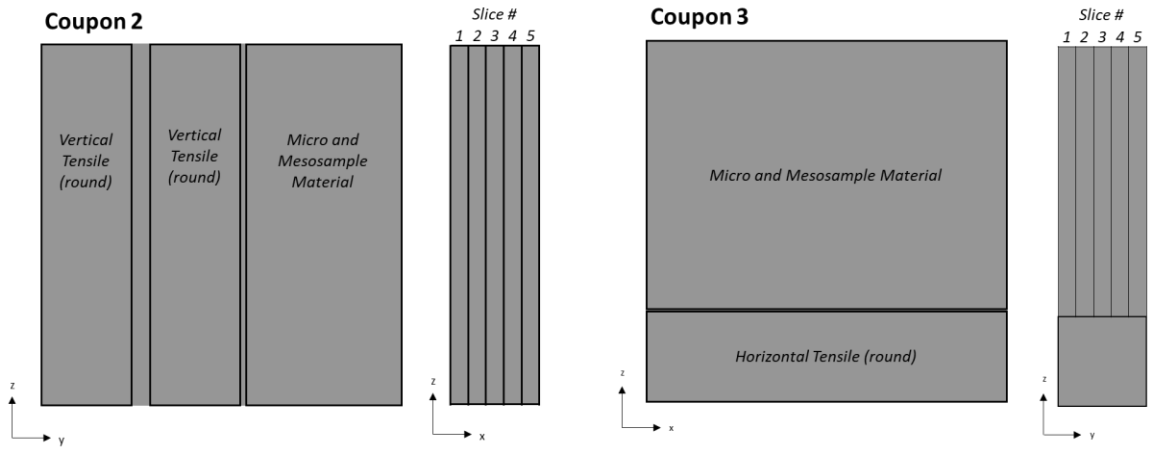

Figure 18 Location of tension samples cut from coupons 2 and 3. Includes all microsamples, mesosamples, and a portion of the ASTM E8 round bar samples. Indicates the slices in the micro and mesosample region used to increase the total number of mesosamples for testing.

All samples were cut using wire electrical discharge machining (EDM). They were then freed using the South Bay Technology Low Speed Diamond Wheel Saw Model 650 seen in Figure 19.

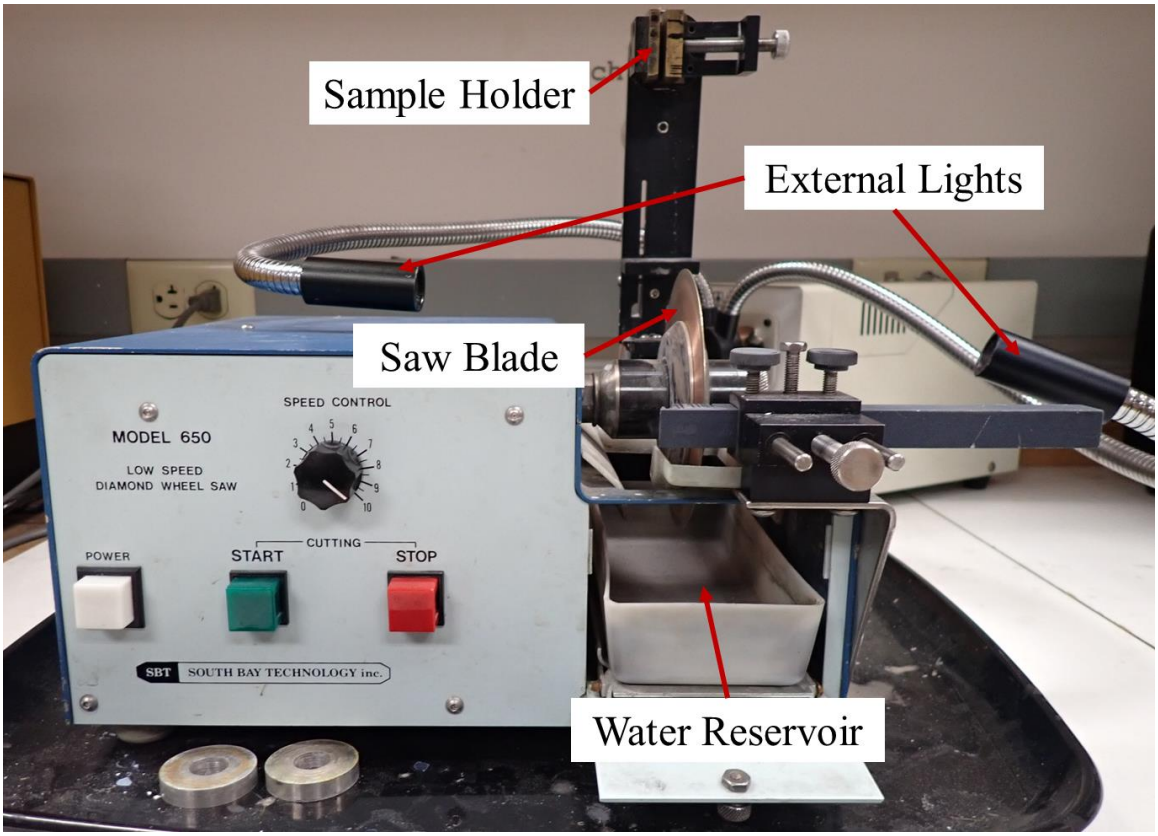

Figure 19 Low speed diamond wheel saw used to free micro- and mesosamples after they were cut using the wire EDM.

The area designated for the micro- and mesosamples was sectioned into five thinner slices to cut more mesosamples for testing. The positioning of the micro- and mesosamples within coupons 2 and 3 can be seen in Figure 20.

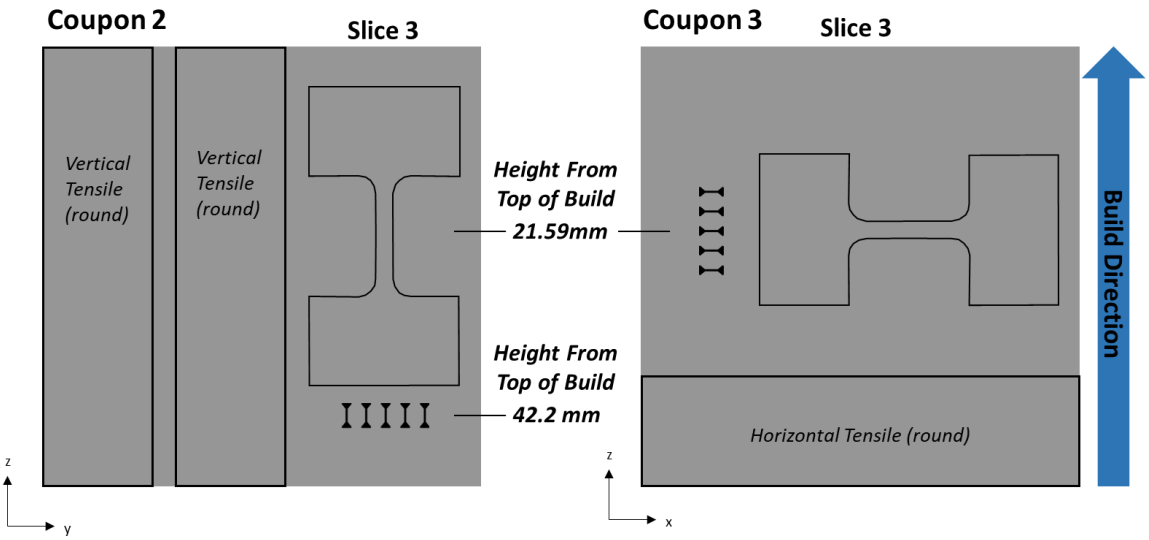

Figure 20 Location of micro and mesosamples within coupons 2 and 3. Indicates the height from the top of the build where the samples were positioned.

Coupon 2 was designed to create samples oriented vertically, i.e., samples with gauge sections parallel to the build direction, and coupon 3 was designed for horizontal samples, i.e., samples with gauge sections perpendicular to the build direction. The positioning of the mesosamples was designed to align the center of their gauge sections. In coupons 2 and 3, a single mesosample was cut from slices 2-4 for a total of three mesosamples, and a row of five microsamples was cut from slice 3. Additional round bar tension samples were extracted from coupon 1, specifically from section A of coupon 1, indicated in Figure 21.

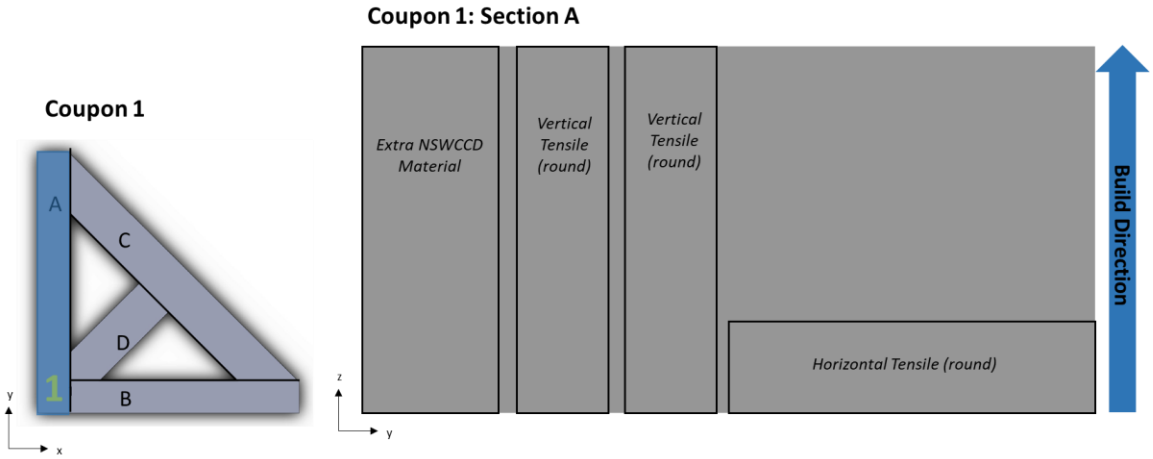

Figure 21 ASTM E8 round bar tension sample cut from section A (indicated in the image on the right) of coupon 1.

The final round bar samples were machined from coupons 4 and 5, shown in Figure 22. An external commercial vendor collaborated with NSWCCD to provide the data from the six vertical and two horizontal round bar samples for each build that was tested.

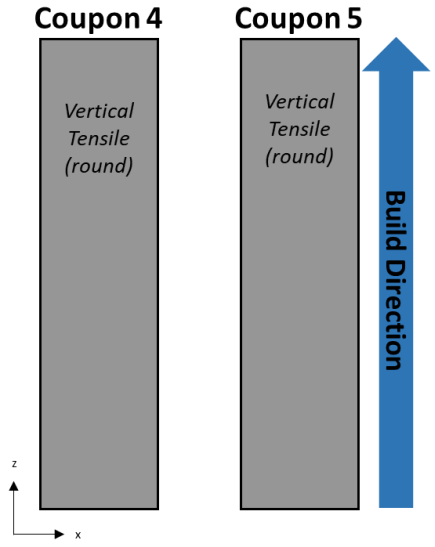

Figure 22 ASTM E8 round bar tension sample machined from coupons 4 and 5.

The sample naming convention in this study is designated by the build number corresponding to material from NSWC Panama City. An example is PC2 which corresponds to build 2 from NSWC Panama City.

3.3 Heat Treatment

All material in this study was heat treated using a three-stage process designed for PH stainless steels and adapted from a standard H1025 heat treatment. Heat treatments were performed using a Thermofisher Lindberg/MPH Blue M model 51663-R Box Furnace, rated to 1500°C. A Thermofisher Lindberg/MPH Model 59166-H High Temperature Alloy Retort insert was included in the furnace for the last two stages of the heat treatment. Figure 23 shows the furnace and retort. Temperature data was recorded during the heat treatment using a K-type thermocouple welded directly to the material and another K-type thermocouple inside the furnace, suspended over the build, to record the air temperature. All temperature data was collected and processed using Picolog 6 software.

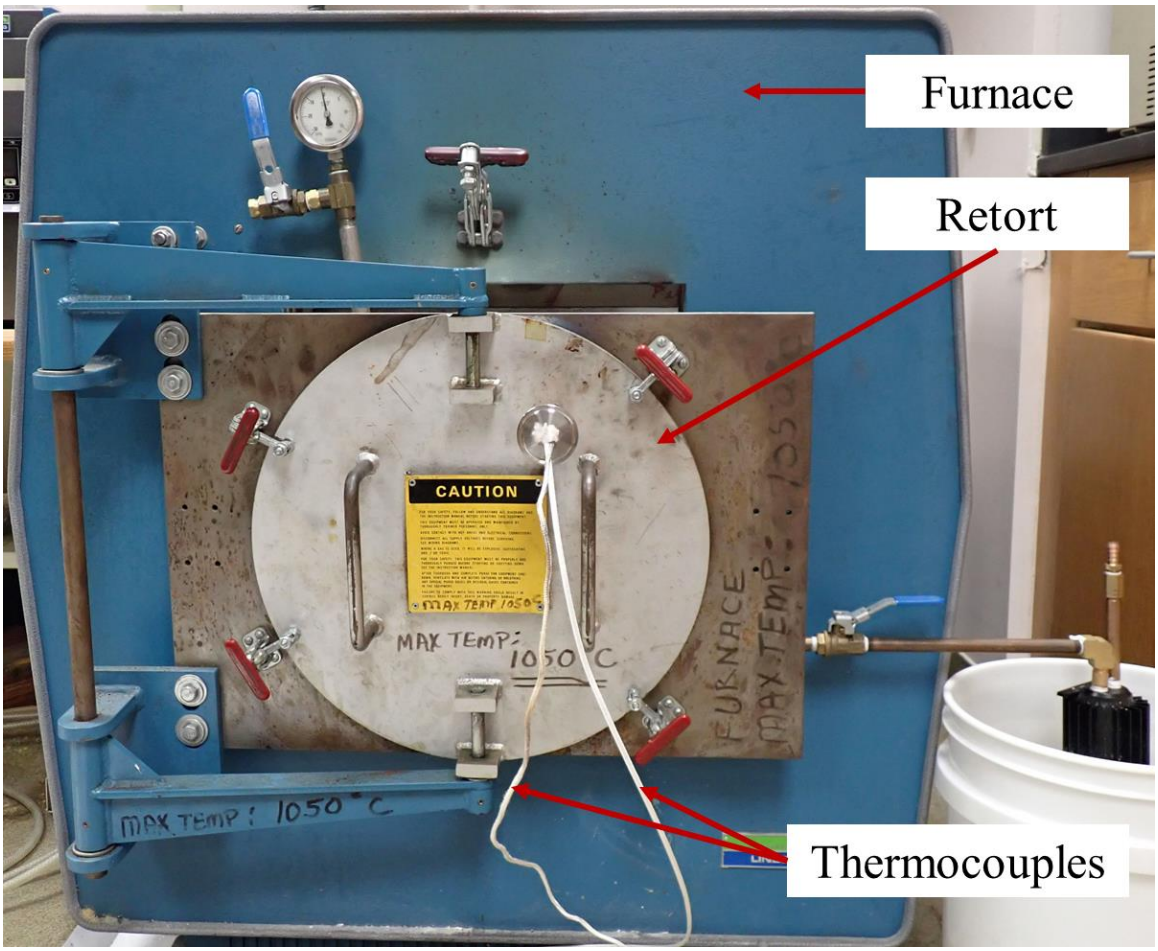

Figure 23 Thermofisher Lindberg/MPH furnace, retort, and thermocouples used during heat treatments.

The three-step heat treatment included a stress relief, solution treatment, and aging for all material. Each build was stress relived in its entirety at 650°C for one hour under an atmospheric environment, followed by an overnight furnace cooling. After the stress relief, the material was cut off the build plate for the subsequent heat treatments. The material for the micro- and mesosamples was heat treated together, and the material for the round bar samples was heat treated separately from the other material. Figure 24 shows an example of a batch of material that was heat treated together during the solution

treatment and aging processes. This batch included thin fins from two different builds and coupons 2 and 3 from PC2 resting on top of a refractory brick designated for furnace use.

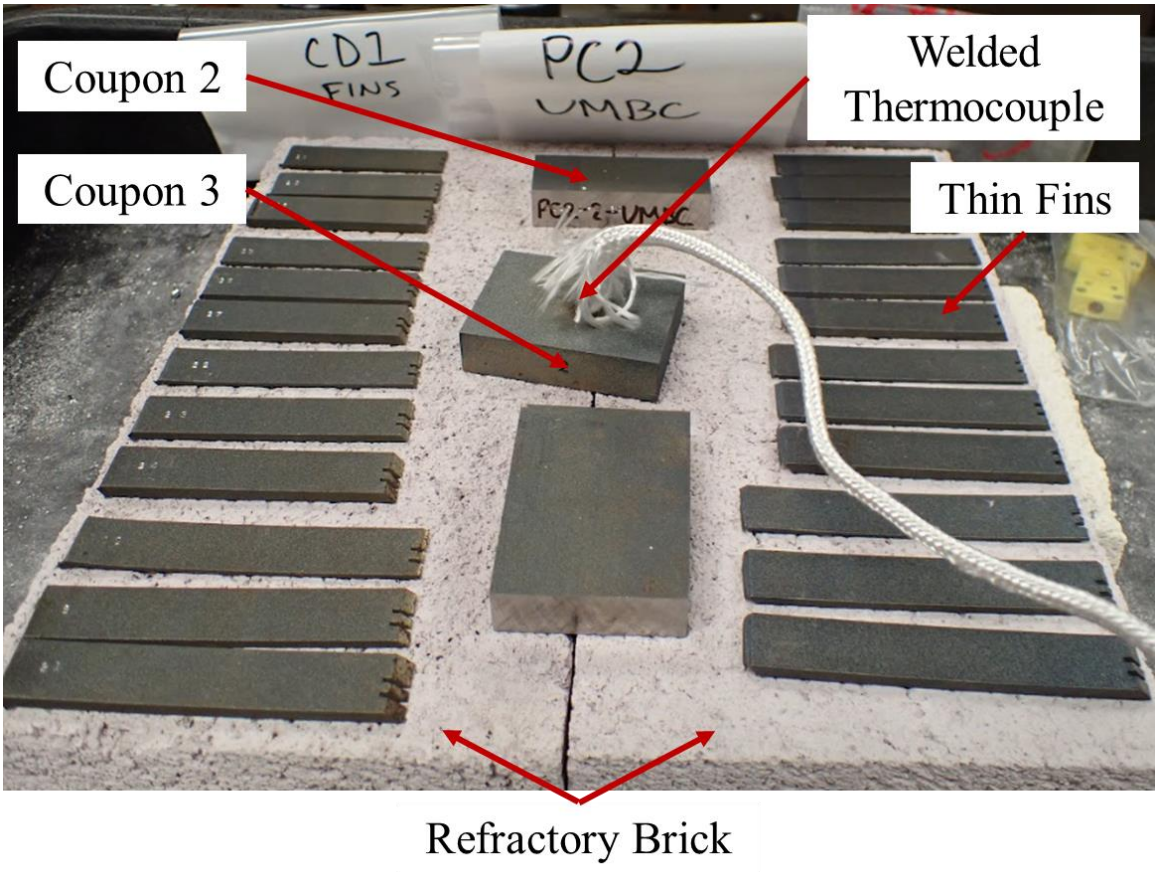

Figure 24 Example heat treatment of thin fins and coupons 2 and 3 for micro- and mesosamples.

Following the stress relief, the solution treatment for all samples occurred for one hour at 1050°C under an argon gas environment, followed by an overnight furnace cooling under argon gas. The aging process occurred at 550°C for one hour-under argon with a subsequent overnight furnace cooling under argon. Figure 25 shows an example time-temperature diagram of the entire heat treatment process.

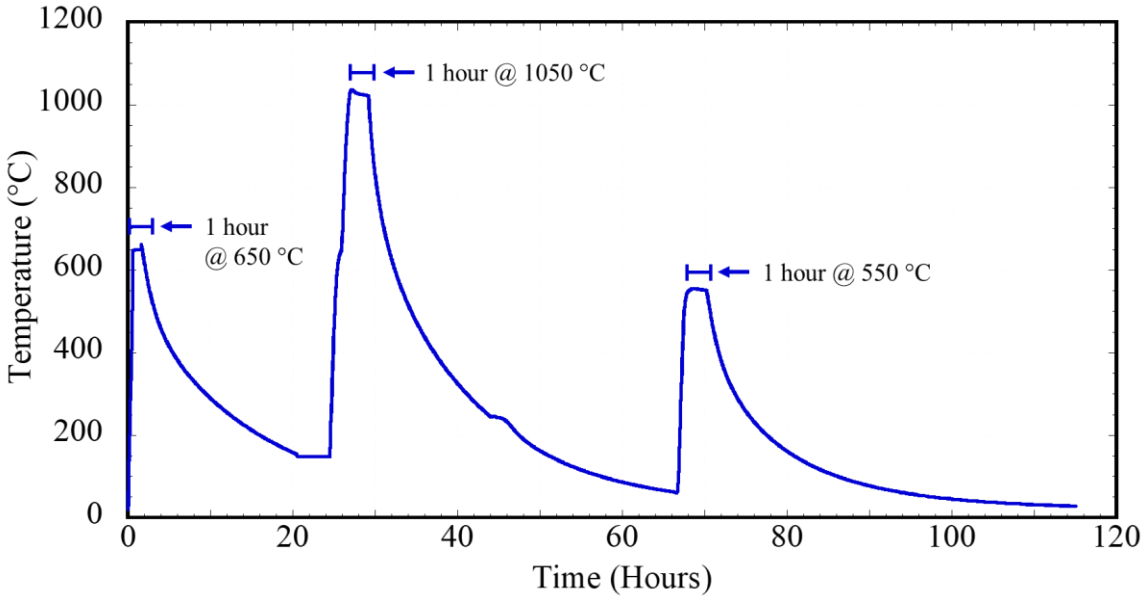

Figure 25 Example time-temperature diagram of the heat treatment process in order of stress relief, solution treatment, and aging [59].

3.4 Microsample Tensile Testing Technique

Multi-scale mechanical characterization provides further insight into the mechanical behavior of a material since some behaviors might only be apparent in a specific length scale. Standard size tensile testing is considered at the macroscale, which can include multiple microstructures in one sample, thus creating a bulk average of the mechanical behavior. Microscale tensile testing provides the opportunity to develop a localized understanding of the mechanical behavior of a material. Additionally, this form of testing requires very little material, making it an ideal technique for testing when the amount of material is limited. Microsample tensile testing has successfully characterized thin films [61, 62] and metal alloys [63-68].

3.4.1. Microsample Preparation

The microsamples used in the microtensile testing were cut to 1mm thick from the bulk material using wire electrical discharge machining (EDM), seen in Figure 26.

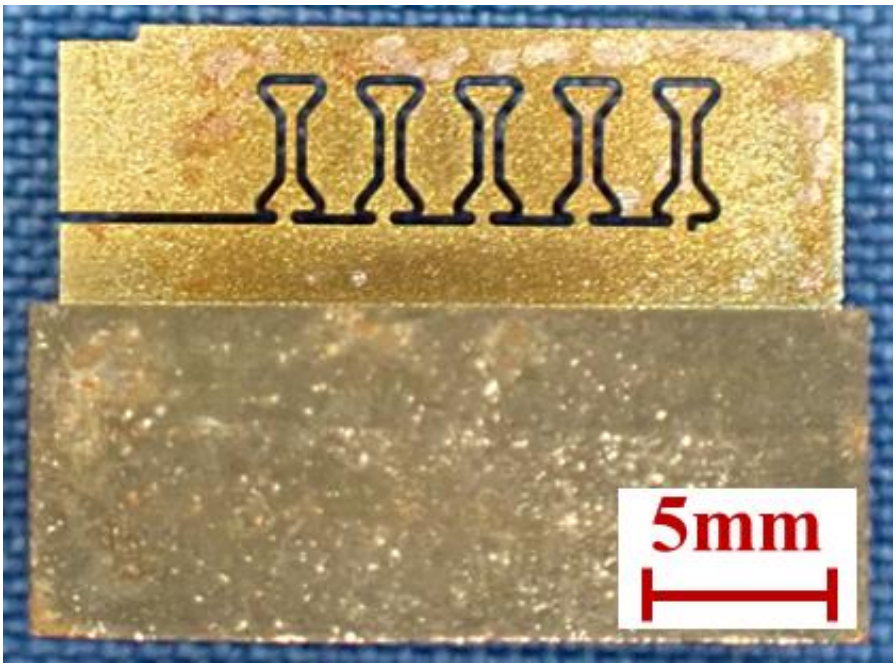

Figure 26 Vertical microsamples after they were cut using wire EDM, but before they were freed.

The microsample geometry used in this study was adapted from ASTM standard tensile specimen geometry and can be seen in Figure 27.

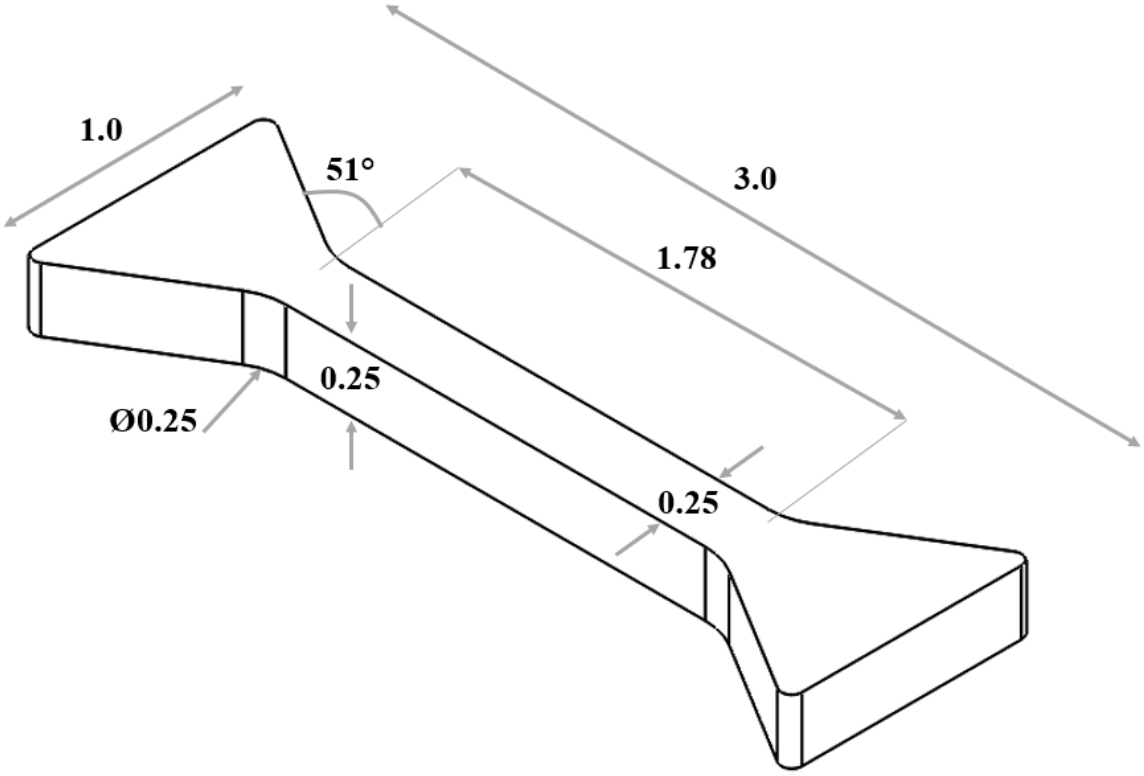

Figure 27 Microsample geometry (units in mm) [64].

After the samples were cut using wire EDM, they were freed from the bulk material using the low speed diamond wheel saw seen in Figure 28.

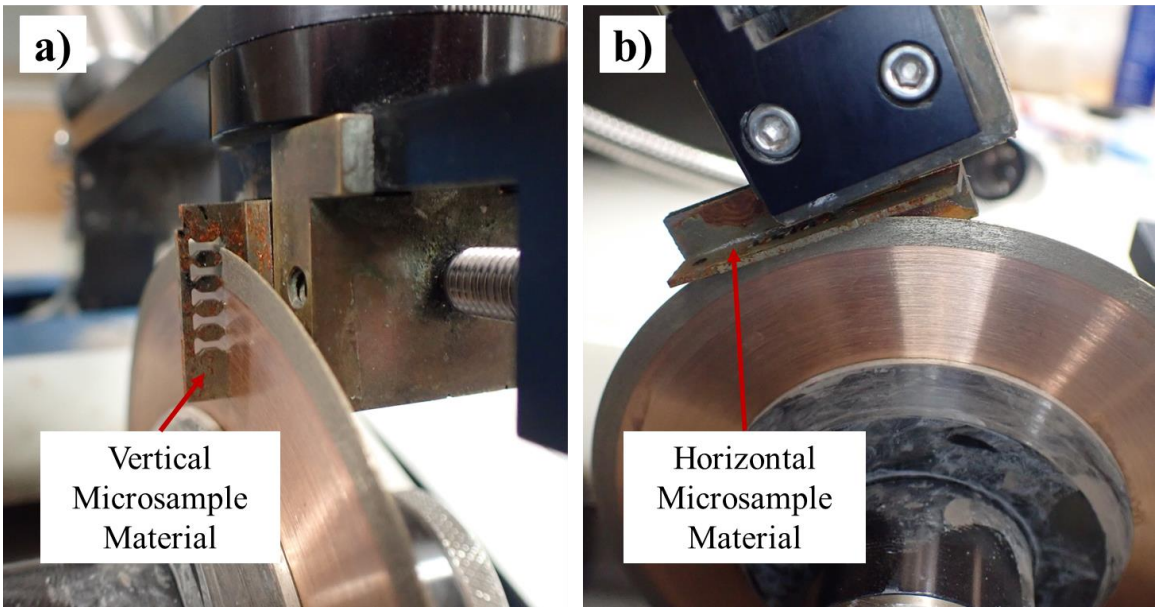

Figure 28 Microsamples were freed from bulk material after wire EDM using the low speed diamond wheel saw. a) Vertical microsample freeing technique and b) horizontal microsample freeing technique.

After the microsamples were cut and freed, they were mounted on borosilicate glass discs using clear Crystalbond 509. Five samples were evenly spaced across the glass discs for polishing, shown in Figure 29.

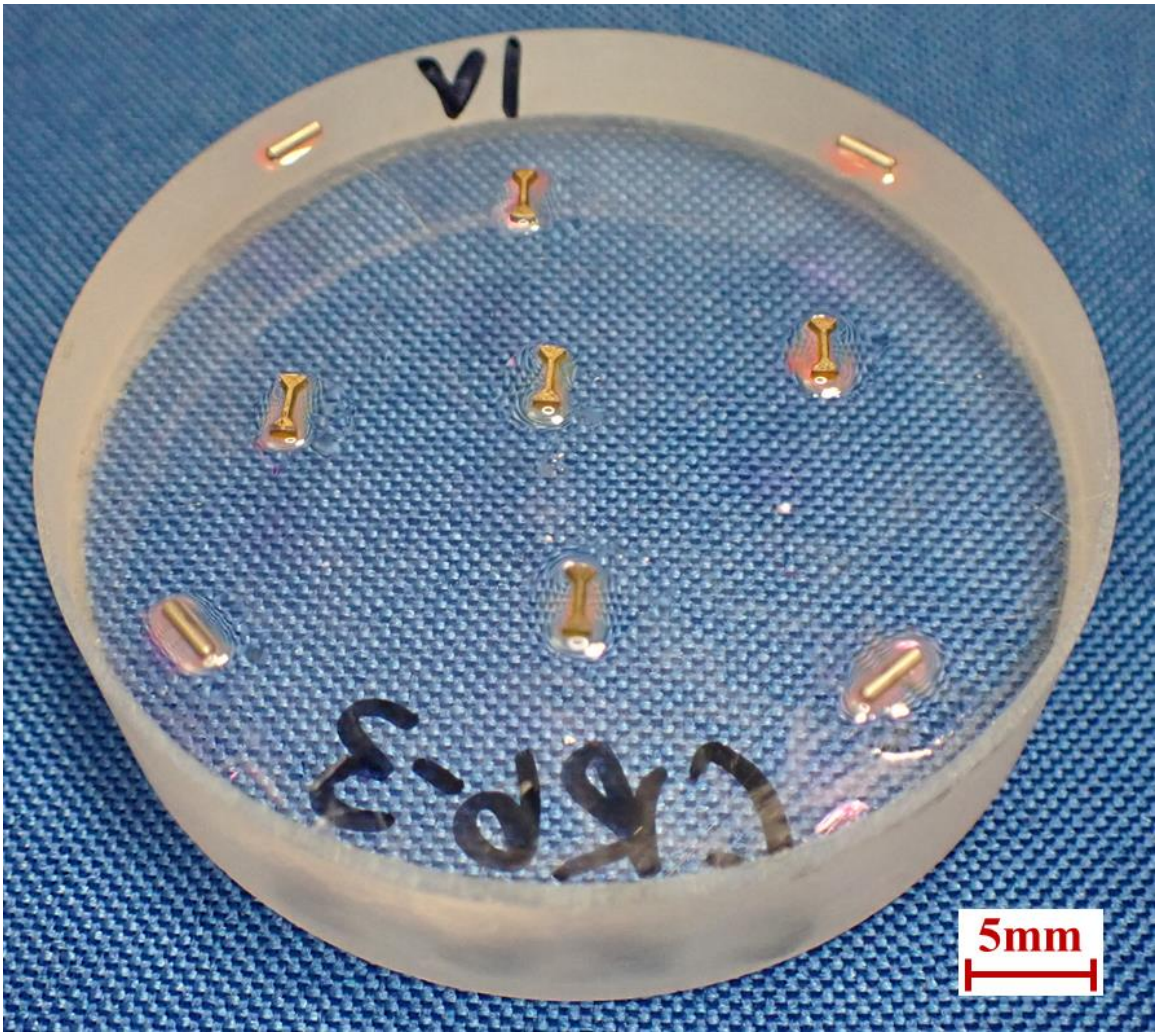

Figure 29 Five microsamples mounted on glass disc for polishing. Four cylindrical stainless steel pins were mounted on the outside of the disc to measure sample thickness throughout polishing.

Samples were polished to a thickness of nominally 250μm using first SiC papers of 180, 320, 600, 800, and 1200 grit, then followed by a final polish using 0.05μm colloidal silica suspension on a synthetic velvet cloth. Following polishing, the width and thickness of all microsamples were measured under a metallurgical microscope.

3.4.2. Microsample Tensile Testing System

The system used for microtensile testing in this study was developed by Dr. Salahudin Nimer as part of his doctoral work [64]. Figure 30 shows the microsample tensile testing system equipped for elevated temperature testing. This system uses an actuator, LTA-HL from Newport, with a minimal incremental motion of 0.05μm and a maximum stroke of 25mm. The actuator can produce a quasi-static strain rate and a maximum strain rate of $1s^{-1}$. This study tested samples at a quasi-static strain rate of $1x10^{-4}s^{-1}$ until total separation. The actuator has a maximum axial load capacity of 120N in the push direction and 100N in the pull direction, and the microsample tensile testing uses it in the pull direction. The in-line load cell used in this system, MLP-25 from Transducer Techniques, has a maximum of 111N. Its output is 2mV/V, and it is set up to operate on a 10V scale instead, creating a resolution of 0.0022N. The system is a horizontal load frame, so an air bearing is placed between the in-line load cell and a single side of the sample grips to reduce frictional loading during testing. The microsample tensile testing system was originally designed to test at elevated temperatures ranging from 21 to 600°C. The system includes a tubular heater, LTA750-01 from Micropyretics Heaters International, to operate at elevated temperatures [63], however all testing in this study was conducted at room temperature.

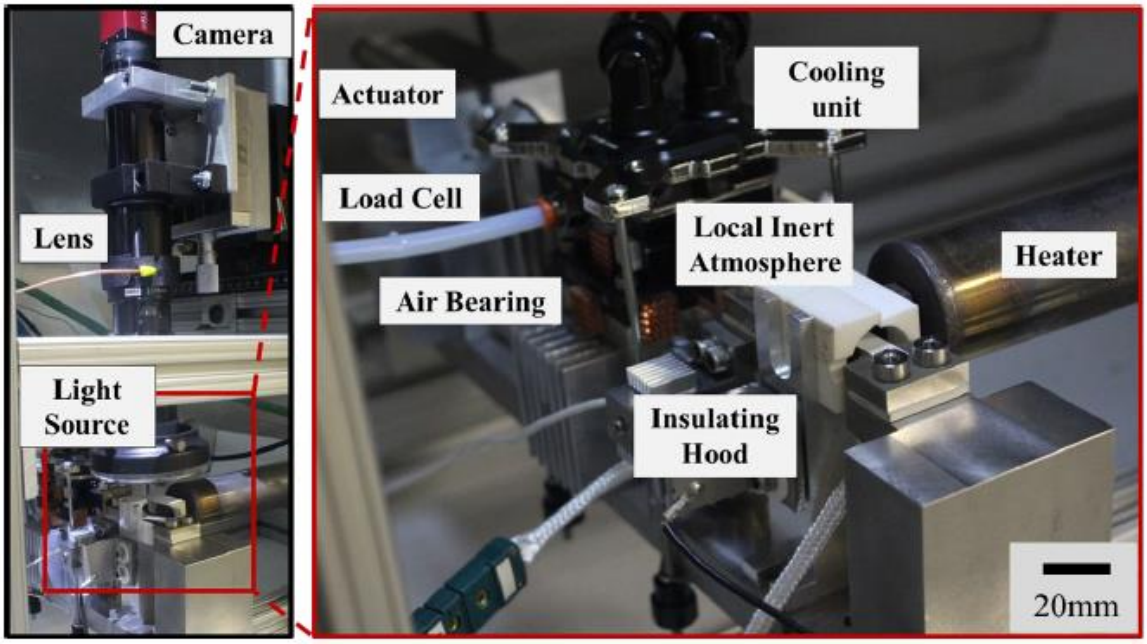

Figure 30 Microsample tensile testing system at UMBC equipped for elevated temperature testing [64].

3.4.3. Digital Image Correlation (DIC)

The microsample tensile testing system uses digital image correlation (DIC) to record strain measurements. Prior to testing, samples were coated with a speckle pattern using white and black paint. The white paint was applied first to create a solid base coat, followed by the black paint diluted with acetone in a 20g:24g ratio. An airbrush was used to apply the black paint in a speckle pattern along the gauge section, seen in Figure 31. Each sample was visually inspected using an Olympus BX51 metallurgical microscope to ensure even distribution of the black speckles across the white paint.

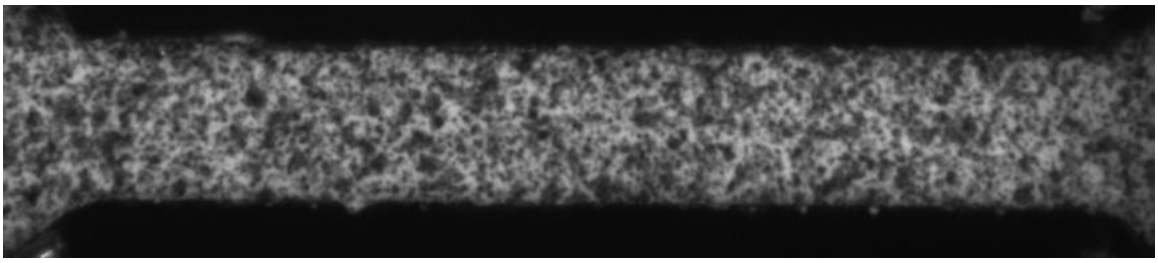

Figure 31 Microsample gauge section with white background and black speckle pattern.

During testing, a PixeLINK ½.3" CMOS 15 MP USB 3.0 camera was used to record images at two frames per second. The load and displacement were recorded simultaneously using LabView, so each load value corresponds to an image. The DIC software VIC-2D by Correlated Solutions was used to obtain full-field strain data from the recorded images. A digital line extensometer was placed across the gauge section, and its displacement and deformation were tracked to obtain the strain data.

3.5 Mesosample Tensile Testing Technique

Mesoscale samples fall on a length scale between the standard size tensile samples traditionally used and the microscale samples used in this study. They were designed to understand the mechanical behavior of the material in a more localized manner than the macroscale samples but more broadly than the microsamples. The mesoscale method of characterization has proven successful previously when evaluating bulk stainless steel [31, 69].

3.5.1. Mesosample Preparation

The mesosamples were prepared similarly to the microsamples. All mesosamples were cut from the bulk material using wire EDM. Figure 32 shows the mesosample

geometry used in this study. The dimensions were adapted from ASTM standard size tensile specimens.

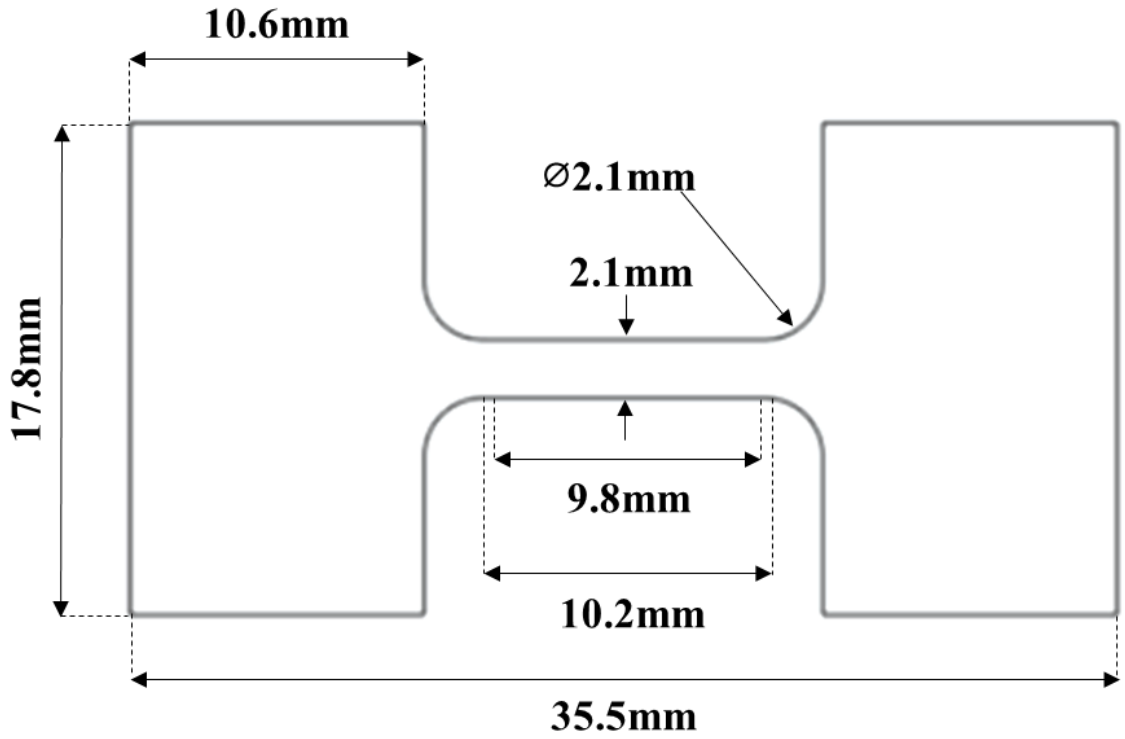

Figure 32 Mesosample geometry (units in mm) [31].

Once the mesosamples were cut and freed, they were polished to a thickness of nominally 2mm using the Buehler ECOMET 6/AUTOMET 3 Dual Grinder/Polisher, seen in Figure 33.

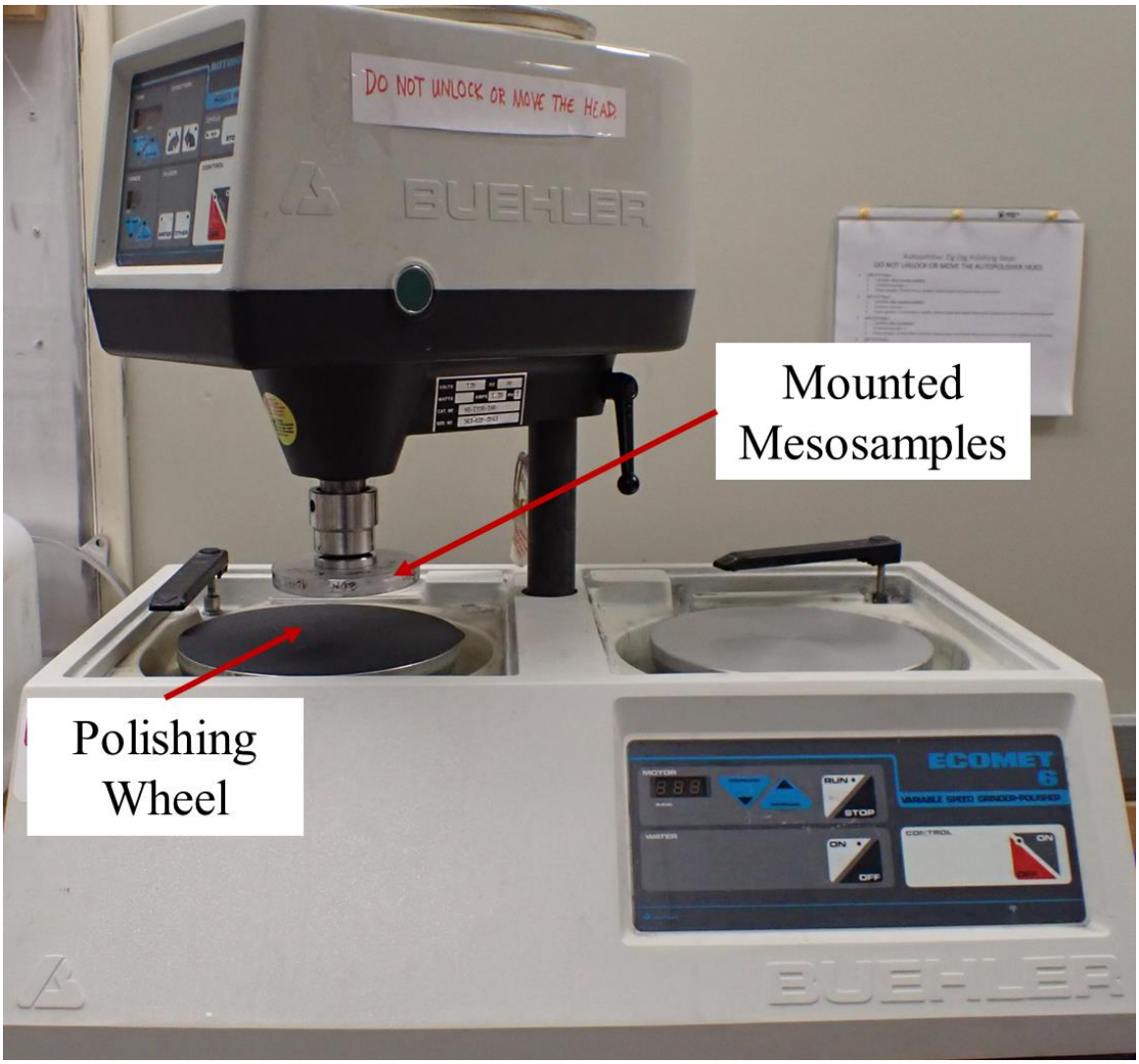

Figure 33 Buehler ECOMET 6/AUTOMET 3 Dual Grinder/Polisher used to polish the mesosamples.

Samples were mounted on an aluminum disc that mounted to the autopolisher head. Three samples were evenly mounted on the aluminum disc using clear Crystalbond 509 for polishing, shown in Figure 34.

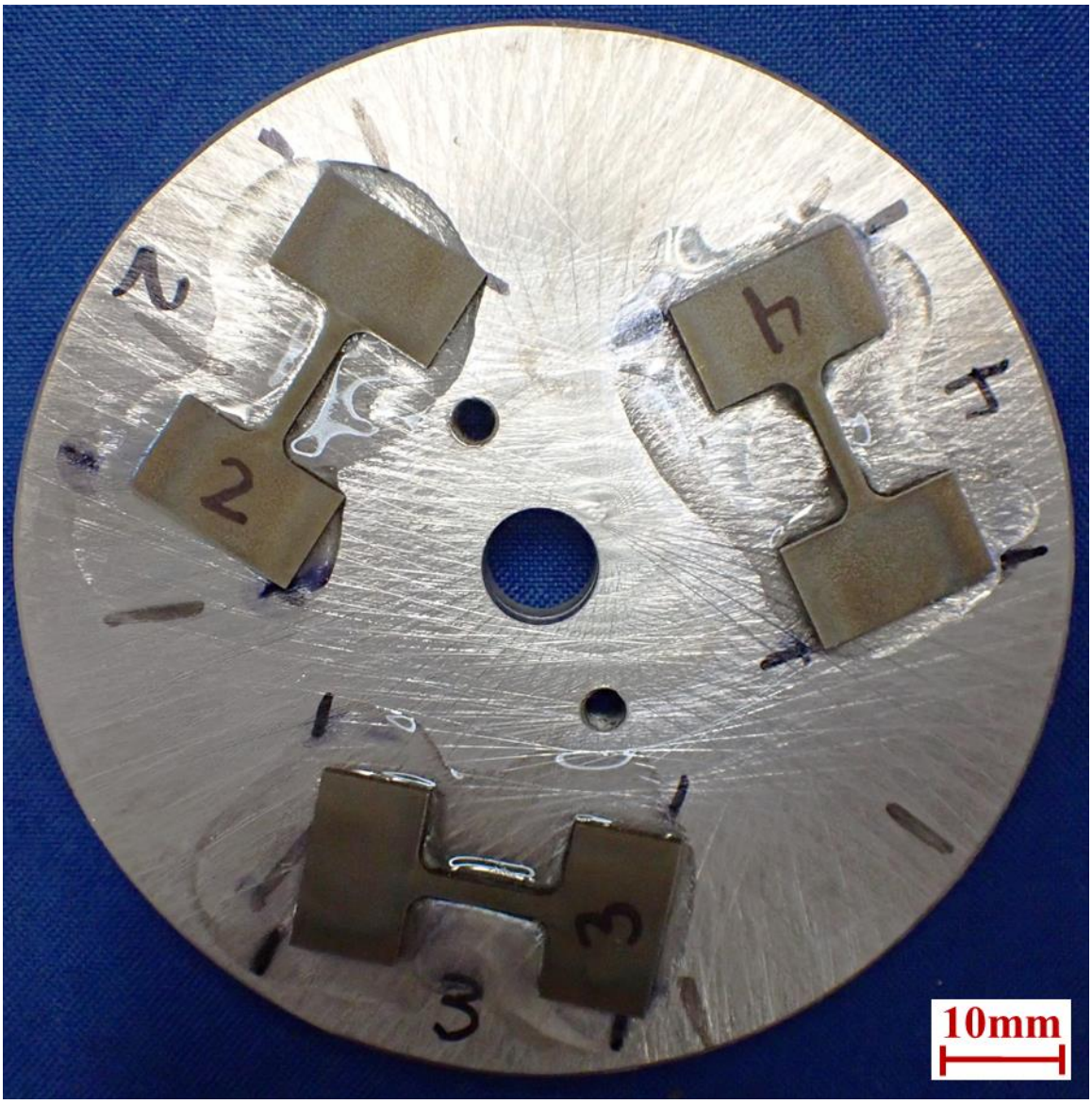

Figure 34 Three mesosamples mounted on aluminum disc for polishing.

The same polishing protocol for the microsamples was used for the mesosamples: 180, 320, 600, 800, and 1200 SiC grit paper, followed by a 0.05μm colloidal silica suspension. Following polishing, the width and thickness of all mesosamples were measured using digital calipers. Reflective tape was applied to the gauge section to indicate the 9.8mm gauge length during testing.

3.5.2. Mesosample Tensile Testing System

The mesosample tensile testing was performed using an Instron 3369 Dual Column Tabletop Testing System with a non-contact laser extensometer, seen in Figure 35.

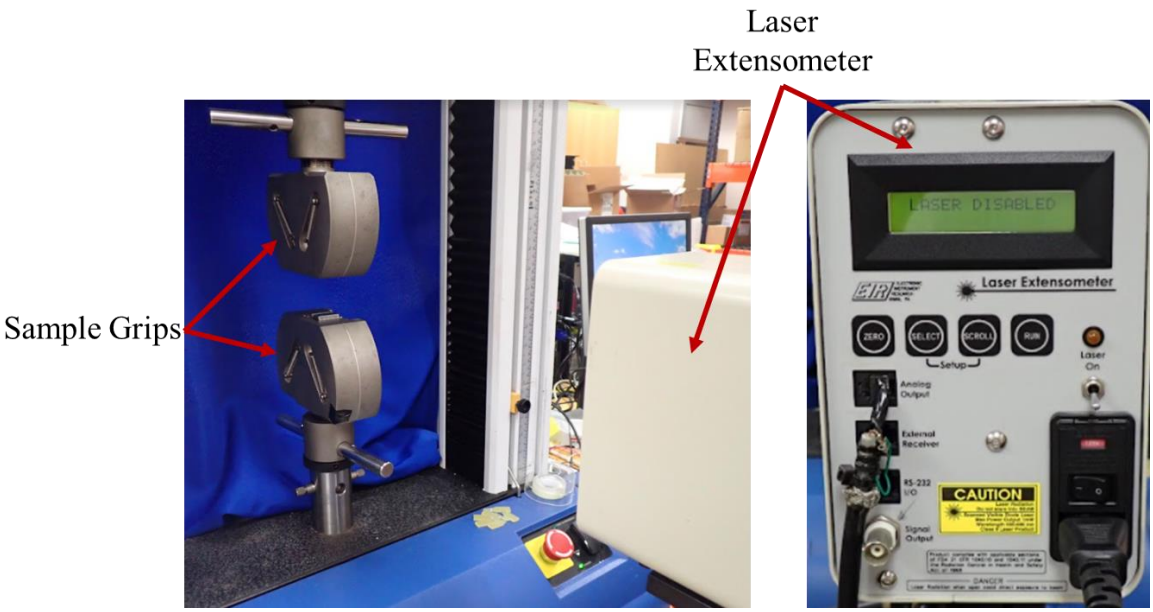

Figure 35 Mesosample tensile testing system at UMBC using an Instron 3369 Dual Column Tabletop Testing System with a non-contact laser extensometer.

The laser extensometer recorded the change in position of the reflective tape on the mesosample during testing, and the applied load was recorded until fracture. Figure 36 shows a sample mounted in the system.

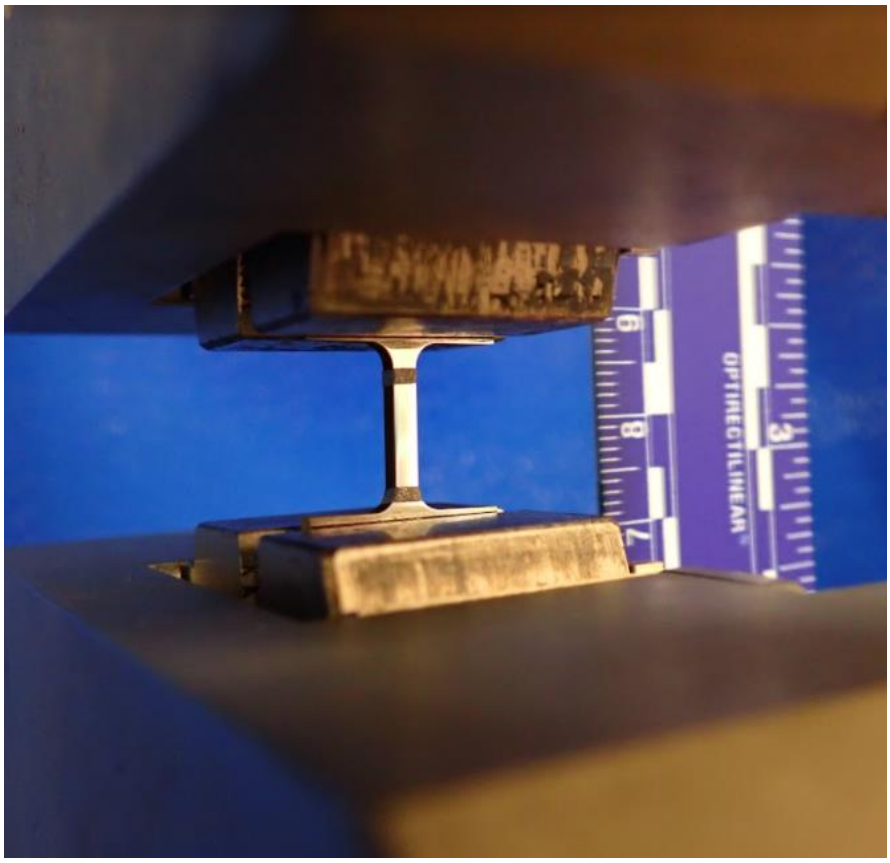

Figure 36 Mesosample inserted into Instron grips during testing.

3.6 Round Bar Tensile Testing Technique

Tensile testing traditionally uses macroscale tensile specimens to conduct tensile testing, and many standards exist for these geometries. This testing will show the average mechanical behavior of the material rather than the more localized behavior seen from the micro- and mesoscale samples. NSWCCD collaborated with an external team to run the macroscale tensile testing, following ASTM E8 13a, Specimen #4 sample dimensions seen in Figure 37. Based on this geometry, these samples will be referred to as round bar tensile samples.

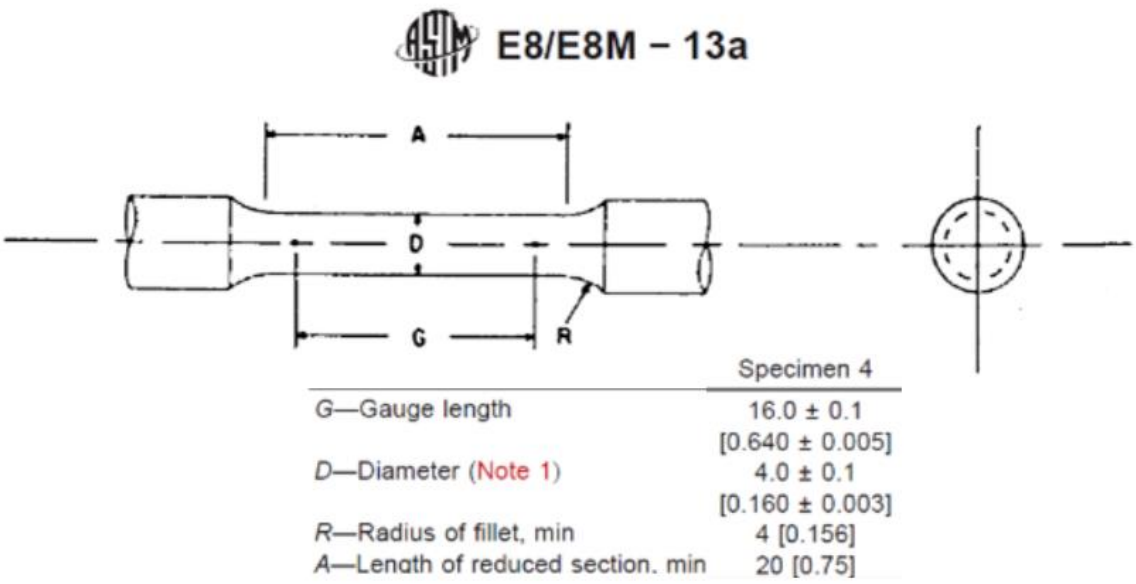

Figure 37 ASTM E8 round bar tensile sample dimensions (units in mm) [70].

3.7 Mechanical Property Measurements

An engineering stress-strain curve was created from each micro- and mesosample tested to obtain mechanical properties essential to characterizing the material's behavior. A typical stress-strain curve can be seen in Figure 38 with the relevant mechanical properties indicated. The Young's modulus, E, is determined by finding the slope of the linear elastic region of the engineering stress-strain curve. The yield strength, YS, corresponds to the stress value found using the 0.2% offset method, seen more clearly in Figure 38b. The ultimate tensile strength, UTS, is identified as the maximum stress value obtained during testing. The strain to failure, ε_f, corresponds to the maximum strain value obtained prior to sample separation.

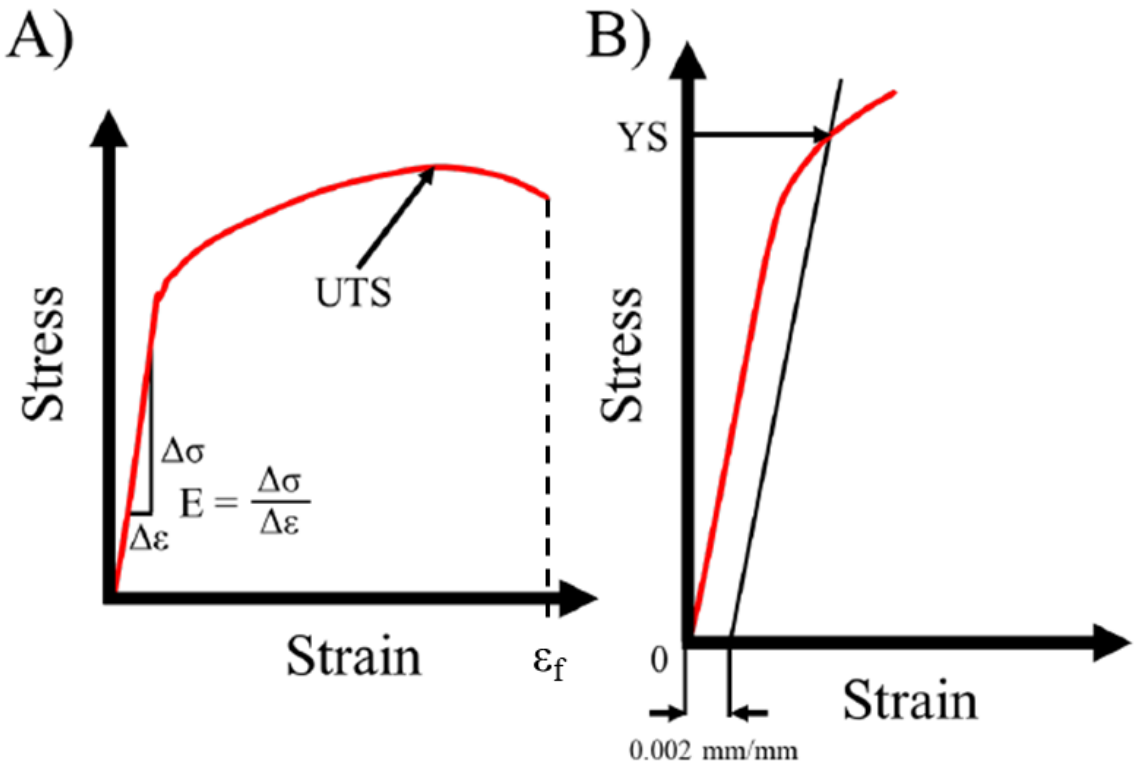

Figure 38 a) Typical engineering stress-strain curve with Young's modulus (E), ultimate tensile strength (UTS), and strain to failure (ε_f). b) Closer view of linear elastic region showing how 0.2% yield strength (YS) is determined [63].

4. Results and Discussion

The relevant results from the multiscale tension testing will be presented in this section for the AM 17-4 PH stainless steel material. 60 microsamples were tested from six different builds in two different orientations (5 samples per build per direction). 36 mesosamples were tested from the same six builds in two different orientations (3 samples per build per direction). 48 round bar samples underwent tensile testing from the same six builds in two different orientations (6 samples per build in the vertical direction and 2 samples per build in the horizontal direction). The evaluated mechanical properties include 0.2% offset yield strength (YS), ultimate tensile strength (UTS), and strain to failure (ε_f). Stress-strain curves will be presented for the micro- and mesosamples.

A summary of the experimentally determined mechanical properties for AM 17-4 PH stainless steel microsamples in the vertical direction can be seen in Table 9. Figure 39 shows the representative engineering stress-strain curves for the vertical microsample material from each build. The summary of the experimentally determined mechanical properties for the mesosamples in the vertical direction can be seen in Table 10, with the representative engineering stress-strain curves shown in Figure 40. Table 11 shows the summary of the experimentally determined mechanical properties for the vertically oriented round bar samples. No stress-strain curves were provided by NSWCCD for the round bar samples at this time. Additional mechanical properties for the microsamples, mesosamples, and round bar samples can be found in Appendix A. Microsamples Mechanical Properties Appendix B. Mesosamples Mechanical Properties, and Appendix C. Round Bar Samples Mechanical Properties, respectively.

Table 9 Summary of AM 17-4 PH stainless steel vertically oriented microsamples' mechanical properties by manufactured build.

Microsamples Vertical Orientation			
Build	Yield Strength (MPa)	Ultimate Tensile Strength (MPa)	Strain to Failure (%)
PC2	1017.27 ± 27.18	1046.76 ± 29.39	14.16 ± 1.19
PC2B	1021.08 ± 21.29	1042.88 ± 23.55	15.84 ± 2.48
PC3	1012.89 ± 24.01	1044.86 ± 23.21	17.13 ± 2.01
PC4	989.352 ± 13.66	1006.97 ± 14.22	14.68 ± 2.53
PC5	1033.22 ± 32.74	1052.33 ± 34.18	14.35 ± 1.78
PC6	1040.96 ± 8.65	1077.52 ± 8.86	17.12 ± 1.04

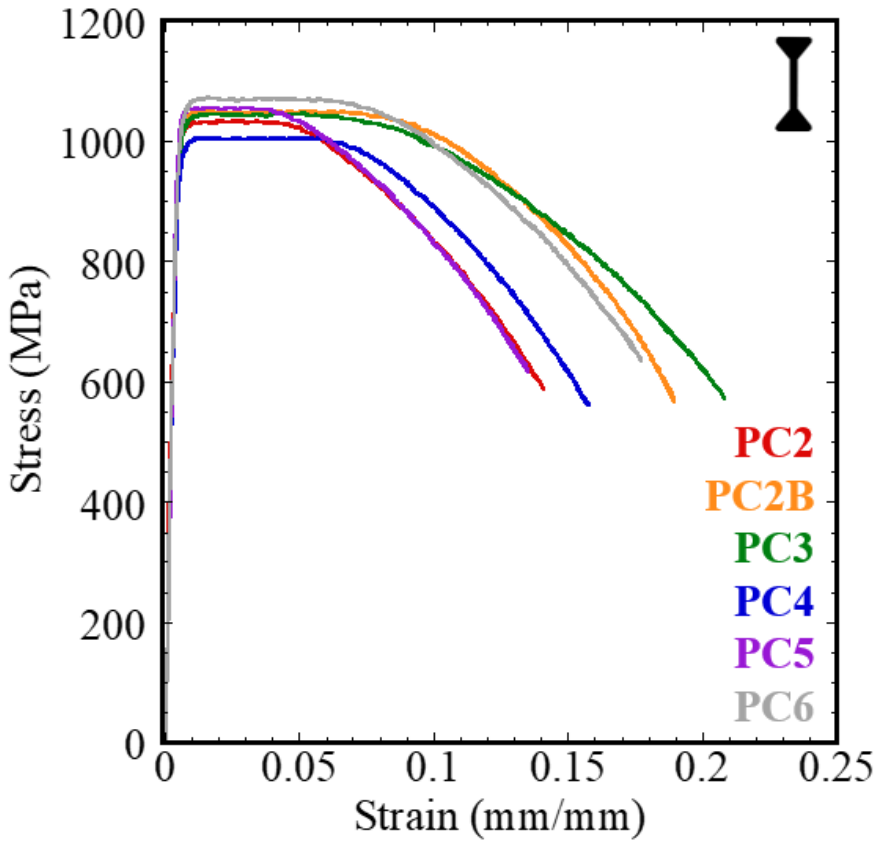

Figure 39 Representative stress-strain curves of the vertically orientated AM 17-4 PH stainless steel microsamples from each manufactured build.

Table 10 Summary of AM 17-4 PH stainless steel vertically oriented mesosamples' mechanical properties by manufactured build.

Mesosamples Vertical Orientation			
Build	Yield Strength (MPa)	Ultimate Tensile Strength (MPa)	Strain to Failure (%)
PC2	1008.35 ± 2.75	1021.15 ± 8.25	18.25 ± 0.65
PC2B	999.10 ± 6.63	1022.27 ± 3.73	17.5 ± 0.73
PC3	978.83 ± 27.56	1010.57 ± 18.63	18.47 ± 0.41
PC4	1016.67 ± 4.53	1021.63 ± 1.81	17.77 ± 0.83
PC5	1059.27 ± 6.94	1072.70 ± 2.61	17.23 ± 1.09
PC6	1097.23 ± 5.67	1107.13 ± 2.65	17.47 ± 0.52

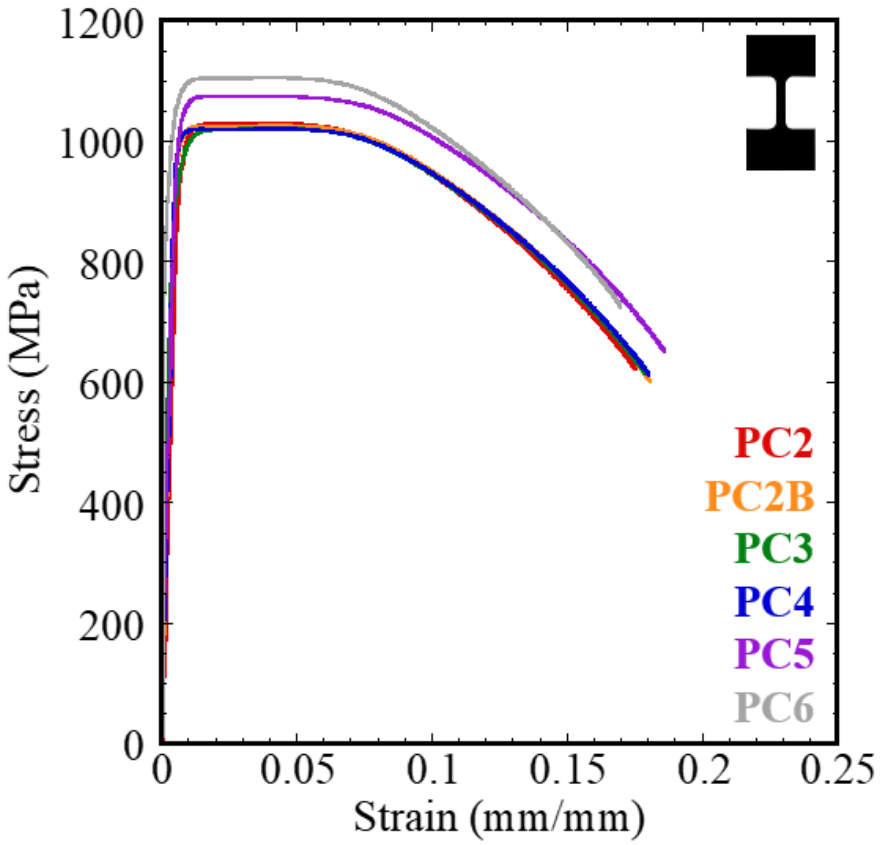

Figure 40 Representative stress-strain curves of the vertically orientated AM 17-4 PH stainless steel mesosamples from each manufactured build.

Table 11 Summary of AM 17-4 PH stainless steel vertically oriented round bar samples' mechanical properties by manufactured build.

Round Bar Samples Vertical Orientation			
Build	Yield Strength (MPa)	Ultimate Tensile Strength (MPa)	Strain to Failure (%)
PC2	1050.19 ± 6.27	1066.16 ± 7.94	15 ± 1.00
PC2B	1085.92 ± 19.47	1106.26 ± 23.21	15 ± 1.41
PC3	1040.42 ± 10.66	1053.86 ± 12.79	15.67 ± 1.89
PC4	1108.79 ± 27.22	1132.46 ± 30.0	15 ± 1.41
PC5	1039.96 ± 9.19	1052.94 ± 11.06	15.67 ± 1.89
PC6	1024.10 ± 3.60	1032.72 ± 4.53	15.17 ± 1.21

A one-way ANOVA test was conducted to characterize the effect of length-scales on the AM 17-4 PH stainless steel material, with the results for vertically oriented samples presented currently. The experimentally determined mechanical properties (YS, UTS, and ε_f) from each sample were classified into 18 groups based on sample size and build number: microsamples from builds PC2 (n = 5), PC2B (n = 5), PC3 (n = 5), PC4 (n = 5), PC5 (n = 5), and PC6 (n = 5), mesosamples from builds PC2 (n = 3), PC2B (n = 3), PC3 (n = 3), PC4 (n = 3), PC5 (n = 3), and PC6 (n = 3), and round bar samples from builds PC2 (n = 6), PC2B (n = 6), PC3 (n = 6), PC4 (n = 6), PC5 (n = 6), PC6 (n = 6). The data are presented as mean ± standard deviation.

The YS was statistically significantly different between builds across the three length scales, $F(17, 65) = 13.688$, $p < 0.0001$, $\omega^2 = 0.722$. The YS increased from PC3 mesosample (978.83 ± 27.56) to PC4 microsample (989.352 ± 13.66) to PC2B mesosample (999.10 ± 6.63) to PC2 mesosample (1008.35 ± 2.75) to PC3 microsample (1012.89 ± 24.01) to PC4 mesosample (1016.67 ± 4.53) to PC2 microsample (1017.27 ± 27.18) to PC2B microsample (1021.08 ± 21.29) to PC6 round bar (1024.10 ± 3.60) to PC5 microsample (1033.22 ± 32.74) to PC5 round bar (1039.96 ± 9.19) to PC3 round bar

(1040.42 ± 10.66) to PC6 microsample (1040.96 ± 8.65) to PC2 round bar (1050.19 ± 6.27) to PC5 mesosample (1059.27 ± 6.94) to PC2B round bar (1085.92 ± 19.47) to PC6 mesosample (1097.23 ± 5.67) to PC4 round bar (1108.79 ± 27.22), in that order. Tukey HSD post-hoc analysis showed that 52 different comparisons were statistically significantly different.

Comparing against PC4 round bar, the sample with the largest YS value, Tukey HSD post-hoc analysis showed that the mean differences to the following samples were statistically significant ($p < 0.0001$): PC3 mesosample with a mean difference of 129.96 (95% CI (78.14 to 181.78)), PC4 microsample with a mean difference of 119.44 (95% CI (75.06 to 163.82)), PC2B mesosample with a mean difference of 109.69 (95% CI (57.87 to 161.52)), PC2 mesosample with a mean difference of 100.44 (95% CI (40.60 to 160.28)), PC3 microsample with a mean difference of 95.90 (95% CI (51.52 to 140.28)), PC4 mesosample with a mean difference of 92.13 (95% CI (40.30 to 143.95)), PC2 microsample with a mean difference of 91.52 (95% CI (47.14 to 135.90)), PC2B microsample with a mean difference of 87.71 (95% CI (43.33 to 132.09)), PC6 round bar with a mean difference of 84.69 (95% CI (42.38 to 127.00)), PC5 microsample with a mean difference of 75.57 (95% CI (31.20 to 119.95)), PC5 round bar with a mean difference of 68.83 (95% CI (26.52 to 111.15)), PC3 round bar with a mean difference of 68.37 (95% CI (26.06 to 110.69)), and PC6 microsample with a mean difference of 67.83 (95% CI (23.45 to 112.21)). Additionally, the mean difference of 58.61 from PC2 round bar to PC4 round bar (95% CI (16.291 to 100.92)) was statistically significant ($p = 0.0005$).

Comparing against PC6 mesosample, the sample with the second largest YS value, Tukey HSD post-hoc analysis showed that the mean differences to the following samples were statistically significant ($p < 0.0001$): PC3 mesosample with a mean difference of 118.40 (95% CI (58.56 to 178.24)), PC4 microsample with a mean difference of 107.88 (95% CI (54.36 to 161.40)), PC2B mesosample with a mean difference of 98.13 (95% CI (38.29 to 157.97)), and PC3 microsample with a mean difference of 84.34 (95% CI (30.818 to 137.86)). Listed in decreasing order of statistical significance, additional comparison against PC6 mesosample showed PC2 microsample with a mean difference of 79.96 (95% CI (26.436 to 133.48)) was statistically significant ($p = 0.0001$), PC2B microsample with a mean difference of 76.15 (95% CI (22.63 to 129.68)) was statistically significant ($p = 0.0003$), PC6 round bar with a mean difference of 73.13 (95% CI (21.308 to 124.96)) was statistically significant ($p = 0.0004$), PC4 mesosample with a mean difference of 80.57 (95% CI (20.73 to 140.41)) was statistically significant ($p = 0.0009$), PC2 mesosample with a mean difference of 88.88 (95% CI (22.00 to 155.79)) was statistically significant ($p = 0.0011$), PC5 microsample with a mean difference of 64.02 (95% CI (10.49 to 117.54)) was statistically significant ($p = 0.0058$), PC5 round bar with a mean difference of 57.27 (95% CI (5.45 to 109.10)) was statistically significant ($p = 0.0164$), PC3 round bar with a mean difference of 56.81 (95% CI (4.99 to 108.64)) was statistically significant ($p = 0.0181$), and PC6 microsample with a mean difference of 56.27 (95% CI (2.75 to 109.80)) was statistically significant ($p = 0.0295$).

Comparing against PC2B round bar, the sample with the third largest YS value, Tukey HSD post-hoc analysis showed that the mean differences to the following samples

were statistically significant ($p < 0.0001$): PC3 mesosample with a mean difference of 107.09 (95% CI (55.27 to 158.91)), PC4 microsample with a mean difference of 96.57 (95% CI (52.19 to 140.95)), PC2B mesosample with a mean difference of 86.82 (95% CI (35.00 to 138.65)), PC3 microsample with a mean difference of 73.03 (95% CI (28.65 to 117.41)), and PC2 microsample with a mean difference of 68.65 (95% CI (24.27 to 113.03)). Listed in decreasing order of statistical significance, additional comparison against PC2B round bar showed that the mean difference of 64.84 from PC2B microsample (95% CI (20.47 to 109.22)) was statistically significant ($p = 0.0002$), the mean difference of 61.82 from PC6 round bar (95% CI (19.51 to 104.14)) was statistically significant ($p = 0.0002$), the mean difference of 69.26 from PC4 mesosample (95% CI (17.43 to 121.08)) was statistically significant ($p = 0.001$), the mean difference of 77.57 from PC2 mesosample (95% CI (17.73 to 137.42)) was statistically significant ($p = 0.0017$), the mean difference of 52.71 from PC5 microsample (95% CI (8.327 to 97.086)) was statistically significant ($p = 0.0064$), the mean difference of 45.97 from PC5 round bar (95% CI (3.65 to 88.28)) was statistically significant ($p = 0.0203$), the mean difference of 45.51 from PC3 round bar (95% CI (3.19 to 87.82)) was statistically significant ($p = 0.0228$) , and the mean difference of 44.96 from PC6 microsample (95% CI (0.58 to 89.34)) was statistically significant ($p = 0.0438$).

Comparing against PC3 mesosample, the sample with the smallest YS value, Tukey HSD post-hoc analysis showed that the mean difference of 71.35 from PC3 mesosample to PC2 round bar (95% CI (19.53 to 123.18)) was statistically significant ($p = 0.0006$), the mean difference of 80.43 from PC3 mesosample to PC5 mesosample (95% CI (20.59 to 140.27)) was statistically significant ($p = 0.0009$), the mean difference of

61.59 from PC3 mesosample to PC3 round bar (95% CI (9.76 to 113.41)) was statistically significant (p = 0.0063), the mean difference of 61.13 from PC3 mesosample to PC5 round bar (95% CI (9.30 to 112.95)) was statistically significant (p = 0.007), the mean difference of 62.13 from PC3 mesosample to PC6 microsample (95% CI (8.60 to 115.65)) was statistically significant (p = 0.0087), and the mean difference of 54.38 from PC3 mesosample to PC5 microsample (95% CI (0.86 to 107.91)) was statistically significant (p = 0.0425).

Comparing against PC4 microsample, the sample with the second smallest YS value, Tukey HSD post-hoc analysis showed that the mean difference of 60.83 from PC4 microsample to PC2 round bar (95% CI (16.46 to 105.21)) was statistically significant (p = 0.0006), the mean difference of 69.91 from PC4 microsample to PC5 mesosample (95% CI (16.39 to 123.44)) was statistically significant (p = 0.0015), the mean difference of 51.07 from PC4 microsample to PC3 round bar (95% CI (6.69 to 95.45)) was statistically significant (p = 0.0098), the mean difference of 50.61 from PC4 microsample to PC5 round bar (95% CI (6.23 to 94.99)) was statistically significant (p = 0.0111), and the mean difference of 51.61 from PC4 microsample to PC6 microsample (95% CI (5.26 to 97.96)) was statistically significant (p = 0.015).

Additionally, the Tukey HSD post-hoc analysis showed that the mean difference of 60.17 from PC2B mesosample, the sample with the third smallest YS value, to PC5 mesosample (95% CI (0.33 to 120.01)) was statistically significant (p = 0.0473).

The UTS was statistically significantly different between builds across the three length scales, $F(17, 65) = 12.394$, $p < 0.0001$, $\omega^2 = 0.700$. The UTS increased from PC4 microsample (1006.97 ± 14.22) to PC3 mesosample (1010.57 ± 18.63) to PC2

mesosample (1021.15 ± 8.25) to PC4 mesosample (1021.63 ± 1.81) to PC2B mesosample (1022.27 ± 3.73) to PC6 round bar (1032.72 ± 4.53) to PC2B microsample (1042.88 ± 23.55) to PC3 microsample (1044.86 ± 23.21) to PC2 microsample (1046.76 ± 29.39) to PC5 microsample (1052.33 ± 34.18) to PC5 round bar (1052.94 ± 11.06) to PC3 round bar (1053.86 ± 12.79) to PC2 round bar (1066.16 ± 7.94) to PC5 mesosample (1072.70 ± 2.61) to PC6 microsample (1077.52 ± 8.86) to PC2B round bar (1106.26 ± 23.21) to PC6 mesosample (1107.13 ± 2.65) to PC4 round bar (1132.46 ± 30.0), in that order. Tukey HSD post-hoc analysis showed that 42 different comparisons were statistically significantly different.

Comparing against PC4 round bar, the sample with the largest UTS value, Tukey HSD post-hoc analysis showed that the mean differences to the following samples were statistically significant ($p < 0.0001$): PC4 microsample with a mean difference of 125.49 (95% CI (78.89 to 172.10)), PC3 mesosample with a mean difference of 121.90 (95% CI (67.47 to 176.32)), PC2 mesosample with a mean difference of 111.31 (95% CI (48.47 to 174.16)), PC4 mesosample with a mean difference of 110.83 (95% CI (56.41 to 165.25)), PC2B mesosample with a mean difference of 110.20 (95% CI (55.77 to 164.62)), PC6 round bar with a mean difference of 99.74 (95% CI (55.31 to 144.18)), PC2B microsample with a mean difference of 89.58 (95% CI (42.980 to 136.19)), PC3 microsample with a mean difference of 87.60 (95% CI (41.00 to 134.21)), PC2 microsample with a mean difference of 85.70 (95% CI (39.10 to 132.31)), PC5 microsample with a mean difference of 80.13 (95% CI (33.53 to 126.74)), PC5 round bar with a mean difference of 79.52 (95% CI (35.08 to 123.96)), and PC3 round bar with a mean difference of 78.60 (95% CI (34.164 to 123.04)). Listed in decreasing order of

statistical significance, additional comparison against PC4 round bar showed the mean difference of 66.30 from PC2 round bar (95% CI (21.87 to 110.74)) was statistically significant ($p = 0.0001$), the mean difference of 54.94 from PC6 microsample (95% CI (8.34 to 101.55)) was statistically significant ($p = 0.0071$), and the mean difference of 59.76 (95% CI (5.34 to 114.19)) was statistically significant ($p = 0.0178$).

Comparing against PC6 mesosample, the sample with the second largest UTS value, Tukey HSD post-hoc analysis showed that the mean differences to the following samples were statistically significant ($p < 0.0001$): PC4 microsample with a mean difference of 100.16 (95% CI (43.95 to 156.37)), and PC3 mesosample with a mean difference of 96.57 (95% CI (33.73 to 159.41)). Listed in decreasing order of statistical significance, additional comparison against PC6 mesosample showed PC4 mesosample with a mean difference of 85.50 (95% CI (22.66 to 148.34)) was statistically significant ($p = 0.0007$), PC6 round bar with a mean difference of 74.41 (95% CI (19.99 to 128.84)) was statistically significant ($p = 0.0007$), PC2B mesosample with a mean difference of 84.87 (95% CI (22.03 to 147.71)) was statistically significant ($p = 0.0008$), PC2 mesosample with a mean difference of 85.98 (95% CI (15.72 to 156.24)) was statistically significant ($p = 0.0041$), PC2B microsample with a mean difference of 64.25 (95% CI (8.05 to 120.46)) was statistically significant ($p = 0.0107$), PC3 microsample with a mean difference of 62.27 (95% CI (6.0658 to 118.48)) was statistically significant ($p = 0.0160$), and PC2 microsample with a mean difference of 60.37 (95% CI (4.17 to 116.58)) was statistically significant ($p = 0.0231$).

Comparing against PC2B round bar, the sample with the third largest UTS value, Tukey HSD post-hoc analysis showed that the mean differences to the following samples

were statistically significant ($p < 0.0001$): PC4 microsample with a mean difference of 99.29 (95% CI (52.69 to 145.9)), PC3 mesosample with a mean difference of 95.70 (95% CI (41.27 to 150.12)), PC4 mesosample with a mean difference of 84.63 (95% CI (30.21 to 139.05)), PC2B mesosample with a mean difference of 84.00 (95% CI (29.57 to 138.42)), and PC6 round bar with a mean difference of 73.54 (95% CI (29.108 to 117.98)). Listed in decreasing order of statistical significance, additional comparison against PC2B round bar showed that the mean difference of 63.38 from PC2B microsample (95% CI (16.78 to 109.99)) was statistically significant ($p = 0.0007$), the mean difference of 85.11 from PC2 mesosample (95% CI (22.27 to 147.96)) was statistically significant ($p = 0.0008$), the mean difference of 61.40 from PC3 microsample (95% CI (14.80 to 108.01)) was statistically significant ($p = 0.0013$), the mean difference of 59.50 from PC2 microsample (95% CI (12.90 to 106.11)) was statistically significant ($p = 0.0021$), the mean difference of 53.32 from PC5 round bar (95% CI (8.88 to 97.76)) was statistically significant ($p = 0.0055$), the mean difference of 52.40 from PC3 round bar (95% CI (7.96 to 96.84)) was statistically significant ($p = 0.007$), and the mean difference of 53.93 from PC5 microsample (95% CI (7.33 to 100.54)) was statistically significant ($p = 0.0091$).

Comparing against PC4 microsample, the sample with the smallest UTS value, Tukey HSD post-hoc analysis showed that the mean difference of 70.55 from PC4 microsample to PC6 microsample (95% CI (21.871 to 119.23)) was statistically significant ($p = 0.0002$), the mean difference of 59.19 from PC4 microsample to PC2 round bar (95% CI (12.58 to 105.79)) was statistically significant ($p = 0.0023$), the mean difference of 65.73 from PC4 microsample to PC5 mesosample (95% CI (9.52 to

121.94)) was statistically significant (p = 0.0079), and the mean difference of 46.89 from PC4 microsample to PC3 round bar (95% CI (0.29 to 93.50)) was statistically significant (p = 0.047).

Comparing against PC3 mesosample, the sample with the second smallest UTS value, Tukey HSD post-hoc analysis showed that the mean difference of 66.95 from PC3 mesosample to PC6 microsample (95% CI (10.746 to 123.16)) was statistically significant (p = 0.0061), and the mean difference of 55.59 from PC3 mesosample to PC2 round bar (95% CI (1.17 to 110.02)) was statistically significant (p = 0.0402).

The one-way ANOVA showed that ε_f was statistically significant between builds across the three length scales, F(17, 65) = 2.448, p = 0.00512, ω^2 = 0.229. The ε_f increased from PC2 microsample (14.16 ± 1.19) to PC5 microsample (14.35 ± 1.78) to PC4 microsample (14.68 ± 2.53) to PC2 round bar (15 ± 1.00) to PC2B round bar (15 ± 1.41) to PC4 round bar (15 ± 1.41) to PC6 round bar (15.17 ± 1.21) to PC3 round bar (15.67 ± 1.89) to PC5 round bar (15.67 ± 1.89) to PC2B microsample (15.84 ± 2.48) to PC6 microsample (17.12 ± 1.04) to PC3 microsample (17.13 ± 2.01) to PC5 mesosample (17.23 ± 1.09) to PC6 mesosample (17.47 ± 0.52) to PC2B mesosample (17.5 ± 0.73) to PC4 mesosample (17.77 ± 0.83) to PC2 mesosample (18.25 ± 0.65) to PC3 mesosample (18.47 ± 0.41). Tukey HSD post-hoc analysis showed that no pairwise comparisons were statistically significantly different. This could be attributed to the conservative nature of the Tukey post-hoc analysis or there could be no real statistically significant difference.

A summary of the experimentally determined mechanical properties for AM 17-4 PH stainless steel microsamples in the horizontal direction can be seen in Table 12. Figure 41 shows the representative engineering stress-strain curves for the horizontal

microsample material from each build. The summary of the experimentally determined mechanical properties for the mesosamples in the horizontal direction can be seen in Table 13, with the representative engineering stress-strain curves shown in Figure 42. Table 14 shows the summary of the experimentally determined mechanical properties for the horizontally oriented round bar samples. No stress-strain curves were provided by NSWCCD for the round bar samples at this time

Table 12 Summary of AM 17-4 PH stainless steel horizontally oriented microsamples' mechanical properties by manufactured build.

Microsamples Horizontal Orientation			
Build	Yield Strength (MPa)	Ultimate Tensile Strength (MPa)	Strain to Failure (%)
PC2	979.18 ± 4.00	1026.56 ± 7.82	14.10 ± 1.63
PC2B	983.078 ± 21.21	1017.47 ± 17.40	16.40 ± 1.66
PC3	925.97 ± 131.24	958.91 ± 128.03	17.24 ± 0.92
PC4	994.28 ± 10.17	1032.36 ± 9.93	14.36 ± 3.84
PC5	995.86 ± 11.35	1028.30 ± 7.34	15.87 ± 1.18
PC6	1023.36 ± 10.51	1059.84 ± 9.95	13.78 ± 1.82

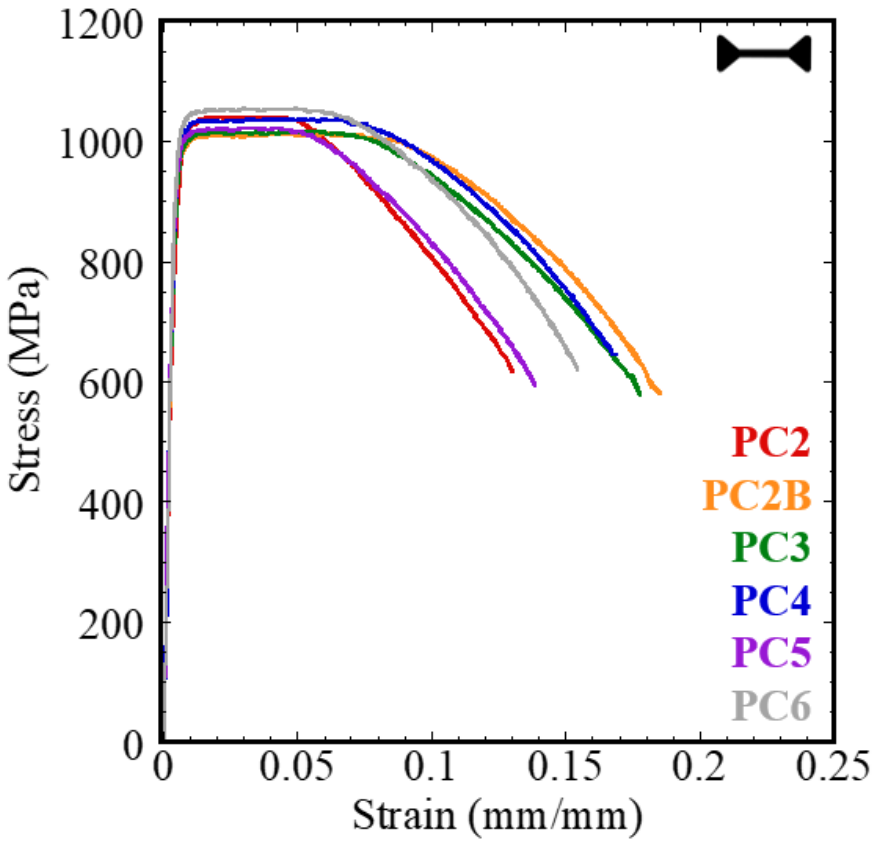

Figure 41 Representative stress-strain curves of the horizontally orientated AM 17-4 PH stainless steel microsamples from each manufactured build.

Table 13 Summary of AM 17-4 PH stainless steel horizontally oriented mesosamples' mechanical properties by manufactured build.

Mesosamples Horizontal Orientation			
Build	Yield Strength (MPa)	Ultimate Tensile Strength (MPa)	Strain to Failure (%)
PC2	1027.8 ± 19.66	1050.53 ± 1.20	21.40 ± 5.18
PC2B	1014.8 ± 5.53	1039.07 ± 1.62	18.57 ± 0.33
PC3	1038.67 ± 10.35	1055.73 ± 13.45	17.90 ± 1.22
PC4	1018.50 ± 3.25	1035.57 ± 1.33	16.90 ± 0.57
PC5	1017.35 ± 10.45	1027.70 ± 7.00	19.55 ± 0.65
PC6	1088.87 ± 7.83	1100.40 ± 1.10	17.43 ± 0.29

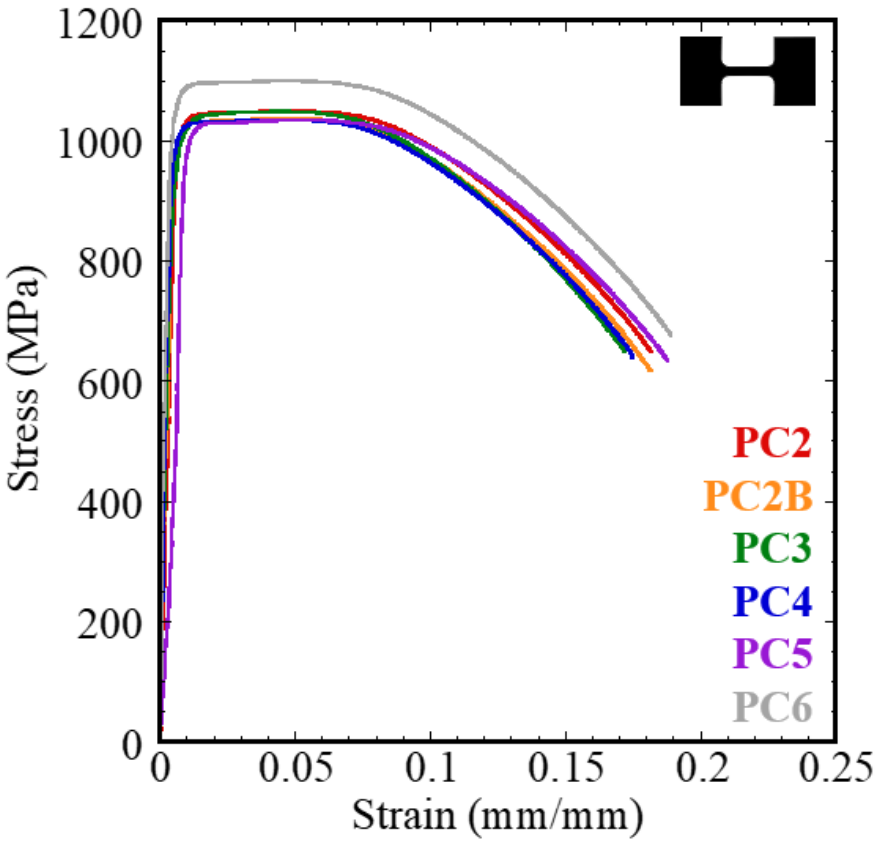

Figure 42 Representative stress-strain curves of the horizontally orientated AM 17-4 PH stainless steel mesosamples from each manufactured build.

Table 14 Summary of AM 17-4 PH stainless steel horizontally oriented round bar samples' mechanical properties by manufactured build.

Round Bar Samples Horizontal Orientation			
Build	Yield Strength (MPa)	Ultimate Tensile Strength (MPa)	Strain to Failure (%)
PC2	1038.35 ± 1.38	1056.62 ± 3.79	16 ± 0
PC2B	1113.16 ± 1.03	1136.60 ± 1.03	15 ± 1.00
PC3	1028.01 ± 5.52	1043.52 ± 8.62	16 ± 0
PC4	1102.13 ± 25.17	1130.40 ± 27.23	16 ± 0
PC5	1043.87 ± 4.83	1060.07 ± 3.79	16.5 ± 0.50
PC6	1028.35 ± 0.34	1044.21 ± 5.86	17 ± 0

A one-way ANOVA test was conducted to characterize the effect of length-scales on the AM 17-4 PH stainless steel material, with the results for horizontally oriented samples presented currently. The experimentally determined mechanical properties (YS, UTS, and ε_f) from each sample were classified into 18 groups based on sample size and build number: microsamples from builds PC2 (n = 5), PC2B (n = 5), PC3 (n = 5), PC4 (n = 5), PC5 (n = 5), and PC6 (n = 5), mesosamples from builds PC2 (n = 3), PC2B (n = 3), PC3 (n = 3), PC4 (n = 3), PC5 (n = 3), and PC6 (n = 3), and round bar samples from builds PC2 (n = 2), PC2B (n = 2), PC3 (n = 2), PC4 (n = 2), PC5 (n = 2), PC6 (n = 2). The data are presented as mean ± standard deviation.

The YS was statistically significantly different between builds across the three length scales, $F(17, 41) = 2.884$, $p = 0.003$, $\omega^2 = 0.352$. The YS increased from PC3 microsample (925.97 ± 131.24) to PC2 microsample (979.18 ± 4.00) to PC2B microsample (983.078 ± 21.21) to PC4 microsample (994.28 ± 10.17) to PC5 microsample (995.86 ± 11.35) to PC2B mesosample (1014.8 ± 5.53) to PC5 mesosample (1017.35 ± 10.45) to PC4 mesosample (1018.50 ± 3.25) to PC6 microsample (1023.36 ± 10.51) to PC2 mesosample (1027.8 ± 19.66) to PC3 round bar (1028.01 ± 5.52) to PC6 round bar (1028.35 ± 0.34) to PC2 round bar (1038.35 ± 1.38) to PC3 mesosample (1038.67 ± 10.35) to PC5 round bar (1043.87 ± 4.83) to PC6 mesosample (1088.87 ± 7.830) to PC4 round bar (1102.13 ± 25.17) to PC2B round bar (1113.16 ± 1.03). Three different comparisons were found to be statistically significantly different during the post-hoc analysis.

Tukey HSD post-hoc analysis showed that the mean difference of 187.19 from PC3 microsample to PC2B round bar (95% CI (38.60 to 335.77)) was statistically

significant (p = 0.0034), as well as the mean difference of 162.89 from PC3 microsample to PC6 mesosample (95% CI (33.20 to 292.59)) was statistically significant (p = 0.0036), and the mean difference of 176.15 from PC3 microsample to PC4 round bar (95% CI (27.57 to 324.74)) was statistically significant (p = 0.0077).

The UTS was statistically significantly different between builds across the three length scales, F(17, 41) = 2.424, p = 0.010, ω^2 = 0.291. The UTS increased from PC3 microsample (958.91 ± 128.03) to PC2B microsample (1017.47 ± 17.40) to PC2 microsample (1026.56 ± 7.82) to PC5 mesosample (1027.70 ± 7.00) to PC5 microsample (1028.30 ± 7.34) to PC4 microsample (1032.36 ± 9.93) to PC4 mesosample (1035.57 ± 1.33) to PC2B mesosample (1039.07 ± 1.62) to PC3 round bar (1043.52 ± 8.62) to PC6 round bar (1044.21 ± 5.86) to PC2 mesosample (1050.53 ± 1.20) to PC3 mesosample (1055.73 ± 13.45) to PC2 round bar (1056.62 ± 3.79) to PC6 microsample (1059.84 ± 9.95) to PC5 round bar (1060.07 ± 3.79) to PC6 mesosample (1100.40 ± 1.10) to PC4 round bar (1130.40 ± 27.23) to PC2B round bar (1136.60 ± 1.03). Three different comparisons were found to be statistically significantly different during the post-hoc analysis.

Tukey HSD post-hoc analysis showed that the mean difference of 177.69 from PC3 microsample to PC2B round bar (95% CI (34.03 to 321.36)) was statistically significant (p = 0.0044), as well as the mean difference of 171.49 from PC3 microsample to PC4 round bar (95% CI (27.82 to 315.15)) was statistically significant (p = 0.0071), and the mean difference of 141.49 from PC3 microsample to PC6 mesosample (95% CI (16.086 to 266.89)) was statistically significant (p = 0.0141).

The one-way ANOVA showed that ε_f was statistically significantly different between builds across the three length scales, $F(17, 41) = 2.331$, $p = 0.014$, $\omega^2 = 0.277$. The ε_f increased from PC6 microsample (13.78 ± 1.82) to PC2 microsample (14.10 ± 1.63) to PC4 microsample (14.36 ± 3.84) to PC2B round bar (15 ± 1.00) to PC5 microsample (15.87 ± 1.18) to PC2 round bar (16 ± 0) to PC3 round bar (16 ± 0) to PC4 round bar (16 ± 0) to PC2B microsample (16.40 ± 1.66) to PC5 round bar (16.5 ± 0.50) to PC4 mesosample (16.90 ± 0.57) to PC6 round bar (17 ± 0) to PC3 microsample (17.24 ± 0.92) to PC6 mesosample (17.43 ± 0.29) to PC3 mesosample (17.90 ± 1.22) to PC2B mesosample (18.57 ± 0.33) to PC5 mesosample (19.55 ± 0.65) to PC2 mesosample (21.40 ± 5.18). Three different comparisons were found to be statistically significantly different during the post-hoc analysis.

Tukey HSD post-hoc analysis showed that the mean difference of 7.62 from PC6 microsample to PC2 mesosample (95% CI (1.34 to 13.89)) was statistically significant ($p = 0.0057$), as well as the mean difference of 7.30 from PC2 microsample to PC2 mesosample (95% CI (1.03 to 13.57)) was statistically significant ($p = 0.0097$), and the mean difference of 7.03 from PC4 microsample to PC2 mesosample (95% CI (0.76 to 13.30)) was statistically significant ($p = 0.0152$).

Additional one-way ANOVA testing was conducted to characterize the effect of length-scales on the AM 17-4 PH stainless steel material, looking at a single build (PC4). The results for vertically oriented samples will be presented first. The experimentally determined mechanical properties (YS, UTS, and ε_f) from PC4 were classified into 3 groups based on sample geometry: microsamples (n=5), mesosamples (n=3), and round bar samples (n=6). The data are presented as mean ± standard deviation.

The YS was statistically significantly different for PC4 across the three length scales, $F(2, 11) = 42.742$, $p < 0.0001$, $\omega^2 = 0.856$. The YS increased from microsample (989.352 ± 13.66) to mesosample (1016.67 ± 4.53) to round bar (1108.79 ± 27.22). Tukey HSD post-hoc analysis showed that the mean difference of 119.44 from round bar to microsample (95% CI (83.068 to 155.81)) was statistically significant ($p < 0.0001$), as well as the mean difference of 92.13 from round bar to mesosample (95% CI (49.652 to 134.6)) was statistically significant ($p = 0.0003$).

The UTS was statistically significantly different for PC4 across the three length scales, $F(2, 11) = 42.424$, $p < 0.0001$, $\omega^2 = 0.855$. The UTS increased from microsample (1006.97 ± 14.22) to mesosample (1021.63 ± 1.81) to round bar (1132.46 ± 30.0). Tukey HSD post-hoc analysis showed that the mean difference of 125.49 from round bar to microsample (95% CI (85.883 to 165.1)) was statistically significant ($p < 0.0001$), as well as the mean difference of 110.83 from round bar to mesosample (95% CI (64.577 to 157.08)) was statistically significant ($p = 0.0001$).

The one-way ANOVA test determined that ε_f was not statistically significantly different for PC4 across the three length scales, $F(2, 11) = 2.412$, $p = 0.135$, $\omega^2 = 0.168$.

One-way ANOVA testing was conducted to characterize the effect of length-scales on the AM 17-4 PH stainless steel material, looking at the horizontally oriented samples from a single build (PC4). The experimentally determined mechanical properties (YS, UTS, and ε_f) from PC4 were classified into 3 groups based on sample geometry: microsamples (n=5), mesosamples (n=3), and round bar samples (n=2). The data are presented as mean ± standard deviation.

The YS was statistically significantly different for PC4 across the three length scales, $F(2, 7) = 32.199$, $p = 0.0003$, $\omega^2 = 0.862$. The YS increased from microsample (994.28 ± 10.17) to mesosample (1018.50 ± 3.25) to round bar (1102.13 ± 25.17). Tukey HSD post-hoc analysis showed that the mean difference of 107.85 from round bar to microsample (95% CI (68.158 to 147.53)) was statistically significant ($p = 0.0002$), as well as the mean difference of 83.63 from round bar to mesosample (95% CI (40.325 to 126.93)) was statistically significant ($p = 0.0019$).

The UTS was statistically significantly different for PC4 across the three length scales, $F(2, 7) = 26.537$, $p = 0.0005$, $\omega^2 = 0.836$. The UTS increased from microsample (1032.36 ± 9.93) to mesosample (1035.57 ± 1.33) to round bar (1130.40 ± 27.23). Tukey HSD post-hoc analysis showed that the mean difference of 98.04 from round bar to microsample (95% CI (56.582 to 139.49)) was statistically significant ($p = 0.0006$), as well as the mean difference of 94.83 from round bar to mesosample (95% CI (49.599 to 140.06)) was statistically significant ($p = 0.0011$).

The one-way ANOVA test determined that ε_f was not statistically significantly different for PC4 across the three length scales, $F(2, 7) = 0.597$, $p = 0.576$, $\omega^2 = -0.088$.

Table 15 presents a summary of the 17-4 PH stainless steel mechanical properties from the published values supplied by EOS for the EOS M290 and the microsample experimental data. The EOS supplied data includes mechanical properties from as-built material and from an argon atmospheric heat treatment (solution treatment at 1040°C for 30 min followed by aging at 460°C for 1 hr). Comparing the experimentally determined mechanical properties to the EOS supplied data shows that the microsample mechanical properties fall between the as-built and heat treated EOS supplied data.

Table 15 Mechanical properties from the microsamples and the published values from EOS M290.

Sample Type	Orientation	Yield Strength (MPa)	Ultimate Tensile Strength (MPa)	Strain to Failure (%)
EOS M290 As-Built [47]	Vertical	861.3 ± 44.7	924.2 ± 65.9	20.1 ± 1.5
	Horizontal	860.6 ± 75.7	886.0 ± 70.4	19.9 ± 1.2
EOS M290 HT[3] [47]	Vertical	1242.6 ± 10.1	1345.5 ± 2.8	12.6 ± 0.9
	Horizontal	1235.5 ± 8.7	1340.0 ± 5.9	13.5 ± 0.9
PC2 microsamples	Vertical	1017.27 ± 27.18	1046.76 ± 29.39	14.16 ± 1.19
	Horizontal	979.18 ± 4.00	1026.56 ± 7.82	14.10 ± 1.63
PC2B microsamples	Vertical	1021.08 ± 21.29	1042.88 ± 23.55	15.84 ± 2.48
	Horizontal	983.078 ± 21.21	1017.47 ± 17.40	16.40 ± 1.66
PC3 microsamples	Vertical	1012.89 ± 24.01	1044.86 ± 23.21	17.13 ± 2.01
	Horizontal	925.97 ± 131.24	958.91 ± 128.03	17.24 ± 0.92
PC4 microsamples	Vertical	989.352 ± 13.66	1006.97 ± 14.22	14.68 ± 2.53
	Horizontal	994.28 ± 10.17	1032.36 ± 9.93	14.36 ± 3.84
PC5 microsamples	Vertical	1033.22 ± 32.74	1052.33 ± 34.18	14.35 ± 1.78
	Horizontal	995.86 ± 11.35	1028.30 ± 7.34	15.87 ± 1.18
PC6 microsamples	Vertical	1040.96 ± 8.65	1077.52 ± 8.86	17.12 ± 1.04
	Horizontal	1023.36 ± 10.51	1059.84 ± 9.95	13.78 ± 1.82

[3]Argon Atmospheric HT (Condition A (1040°C for 30 min) followed by 460°C for 1 hr)

Table 16 presents a summary of the 17-4 PH stainless steel mechanical properties from the published values supplied by EOS for the EOS M290 and the mesosample experimental data. The EOS supplied data includes mechanical properties from as-built material and from an argon atmospheric heat treatment. Comparing the experimentally determined mechanical properties to the EOS supplied data shows that the mesosample mechanical properties fall between the as-built and heat treated EOS supplied data.

Table 16 Mechanical properties from the mesosamples and the published values from EOS M290.

Sample Type	Orientation	Yield Strength (MPa)	Ultimate Tensile Strength (MPa)	Strain to Failure (%)
EOS M290 As-Built [47]	Vertical	861.3 ± 44.7	924.2 ± 65.9	20.1 ± 1.5
	Horizontal	860.6 ± 75.7	886.0 ± 70.4	19.9 ± 1.2
EOS M290 HT[3] [47]	Vertical	1242.6 ± 10.1	1345.5 ± 2.8	12.6 ± 0.9
	Horizontal	1235.5 ± 8.7	1340.0 ± 5.9	13.5 ± 0.9
PC2 mesosamples	Vertical	1008.35 ± 2.75	1021.15 ± 8.25	18.25 ± 0.65
	Horizontal	1027.8 ± 19.66	1050.53 ± 1.20	21.40 ± 5.18
PC2B mesosamples	Vertical	999.10 ± 6.63	1022.27 ± 3.73	17.5 ± 0.73
	Horizontal	1014.8 ± 5.53	1039.07 ± 1.62	18.57 ± 0.33
PC3 mesosamples	Vertical	978.83 ± 27.56	1010.57 ± 18.63	18.47 ± 0.41
	Horizontal	1038.67 ± 10.35	1055.73 ± 13.45	17.90 ± 1.22
PC4 mesosamples	Vertical	1016.67 ± 4.53	1021.63 ± 1.81	17.77 ± 0.83
	Horizontal	1018.50 ± 3.25	1035.57 ± 1.33	16.90 ± 0.57
PC5 mesosamples	Vertical	1059.27 ± 6.94	1072.70 ± 2.61	17.23 ± 1.09
	Horizontal	1017.35 ± 10.45	1027.70 ± 7.00	19.55 ± 0.65
PC6 mesosamples	Vertical	1097.23 ± 5.67	1107.13 ± 2.65	17.47 ± 0.52
	Horizontal	1088.87 ± 7.83	1100.40 ± 1.10	17.43 ± 0.29

[3]Argon Atmospheric HT (CA (1040°C for 30 min) followed by 460°C for 1 hr)

Table 17 presents a summary of the 17-4 PH stainless steel mechanical properties from the published values supplied by EOS for the EOS M290 and the round bar experimental data. The EOS supplied data includes mechanical properties from as-built material and from an argon atmospheric heat treatment. Comparing the experimentally determined mechanical properties to the EOS supplied data shows that the round bar mechanical properties fall between the as-built and heat treated EOS supplied data.

Table 17 Mechanical properties from the round bars and the published values from EOS M290.

Sample Type	Orientation	Yield Strength (MPa)	Ultimate Tensile Strength (MPa)	Strain to Failure (%)
EOS M290 As-Built [47]	Vertical	861.3 ± 44.7	924.2 ± 65.9	20.1 ± 1.5
	Horizontal	860.6 ± 75.7	886.0 ± 70.4	19.9 ± 1.2
EOS M290 HT[3] [47]	Vertical	1242.6 ± 10.1	1345.5 ± 2.8	12.6 ± 0.9
	Horizontal	1235.5 ± 8.7	1340.0 ± 5.9	13.5 ± 0.9
PC2 round bar	Vertical	1050.19 ± 6.27	1066.16 ± 7.94	15 ± 1.00
	Horizontal	1038.35 ± 1.38	1056.62 ± 3.79	16 ± 0
PC2B round bar	Vertical	1085.92 ± 19.47	1106.26 ± 23.21	15 ± 1.41
	Horizontal	1113.16 ± 1.03	1136.60 ± 1.03	15 ± 1.00
PC3 round bar	Vertical	1040.42 ± 10.66	1053.86 ± 12.79	15.67 ± 1.89
	Horizontal	1028.01 ± 5.52	1043.52 ± 8.62	16 ± 0
PC4 round bar	Vertical	1108.79 ± 27.22	1132.46 ± 30.0	15 ± 1.41
	Horizontal	1102.13 ± 25.17	1130.40 ± 27.23	16 ± 0
PC5 round bar	Vertical	1039.96 ± 9.19	1052.94 ± 11.06	15.67 ± 1.89
	Horizontal	1043.87 ± 4.83	1060.07 ± 3.79	16.5 ± 0.50
PC6 round bar	Vertical	1024.10 ± 3.60	1032.72 ± 4.53	15.17 ± 1.21
	Horizontal	1028.35 ± 0.34	1044.21 ± 5.86	17 ± 0

[3]Argon Atmospheric HT (CA (1040°C for 30 min) followed by 460°C for 1 hr)

5. Summary and Future Work

5.1 Conclusions

This work presented the multiscale tensile characterization and repeatability of additively manufactured 17-4 PH stainless steel. Material manufactured using the same EOS M290 DMLS system with manufacturer recommended processing parameters was mechanically evaluated across three different length scales: microscale (cross-section of 0.25mm x 0.25mm), mesoscale (cross-section of 2mm x 2mm), and macroscale (cross-section of nominally 4mm x 4mm). All material underwent a heat treatment process, adapted from a standard H1025 heat treatment, with the aging step reduced from four hours to one hour. The mechanical characterization occurred in two different sample orientations; some samples were oriented with gauge sections parallel to the build direction, classified as vertical samples, and others were oriented with gauge sections perpendicular to the build direction, classified as horizontal samples. The behavior across the length scales and builds was evaluated using a one-way ANOVA with a Tukey HSD post-hoc test.

- Considering the YS of all vertical samples, there was a statistically significant difference across the various builds and length scales, with 52 different comparisons identified as statistically significantly different.
- Considering the UTS of all vertical samples, there was a statistically significant difference across the various builds and length scales, with 42 different comparisons identified as statistically significantly different.
- Considering the ε_f of all vertical samples, there was a statistically significant difference across the various builds and length scales. No comparisons were

identified as statistically significantly different, likely due to the conservative nature of the Tukey HSD post-hoc analysis.

- Considering the YS of all horizontal samples, there was a statistically significant difference across the various builds and length scales, with 3 different comparisons identified as statistically significantly different.
- Considering the UTS of all horizontal samples, there was a statistically significant difference across the various builds and length scales, with 3 different comparisons identified as statistically significantly different.
- Considering the ε_f of all horizontal samples, there was a statistically significant difference across the various builds and length scales, with 3 different comparisons identified as statistically significantly different.

The statistically significant differences identified across the different length scales indicates that one type of tensile testing is not sufficient to fully characterize AM 17-4 PH stainless steel material. To develop a comprehensive understanding of the material's mechanical behavior, tensile testing needs to occur at different length scales, otherwise the characterization process is incomplete.

5.2 Future Work

As mentioned previously in this work's state of the art, even though AM has the potential to revolutionize manufacturing and create parts unable to be manufactured using traditional means, it is still a relatively new technology that requires further research. The scope of this work was limited to only one metal AM machine: EOS M290 DMLS. The testing and statistical analysis conducted in this work should be expanded across all metal AM systems to better understand repeatability with AM 17-4 PH stainless steel.

Additionally, a larger sample size should have been used for each set of tensile testing. More samples would have created a larger data set for better statistical analysis. Looking at this specific study, future work into understanding the fractography and microstructure of these tensile specimens would create a detailed understanding of the resultant mechanical properties. Additional work for 17-4 PH stainless steel should focus on the effects of different heat treatments regarding the microstructural changes and differences in multiscale tensile testing results.

Appendix A. Microsamples Mechanical Properties

Table A.1 All mechanical properties from the vertically oriented microsamples.

		Vertical Orientation			
Build	Sample #	Young's Modulus (GPa)	Yield Strength (MPa)	UTS (MPa)	Strain to Failure (%)
PC2	1	202.75	1008.80	1033.90	14.39
	2	201.27	993.27	1034.40	15.96
	3	203.60	1070.20	1105.20	12.22
	4	203.22	1002.80	1026.00	14.16
	5	202.73	1011.30	1034.30	14.10
	Avg	202.71	1017.27	1046.76	14.16
	Std	0.791	27.182	29.393	1.189
PC2B	1	204.06	1004.00	1026.40	13.06
	2	202.78	1060.70	1086.00	14.33
	3	201.27	1005.20	1027.60	18.69
	4	201.40	1025.80	1050.30	18.96
	5	197.69	1009.70	1024.10	14.15
	Avg	201.44	1021.08	1042.88	15.84
	Std	2.134	21.286	23.546	2.480
PC3	1	201.90	1053.00	1081.60	17.00
	2	202.70	1018.80	1045.70	20.85
	3	205.45	1016.30	1056.10	16.10
	4	206.18	989.71	1024.00	14.85
	5	201.43	986.65	1016.90	16.84
	Avg	203.53	1012.89	1044.86	17.13
	Std	1.921	24.005	23.211	2.011
PC4	1	209.82	967.88	986.30	14.40
	2	217.33	995.74	997.46	9.98
	3	204.27	980.17	1005.80	15.77
	4	206.63	996.37	1022.40	15.91
	5	222.28	1006.60	1022.90	17.36
	Avg	212.07	989.35	1006.97	14.68
	Std	6.744	13.659	14.219	2.532
PC5	1	203.32	1044.70	1055.90	13.52
	2	206.49	1070.60	1087.10	11.26
	3	204.04	1055.60	1085.60	15.68

	4	203.75	1017.50	1038.30	15.16
	5	207.88	977.69	994.76	16.15
	Avg	205.10	1033.22	1052.33	14.35
	Std	1.778	32.743	34.175	1.785
PC6	1	202.67	1025.30	1065.60	16.36
	2	202.42	1051.10	1088.40	15.81
	3	202.08	1045.90	1087.20	18.75
	4	202.96	1042.20	1073.90	16.96
	5	202.25	1040.30	1072.50	17.74
	Avg	202.48	1040.96	1077.52	17.12
	Std	0.312	8.654	8.860	1.035

Table A.2 All mechanical properties from the horizontally oriented microsamples.

		Horizontal Orientation			
Build	Sample #	Young's Modulus (GPa)	Yield Strength (MPa)	UTS (MPa)	Strain to Failure (%)
PC2	1	207.90	978.82	1022.60	16.43
	2	199.37	985.50	1027.40	14.35
	3	208.45	981.49	1040.80	13.02
	4	201.19	975.50	1017.50	11.69
	5	203.62	974.59	1024.50	15.02
	Avg	204.11	979.18	1026.56	14.10
	Std	3.592	4.000	7.817	1.631
PC2B	1	202.68	969.81	1000.10	16.21
	2	208.26	1017.30	1042.50	13.46
	3	204.56	971.32	1012.00	18.55
	4	201.88	959.48	999.74	17.03
	5	201.89	997.48	1033.00	16.76
	Avg	203.85	983.08	1017.47	16.40
	Std	2.409	21.212	17.399	1.662
PC3	1	209.02	989.41	1018.90	18.03
	2	203.60	1012.90	1038.00	15.44
	3	205.73	664.54	703.34	17.53
	4	202.51	984.48	1018.60	17.40
	5	202.60	978.54	1015.70	17.78
	Avg	204.69	925.97	958.91	17.24
	Std	2.455	131.236	128.030	0.924

PC4	1	201.52	991.04	1027.10	7.49
	2	204.48	997.84	1037.00	16.88
	3	200.63	1006.60	1045.30	14.21
	4	204.10	999.43	1036.20	14.40
	5	207.73	976.50	1016.20	18.86
	Avg	203.69	994.28	1032.36	14.36
	Std	2.498	10.175	9.925	3.841
PC5	1	202.56	994.26	1022.20	13.89
	2	201.40	987.54	1022.80	16.18
	3	202.62	1008.10	1028.90	16.83
	4	201.89	1009.20	1042.20	17.17
	5	200.57	980.22	1025.40	15.29
	Avg	201.81	995.86	1028.30	15.87
	Std	0.765	11.350	7.341	1.180
PC6	1	201.67	1010.60	1054.30	10.93
	2	203.19	1036.70	1076.80	13.28
	3	203.84	1018.80	1054.40	15.46
	4	204.17	1034.90	1064.90	16.05
	5	206.20	1015.80	1048.80	13.20
	Avg	203.81	1023.36	1059.84	13.78
	Std	1.470	10.506	9.954	1.824

Appendix B. Mesosamples Mechanical Properties

Table B.1 All mechanical properties from the vertically oriented mesosamples.

		Vertical Orientation			
Build	Sample #	Young's Modulus (GPa)	Yield Strength (MPa)	UTS (MPa)	Strain to Failure (%)
PC2	2	155.10	1011.10	1029.40	0.18
	3	207.20	1005.60	1012.90	0.19
	4	-	-	-	-
	Avg	181.15	1008.35	1021.15	0.18
	Std	26.050	2.750	8.250	0.007
PC2B	2	194.70	1005.60	1026.30	0.18
	3	180.90	1001.70	1017.30	0.17
	4	235.70	990.00	1023.20	0.18
	Avg	203.77	999.10	1022.27	0.18
	Std	23.272	6.629	3.733	0.007
PC3	2	246.60	942.00	984.30	0.19
	3	157.50	1008.30	1025.50	0.18
	4	245.30	986.20	1021.90	0.18
	Avg	216.47	978.83	1010.57	0.18
	Std	41.699	27.564	18.631	0.004
PC4	2	169.80	1011.10	1019.80	0.19
	3	189.90	1022.20	1024.10	0.17
	4	175.00	1016.70	1021.00	0.18
	Avg	178.23	1016.67	1021.63	0.18
	Std	8.518	4.532	1.812	0.008
PC5	2	206.60	1050.00	1069.10	0.17
	3	195.00	1066.70	1073.80	0.16
	4	166.40	1061.10	1075.20	0.19
	Avg	189.33	1059.27	1072.70	0.17
	Std	16.894	6.940	2.609	0.011
PC6	2	249.10	1097.20	1106.00	0.17
	3	198.10	1090.30	1104.60	0.17
	4	202.70	1104.20	1110.80	0.18
	Avg	216.63	1097.23	1107.13	0.17
	Std	23.034	5.675	2.655	0.005

Table B.2 All mechanical properties from the horizontally oriented mesosamples.

		Horizontal Orientation			
Build	Sample #	Young's Modulus (GPa)	Yield Strength (MPa)	UTS (MPa)	Strain to Failure (%)
PC2	2	159.60	1041.70	1050.00	0.18
	3	150.50	1000.00	1049.40	0.29
	4	176.00	1041.70	1052.20	0.17
	Avg	162.03	1027.80	1050.53	0.21
	Std	10.552	19.658	1.204	0.052
PC2B	2	149.40	1013.30	1036.80	0.18
	3	243.20	1022.20	1039.90	0.19
	4	194.40	1008.90	1040.50	0.19
	Avg	195.67	1014.80	1039.07	0.19
	Std	38.304	5.532	1.621	0.003
PC3	2	220.40	1027.60	1043.70	0.17
	3	157.90	1052.50	1074.50	0.20
	4	200.70	1035.90	1049.00	0.17
	Avg	193.00	1038.67	1055.73	0.18
	Std	26.090	10.352	13.445	0.012
PC4	2	265.30	1020.80	1034.30	0.17
	3	260.90	1020.80	1035.00	0.18
	4	195.60	1013.90	1037.40	0.16
	Avg	240.60	1018.50	1035.57	0.17
	Std	31.870	3.253	1.327	0.006
PC5	2	246.70	1006.90	1020.70	0.20
	3	-	-	-	-
	4	109.90	1027.80	1034.70	0.19
	Avg	178.30	1017.35	1027.70	0.20
	Std	68.400	10.450	7.000	0.007
PC6	2	243.30	1094.40	1099.30	0.17
	3	196.20	1077.80	1101.90	0.17
	4	191.10	1094.40	1099.99	0.18
	Avg	210.20	1088.87	1100.40	0.17
	Std	23.498	7.825	1.100	0.003

Appendix C. Round Bar Samples Mechanical Properties

Table C.1 All mechanical properties from the vertically oriented round bar samples.

		Vertical Orientation			
Build	Sample #	Young's Modulus (GPa)	Yield Strength (MPa)	UTS (MPa)	Strain to Failure (%)
PC2	1	197.19	1057.66	1074.20	14.00
	2	198.57	1049.38	1070.76	14.00
	3	187.54	1054.90	1070.76	16.00
	4	199.95	1054.90	1070.76	16.00
	5	210.29	1040.42	1052.83	16.00
	6	191.67	1043.87	1057.66	14.00
	Avg	197.53	1050.19	1066.16	15.00
	Std	7.118	6.274	7.938	1.000
PC2B	1	216.50	1068.69	1085.23	14.00
	2	208.91	1074.20	1095.58	17.00
	3	204.08	1072.13	1089.37	16.00
	4	204.08	1116.95	1145.22	13.00
	5	214.43	1109.37	1131.43	14.00
	6	202.02	1074.20	1090.75	16.00
	Avg	208.34	1085.92	1106.26	15.00
	Std	5.479	19.469	23.214	1.414
PC3	1	199.26	1039.04	1051.45	19.00
	2	206.84	1026.63	1036.28	16.00
	3	198.57	1032.83	1045.93	14.00
	4	222.70	1036.28	1050.07	14.00
	5	213.05	1059.03	1076.27	14.00
	6	196.50	1048.69	1063.17	17.00
	Avg	206.15	1040.42	1053.86	15.67
	Std	9.310	10.659	12.786	1.886
PC4	1	210.98	1101.09	1125.22	14.00
	2	190.30	1148.67	1178.31	17.00
	3	195.81	1127.29	1152.11	13.00
	4	206.84	1076.27	1096.27	14.00
	5	185.47	1074.89	1095.58	16.00
	6	200.64	1124.53	1147.29	16.00
	Avg	198.34	1108.79	1132.46	15.00

	Std	8.889	27.222	30.087	1.414
PC5	1	199.95	1032.83	1043.87	14.00
	2	198.57	1050.76	1065.93	16.00
	3	213.05	1033.52	1043.87	14.00
	4	197.88	1034.21	1045.25	17.00
	5	188.92	1033.52	1048.00	19.00
	6	201.33	1054.90	1070.76	14.00
	Avg	199.95	1039.96	1052.94	15.67
	Std	7.087	9.187	11.063	1.886
PC6	1	188.92	1021.80	1030.77	14.00
	2	212.36	1024.56	1031.46	14.00
	3	226.84	1023.18	1032.83	17.00
	4	211.67	1018.36	1025.25	16.00
	5	210.29	1029.39	1039.73	16.00
	6	190.98	1027.32	1036.28	14.00
	Avg	206.84	1024.10	1032.72	15.17
	Std	13.154	3.597	4.528	1.213

Table C.2 All mechanical properties from the horizontally oriented round bar samples.

		Horizontal Orientation			
Build	Sample #	Young's Modulus (GPa)	Yield Strength (MPa)	UTS (MPa)	Strain to Failure (%)
PC2	1	199.95	1039.73	1060.41	16.00
	2	204.08	1036.97	1052.83	14.00
	Avg	202.02	1038.35	1056.62	15.00
	Std	2.068	1.379	3.792	1.000
PC2B	1	194.43	1112.12	1135.57	16.00
	2	199.95	1114.19	1137.63	16.00
	Avg	197.19	1113.16	1136.60	16.00
	Std	2.758	1.034	1.034	0.000
PC3	1	201.33	1033.52	1052.14	16.00
	2	208.22	1022.49	1034.90	16.00
	Avg	204.77	1028.01	1043.52	16.00
	Std	3.447	5.516	8.618	0.000
PC4	1	192.36	1076.96	1103.16	16.00
	2	203.40	1127.29	1157.63	16.00

	Avg	197.88	1102.13	1130.40	16.00
	Std	5.516	25.166	27.234	0.000
PC5	1	207.53	1039.04	1056.28	17.00
	2	208.91	1048.69	1063.86	16.00
	Avg	208.22	1043.87	1060.07	16.50
	Std	0.689	4.826	3.792	0.500
PC6	1	191.67	1028.70	1050.07	17.00
	2	215.12	1028.01	1038.35	17.00
	Avg	203.40	1028.35	1044.21	17.00
	Std	11.721	0.345	5.861	0.000

Bibliography

1. ASTM, *ASTM F2792-10 Standard Terminology for Additive Manufacturing Technologies*. 2012, ASTM F2792-10e1: West Conshohocken, PA.
2. Vafadar, A., et al., *Advances in Metal Additive Manufacturing: A Review of Common Processes, Industrial Applications, and Current Challenges.* Applied Sciences, 2021. **11**(3): p. 1213.
3. Beaman, J.J., et al., *Additive Manufacturing Review: Early Past to Current Practice.* Journal of Manufacturing Science and Engineering, 2020. **142**(11): p. 1-50.
4. Huang, Y., et al., *Additive Manufacturing: Current State, Future Potential, Gaps and Needs, and Recommendations.* Journal of Manufacturing Science and Engineering, 2015. **137**(1): p. 014001.
5. Campbell, T., et al., *Could 3D Printing Change the World? Technologies, Potential, and Implications of Additive Manufacturing*. 2011: Atlantic Council.
6. *What Is An STL File? | 3D Systems*. 2017 2017-02-01 [cited 2022 Jan 17]; Available from: https://www.3dsystems.com/quickparts/learning-center/what-is-stl-file.
7. *STL File Format: Everything You Need to Know*. 2021 2021-10-28 [cited 2022 Jan 17]; Available from: https://all3dp.com/1/stl-file-format-3d-printing/.
8. *What is an STL file?* [cited 2022 Jan 16]; Available from: https://www.sculpteo.com/en/3d-learning-hub/create-3d-file/what-is-an-stl-file/.
9. *7 Families of Additive Manufacturing*. 2021, Hybrid Manufacturing Technologies.
10. Merklein, M., et al., *Hybrid Additive Manufacturing Technologies – An Analysis Regarding Potentials and Applications.* Physics Procedia, 2016. **83**: p. 549-559.
11. Scheck, C., et al., *Technical Overview of Additive Manufacturing*. 2014: Naval Surface Warfare Center, Carderock Division.
12. Blakey-Milner, B., et al., *Metal additive manufacturing in aerospace: A review.* Materials & Design, 2021. **209**: p. 110008.
13. Ngo, T.D., et al., *Additive manufacturing (3D printing): A review of materials, methods, applications and challenges.* Composites Part B: Engineering, 2018. **143**: p. 172-196.
14. Airbus. 2022 [cited 2022 Jan 17]; Available from: https://www.airbus.com/en.
15. Altıparmak, S.C. and B. Xiao, *A market assessment of additive manufacturing potential for the aerospace industry.* Journal of Manufacturing Processes, 2021. **68**: p. 728-738.
16. Sarvankar, S.G. and S.N. Yewale, *Additive manufacturing in automobile industry.* Int. J. Res. Aeronaut. Mech. Eng, 2019. **7**(4): p. 1-10.
17. Guo, N. and M.C. Leu, *Additive manufacturing: technology, applications and research needs.* Frontiers of Mechanical Engineering, 2013. **8**(3): p. 215-243.
18. Salmi, M., *Additive Manufacturing Processes in Medical Applications.* Materials, 2021. **14**(1): p. 191.
19. Zadpoor, A.A. and J. Malda, *Additive Manufacturing of Biomaterials, Tissues, and Organs.* Annals of Biomedical Engineering, 2017. **45**(1): p. 1-11.
20. Cooke, S., et al., *Metal additive manufacturing: Technology, metallurgy and modelling.* Journal of Manufacturing Processes, 2020. **57**: p. 978-1003.

21. Lewandowski, J.J. and M. Seifi, *Metal Additive Manufacturing: A Review of Mechanical Properties.* Annual Review of Materials Research, 2016. **46**(1): p. 151-186.
22. Frazier, W.E., *Metal Additive Manufacturing: A Review*. Journal of Materials Engineering and Performance, 2014. **23**(6): p. 1917-1928.
23. ASTM, *ASTM F2792-12a Standard Terminology for Additive Manufacturing Technologies*. 2013, ASTM F2792-12a: West Conshohocken, OA.
24. Sames, W.J., et al., *The metallurgy and processing science of metal additive manufacturing.* International Materials Reviews, 2016. **61**(5): p. 315-360.
25. King, W., et al., *Laser powder bed fusion additive manufacturing of metals; physics, computational, and materials challenges.* Applied Physics Reviews, 2015. **2**: p. 041304.
26. Duda, T. and L.V. Raghavan, *3D Metal Printing Technology.* IFAC-PapersOnLine, 2016. **49**(29): p. 103-110.
27. Jiang, J., X. Xu, and J. Stringer, *Support Structures for Additive Manufacturing: A Review.* Journal of Manufacturing and Materials Processing, 2018. **2**(4): p. 64.
28. Everton, S.K., et al., *Review of in-situ process monitoring and in-situ metrology for metal additive manufacturing.* Materials & Design, 2016. **95**: p. 431-445.
29. Herderick, E.D. *Additive Manufacturing of Metals: A Review*. 2011.
30. Bartlett, J.L. and X. Li, *An overview of residual stresses in metal powder bed fusion.* Additive Manufacturing, 2019. **27**: p. 131-149.
31. Posey, J., *Repeatability of Additively Manufactured Precipitation Hardened 17% Chromium - 4% Nickel Stainless Steel*, in *Mechanical Engineering*. 2020, University of Maryland, Baltimore County: Maryland. p. 260.
32. Kudzal, A., et al., *Effect of scan pattern on the microstructure and mechanical properties of Powder Bed Fusion additive manufactured 17-4 stainless steel.* Materials & Design, 2017. **133**: p. 205-215.
33. Yu, J., et al., *Size effect due to contour laser scanning in 316L stainless steel produced by laser powder bed fusion.* Journal of Materials Research and Technology, 2021. **15**: p. 5554-5568.
34. Hanzl, P., et al., *The Influence of Processing Parameters on the Mechanical Properties of SLM Parts.* Procedia Engineering, 2015. **100**: p. 1405-1413.
35. Gibson, I., et al., *Additive manufacturing technologies*. Vol. 17. 2021: Springer.
36. Oliveira, J.P., A.D. LaLonde, and J. Ma, *Processing parameters in laser powder bed fusion metal additive manufacturing.* Materials & Design, 2020. **193**: p. 108762.
37. Li, C., et al., *Residual Stress in Metal Additive Manufacturing.* Procedia CIRP, 2018. **71**: p. 348-353.
38. Jamal, M. and M.N. Morgan, *Design process control for improved surface finish of metal additive manufactured parts of complex build geometry.* Inventions, 2017. **2**(4): p. 36.
39. Maleki, E., et al., *Surface post-treatments for metal additive manufacturing: Progress, challenges, and opportunities.* Additive Manufacturing, 2021. **37**: p. 101619.
40. Pegues, J., et al., *Surface roughness effects on the fatigue strength of additively manufactured Ti-6Al-4V.* International Journal of Fatigue, 2018. **116**: p. 543-552.

41. Cyr, E., A. Lloyd, and M. Mohammadi, *Tension-compression asymmetry of additively manufactured Maraging steel.* Journal of Manufacturing Processes, 2018. **35**: p. 289-294.
42. Longhitano, G.A., et al., *Correlation between microstructures and mechanical properties under tensile and compression tests of heat-treated Ti-6Al–4V ELI alloy produced by additive manufacturing for biomedical applications.* Journal of Materials Processing Technology, 2018. **252**: p. 202-210.
43. Rodriguez, O.L., et al., *Strain rate effect on the tension and compression stress-state asymmetry for electron beam additive manufactured Ti6Al4V.* Materials Science and Engineering: A, 2018. **713**: p. 125-133.
44. Joseph, J., et al., *Tension/compression asymmetry in additive manufactured face centered cubic high entropy alloy.* Scripta Materialia, 2017. **129**: p. 30-34.
45. Haghdadi, N., et al., *Additive manufacturing of steels: a review of achievements and challenges.* Journal of Materials Science, 2021. **56**(1): p. 64-107.
46. Bajaj, P., et al., *Steels in additive manufacturing: A review of their microstructure and properties.* Materials Science and Engineering: A, 2020. **772**: p. 138633.
47. EOS, *EOS Stainless Steel 17-4 PH*. 2017.
48. Zai, L., et al., *Laser Powder Bed Fusion of Precipitation-Hardened Martensitic Stainless Steels: A Review.* Metals, 2020. **10**(2): p. 255.
49. Sabooni, S., et al., *Laser powder bed fusion of 17–4 PH stainless steel: A comparative study on the effect of heat treatment on the microstructure evolution and mechanical properties.* Additive Manufacturing, 2021. **46**: p. 102176.
50. Rafi, H.K., et al., *Microstructure and Mechanical Behavior of 17-4 Precipitation Hardenable Steel Processed by Selective Laser Melting.* Journal of Materials Engineering and Performance, 2014. **23**(12): p. 4421-4428.
51. Hsu, T.-H., et al., *Microstructure and property of a selective laser melting process induced oxide dispersion strengthened 17-4 PH stainless steel.* Journal of Alloys and Compounds, 2019. **803**: p. 30-41.
52. Yadollahi, A., et al., *Effects of building orientation and heat treatment on fatigue behavior of selective laser melted 17-4 PH stainless steel.* International Journal of Fatigue, 2017. **94**: p. 218-235.
53. LeBrun, T., et al., *Effect of retained austenite on subsequent thermal processing and resultant mechanical properties of selective laser melted 17–4 PH stainless steel.* Materials & Design, 2015. **81**: p. 44-53.
54. Alnajjar, M., et al., *Evidence of austenite by-passing in a stainless steel obtained from laser melting additive manufacturing.* Additive Manufacturing, 2019. **25**: p. 187-195.
55. Sun, Y., R.J. Hebert, and M. Aindow, *Effect of heat treatments on microstructural evolution of additively manufactured and wrought 17-4PH stainless steel.* Materials & Design, 2018. **156**: p. 429-440.
56. Murr, L.E., et al., *Microstructures and Properties of 17-4 PH Stainless Steel Fabricated by Selective Laser Melting.* Journal of Materials Research and Technology, 2012. **1**(3): p. 167-177.
57. Lebrun, T., et al., *Strain rate sensitivity and mechanical anisotropy of selective laser melted 17-4 PH stainless steel.* Mechanical Engineering Journal, 2014. **1**(5): p. SMM0049-SMM0049.

58. EOS, *EOS M 290 Simply Production of Metal Parts*. 2022.
59. Selby, M., et al., *Surface Roughness and Hardness Dependence on Heat Treatment and Geometry of Additively Manufactured Precipitation Hardened 17% Chromium - 4% Nickel Stainless Steel*, in *SAMPE 21*. 2021: Long Beach, CA. p. 15.
60. Stefancik, J., *The Additive Manufacturing Repeatability of 17-4PH Stainless Steel: Component Qualification Methodologies* in *Mechanical Engineering*. 2021, University of Maryland, Baltimore County: Baltimore, MD. p. 242.
61. Gianola, D.S. and W.N. Sharpe, *Techniques for testing thin films in tension.* Experimental Techniques, 2004. **28**: p. 23-27.
62. Sharpe, W., et al., *Strain Measurements of Silicon Dioxide Microspecimens by Digital Imaging Processing.* Experimental Mechanics, 2007. **47**: p. 649-658.
63. Duffy, M.E., *Microtensile Characterization of Additively Manufactured AlSi10Mg*, in *Mechanical Engineering*. 2018, University of Maryland, Baltimore County: Maryland. p. 241.
64. Nimer, S., *Microscale Mechanical experiments at elevated temperatures: system development and material characterization*, in *Mechanical Engineering*. 2016, University of Maryland, Baltimore County: Baltimore, MD.
65. Zupan, M. and K.J. Hemker, *Tension and compression testing of single-crystalline gamma Ti-55.5 pct Al.* Metallurgical and Materials Transactions A, 1998. **29**: p. 65-71.
66. Santos, J., *A Qualification Methodology for Additively Manufactured Parts*, in *Mestrado Integrado em Engenharia Mecânica*. 2016, Faculdade de Engenharia Universidade do Porto.
67. Nimer, S., J. Wolk, and M. Zupan, *Location and Orientation Specific Material Property Evaluation of Friction Stir Welded Ti 5111: A Microsample Approach.* Advanced Engineering Materials, 2014. **16**: p. 452-458.
68. Scheck, C., et al., *Impact of Ultrasonic Impact Treatment on a 5456 Aluminum Alloy Characterized through Micro-Specimen Testing and X-Ray Tomography.* TMS Annual Meeting, 2011. **2**: p. 205-212.
69. Wilkins, J., *Repeatability of the Mechanical Properties of Additively Manufactured Precipitation Hardened 17% Chromium - 4% Nickel Stainless Steel*, in *Mechanical Engineering*. 2021, Universidade do Porto. p. 133.
70. ASTM, *ASTM E8 / E8M-21*, in *Standard Test Methods for Tension Testing of Metallic Materials*. 2021: West Conshohocken, PA.